2008

Investigation of an alpha-parabolic solar concentrator dish

Matthew R. Devlin
Lehigh University

Devlin, Matthew R.

Investigation of an Alpha-Parabolic Solar Concentrator Dish

January 2009

Investigation of an Alpha-Parabolic Solar Concentrator Dish

by

Matthew R. Devlin

A Thesis

Presented to the Graduate and Research Committee

of Lehigh University

in Candidacy for the Degree of

Master of Science

in

Mechanical Engineering

Lehigh University

January 2008

Certificate of Approval

This thesis is accepted and approved in partial fulfillment of the requirements for the Master of Science.

Dec 4, 2008

Date

Dr. Sudhakar Neti, Thesis Advisor

Dr. Gary Harlow, Chairperson of Department

Acknowledgements

I would first like to extend my utmost appreciation to my advisor, Dr. Neti, who presented me with the opportunity to do this work, and was there for anything I needed to guide me every step of the way. I would also like to thank John Fangman, who's ideas are included in this study and was always there to lend advice when I was having a dilemma. I would also like to thank Matt Fangman, who also provided help and guidance throughout my work.

I would also like thank my parents for their endless love and support throughout this project as well as my entire life. Since I was young, they have always instilled in me the importance of education. Without their support I would not have been able to continue my education at Lehigh.

Table of Contents

List of Figures

List of Tables

Abstract

Concentrated solar thermal (CST) power has been used for years to help supply power to certain energy markets and has proven to be fairly successful. Unfortunately the high prices of these solar technologies have prohibited them from really making a large impact on the world's energy scene. This study analyzes the structural, optical, and thermal performance of a parabolic dish concept which could be the basis for large scale commercial concentrated solar thermal electricity. Finite element method (FEM) software was used to simulate the structural integrity of the dish which is modeled after the General Electric dish (described later) under different wind loading conditions. Ray tracing software was used to track optical performance, and computational fluid dynamics (CFD) software was used to simulate the thermal performance of the receiver.

Simulations predict the dish to have minimal deflections in 30mph operation wind loading condition. Optical analysis shows the dish is capable of capturing 95% of the incident solar radiation. This radiation is capable of heating thermic fluid to a maximum enthalpy gain of 749kJ/kg. For the case of VP-1 which was used in this study the maximum outlet temperature from the receiver is 423°C. These results show a dish of this type has good performance in all three (structural, optical, and thermal) areas and has much promise to compete in the current energy markets.

Chapter 1: Background

1.1 Motivation

The energy crisis facing the world today has left an open debate as to where the answers lie for the problem. It is no secret that fossil fuels will not last forever with the worlds growing hunger for energy. With the cost of fossil fuels rising on a daily basis it is becoming more apparent that renewable types of energy must be looked at as possible solutions to the problem. It only makes sense that we should look to the largest source of energy for Earth in the universe for some answers. Many experts believe that solar energy can play a huge part in meeting the world's energy needs.

There is a simple barrier standing in the way between large scale solar power production and implementation into our power grid; that barrier is the price-performance ratio. To date, it just has not been cost efficient to implement solar power; largely because fossil fuels have still been abundant and cheap enough to supply us with the majority of our energy needs. With the recent rise in fuel costs, it is becoming more realistic that solar power will be able to soon compete with other types of energy in the commercial markets.

1.2 History

In the late 1970's and early 1980's solar power became very popular in the U.S. due to economic circumstances similar to those of today. Rising energy costs and

advances in solar technologies left the perfect situation for the first commercialization of large scale solar power plants. Between 1984 and 1990, Luz International Limited built nine solar power plants in southern California; they are often referred to as Solar Electric Generating Stations (SEGS I-IX). One of the main reasons these plants were able to be built was the availability of state and federal investment tax credits. Even with these tax subsidies, it still took over $1.2 billion in capital to finance the construction of these plants. Luz International sold all the plants to independent investors and went bankrupt in 1991, while they were in the process of constructing a tenth plant. Falling energy prices and the reduction in the amount of tax credits are both partially responsible for the demise of Luz. Despite the failure of the company, the power plants were a success. From 1984 to 1991, Luz helped to reduce the cost of solar energy by two-thirds, from 24¢/kWh to 8¢/kWh through marketing and other efforts [11].

After the last SEGS in 1990, there were no new commercial solar power plants built in the U.S. until Nevada Solar One went online in 2007. Located in Nevada's El Dorado Valley, it is the third largest solar power plant in the world. The construction of this plant marks the reemergence of commercially available solar power in the United States. All things considered, this market is poised to grow and once again flourish.

1.3 Objective of Present Work

A parabolic solar concentrator dish concept that could be useful in large scale commercial power plants will be examined through various computer simulations. The

structural, optical, and thermal properties of the dish will be compared to existing concentrated solar thermal (CST) technologies to see if the proposed concept has promise to move forward for further analysis and testing.

Chapter two presents the current state CST technology and examines the opportunity for solar power use in the U.S. Chapter three characterizes the dish and all of its components which this study examines. Chapter four discusses the theory behind the different types of analysis which are used in this study. Chapter five gives an overview of the simulation programs used for analysis. In chapter six, the simulation results are presented and compared to similar types of CST systems already on the market. Conclusions and possible future work to come from this study are summarized in the final chapter.

Chapter 2: Introduction to Existing Solar Technologies

2.1 Solar Resources

Many factors play a part in determining the cost and effectiveness of all of these CST technologies. The one common factor which is most important in the performance of all solar power systems is the availability and power of sunlight. The best system in the world would be of little use if it is located in an area that doesn't receive an ample amount of solar radiation. Electricity is generally measured in kilowatt hours (kWh). 1kWh corresponds to 1Watt of continuous power for a one hour time period. On average, the sun's rays are incident on the U.S. with a power of about $1 W/m^2$ (i.e. $1 kWh/m^2$ per hour of sunlight. The Southwestern United States receives some of the highest amounts of solar radiation (over $2 MWh/m^2$ annually) in the world. This leaves a huge opportunity for the use of CST systems in this region. The following excerpt is taken from a recent article written on the current potential that CST has in the large scale utility market.

> "In the United States, CSP is most suited to the Southwest, where the warm, sunny climate and pancake-flat, unpopulated desert stretches offer vast solar potential. "We have enough suitable land in the Southwest for CSP to support over 6 million megawatts of capacity," according to Mark Mehos, the CSP program manager at the National Renewable Energy Laboratory (NREL) in Golden, Colorado. NREL arrived at this value, which corresponds to a potential CSP contribution of kilowatt-hours equal to over four times U.S. demand, by measuring the solar radiation and subtracting all land area that was unsuitable due to its environmental sensitivity, urban location, or slope [8]."

Figure 2.1 shows the annual direct normal solar radiation for the U.S. [10].

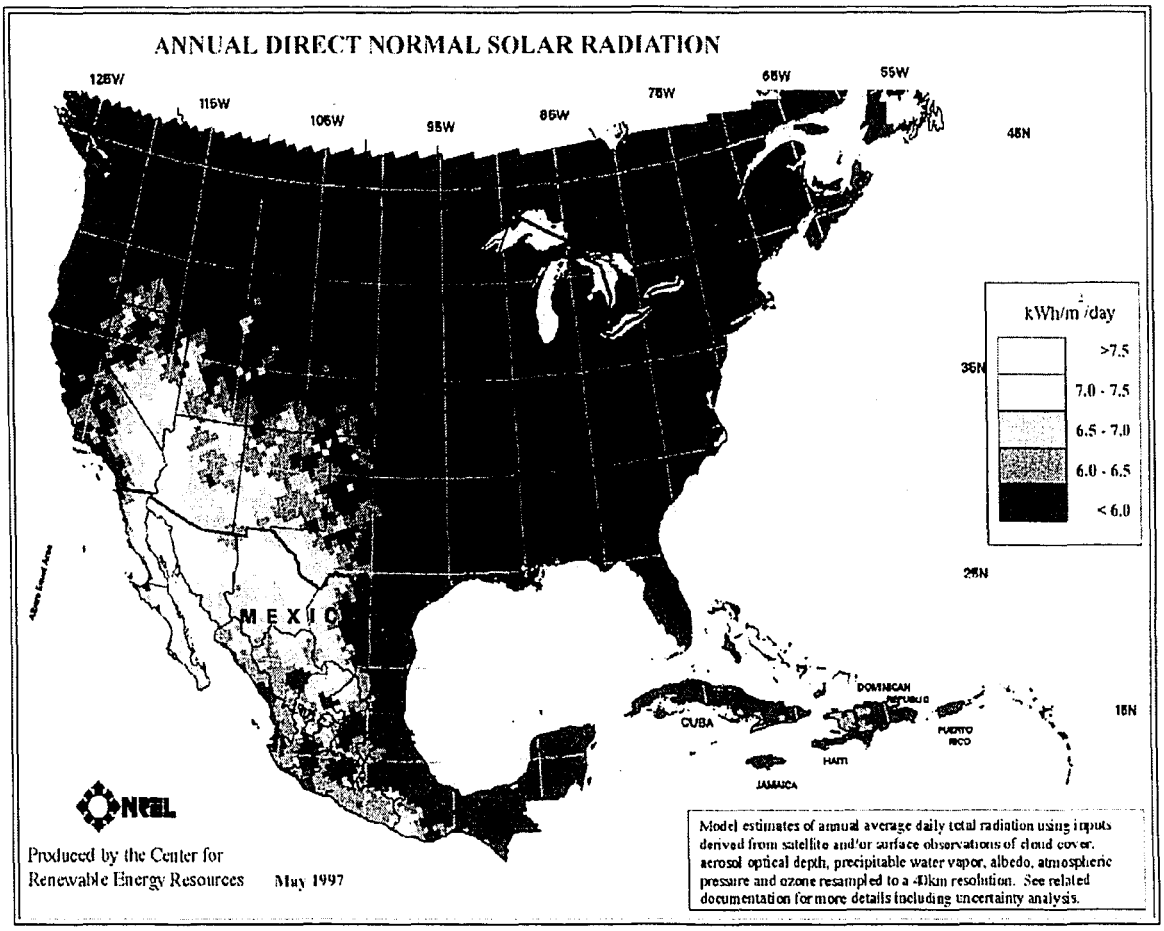

Figure 2.1: U.S. normal direct solar radiation

2.2 Overview

There are many different types of solar technologies, and some of them fall into the concentrated solar thermal (CST) category. Photovoltaic systems are not thermal devices and will not be discussed in this paper since it works on entirely different principles. Most CST systems are comprised of the same basic components which are: support structure, mirrors, receiver, piping for heat transfer fluid, tracking system, and controls. Although all types of CST technologies are made of the same basic components and use

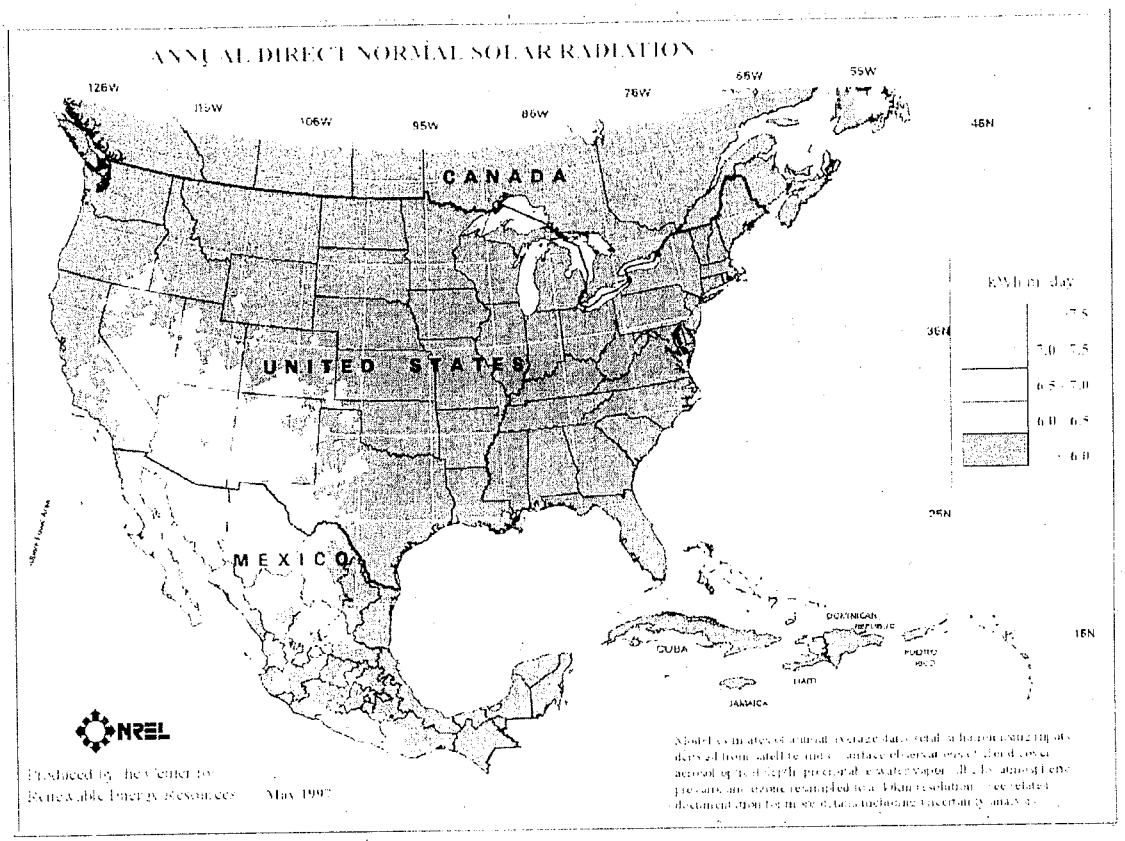

Figure 2.1: U.S. normal direct solar radiation

2.2 Overview

There are many different types of solar technologies, and some of them fall into the concentrated solar thermal (CST) category. Photovoltaic systems are not thermal devices and will not be discussed in this paper since it works on entirely different principles. Most CST systems are comprised of the same basic components which are: support structure, mirrors, receiver, piping for heat transfer fluid, tracking system, and controls. Although all types of CST technologies are made of the same basic components and use

the same principles, the way in which they go about doing so varies greatly. The following sections will describe five types of CST systems which have proven to be useful generators of electricity.

2.3 Parabolic Trough

Parabolic trough systems use a line focusing technique to concentrate the sun's rays. This technology uses long, parabola shaped reflecting surfaces, with a receiver tube running parallel to the reflectors at the line of focus. The tubes contain the heat transfer fluid (usually thermic, organic oil), which are heated to temperatures nearing 400°C. The fluid is then passed through a heat exchanger to produce steam to power the turbine engines. For these types of arrangements, a single axis tracking system is used, based on the N-S or E-W alignment of the trough. The reflector rotates around the axis of the receiver tube following the sun [10]. Figure 2.2 on the following page shows the basic idea.

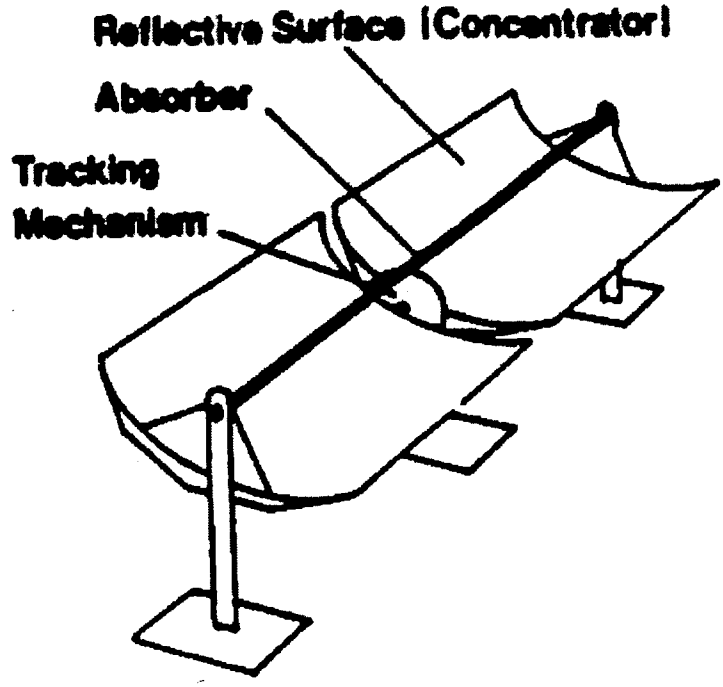

Figure 2.2: Parabolic trough diagram [3]

Parabolic Trough systems are currently accepted as the most reliable option for large scale solar power production. This technology was first put to use in the mid to late 1980's, when nine of these plants, were constructed in the southwestern U.S. (the SEGS plants which were discussed in section 1.2). All of these plants are still in use today and range in size from 14 to 80MW_e, for a combined output of 354MW_e. Five of these plants, each with about 30MW_e capacity, operate at over 100% capacity on most sunny days between the hours of noon and 6pm (to match peak demand). The plant's turbines are hybrid natural gas and solar for times when solar cannot supply all the necessary power (i.e. cloudy days). When the sun is low, the turbines are run on 25% natural gas. These plants have been running for over 18 years now and are considered fairly

successful [11]. Due to the drop in energy costs in the 90's no more large scale solar power plants of this type were produced until recently. In 2007, Acciona Solar (now owned by Abengoa Solar) started operation of a $64MW_e$ plant. This plant, Nevada Solar One, uses the same proven parabolic trough technology as its 18 year old counterparts, with some upgrades to increase efficiency and lower costs. The new plant has better focusing accuracy for improved optical properties, vacuum jacketed receiver tubes to reduce heat losses, and aluminum space frames to provide extra strength while using less material. Technological advances also allowed the Solar One team to reduce the cost of installation and construction in the field. Figure 2.3 shows a row of the parabolic trough system at Nevada Solar One [8].

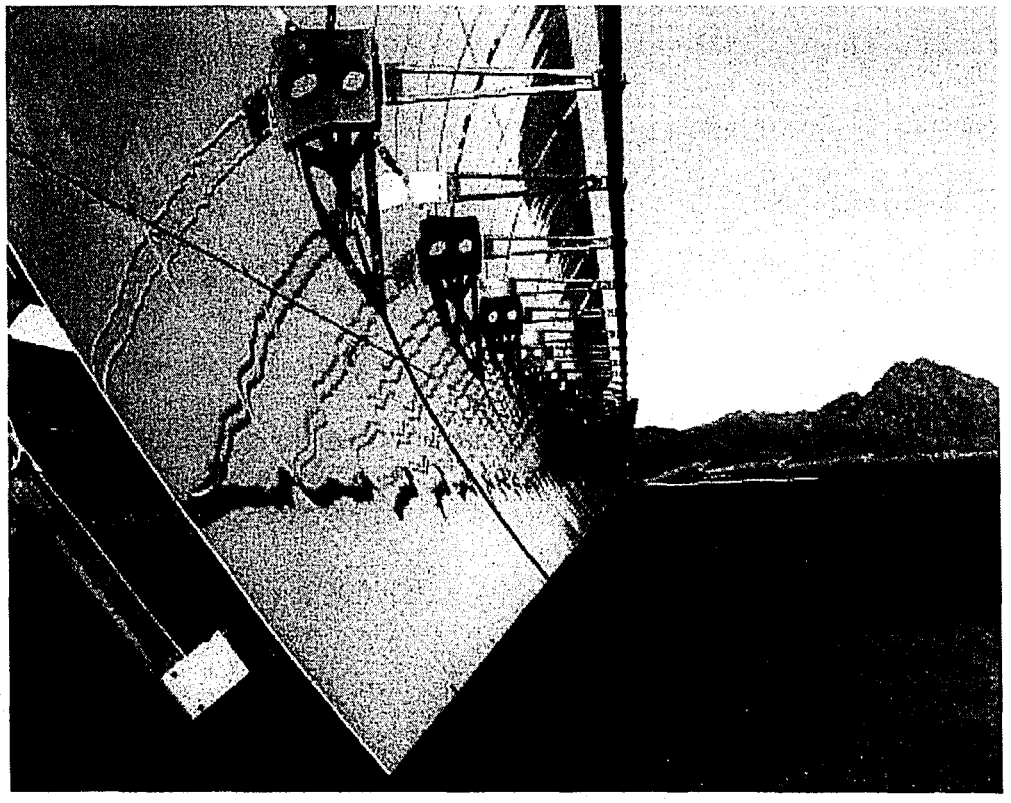

Figure 2.3: Parabolic troughs at Nevada Solar One

2.4 Power Tower

Power Tower systems use a field of mirrors in a circular or semicircular array which reflect to one central receiver located at the top of a tower in the field. Refer to Figure 2.4 for a sketch showing this general idea [3]. Receiver temperatures in these systems can reach up to 565°C. Each mirror, referred to as a heliostat, has an individual tracking system. This type of CST uses far less tubing to carry the heat transfer fluid since there is only one receiver in the tower, which reduces cost in this sense. On the down side, the tracking systems for these are two axis systems, which are a little more complex and expensive than those used for parabolic trough systems. Also, due to the arrangement, all the heliostats cannot be used at high efficiency at all times. This is a major optical and economic disadvantage

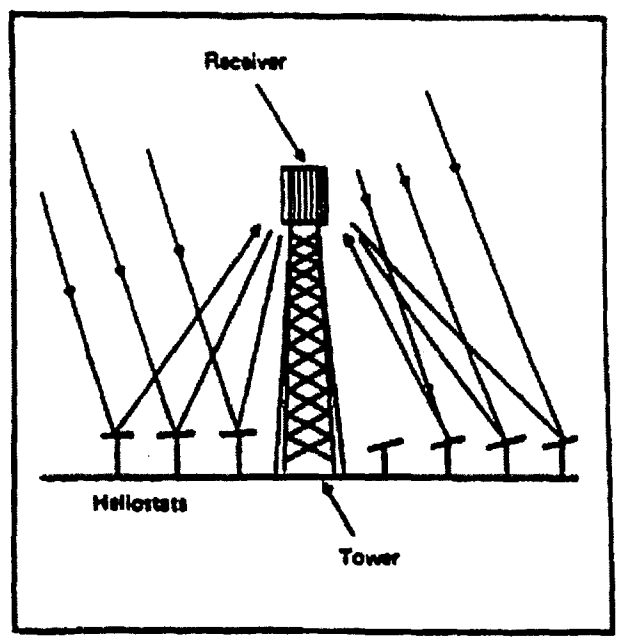

Figure 2.4: Power tower diagram

Power tower technology does not have as much proven use in the commercial market, but still has been around for some time. The first commercial plant began producing power in 1988. It used water in the receiver to generate steam to run turbines. This plant, located in southern California produces $10MW_e$ of power. Adjustments were made to the system in 1992 to use molten salts in the receiver instead of water. This technology is very promising, since the molten salts can be stored at their high temperatures for long periods (3-13 hours). This allows solar power to be produced on demand, not just at peak times during the day [10]. In 2007, Abengoa Solar launched a new $10MW_e$ power tower plant in Spain. A company named Brightsource is currently developing a prototype power tower plant in California. Power tower technology gives much hope for the future of CST power. Below, figure 2.5 depicts Solucar PS10 in Seville, Spain [8].

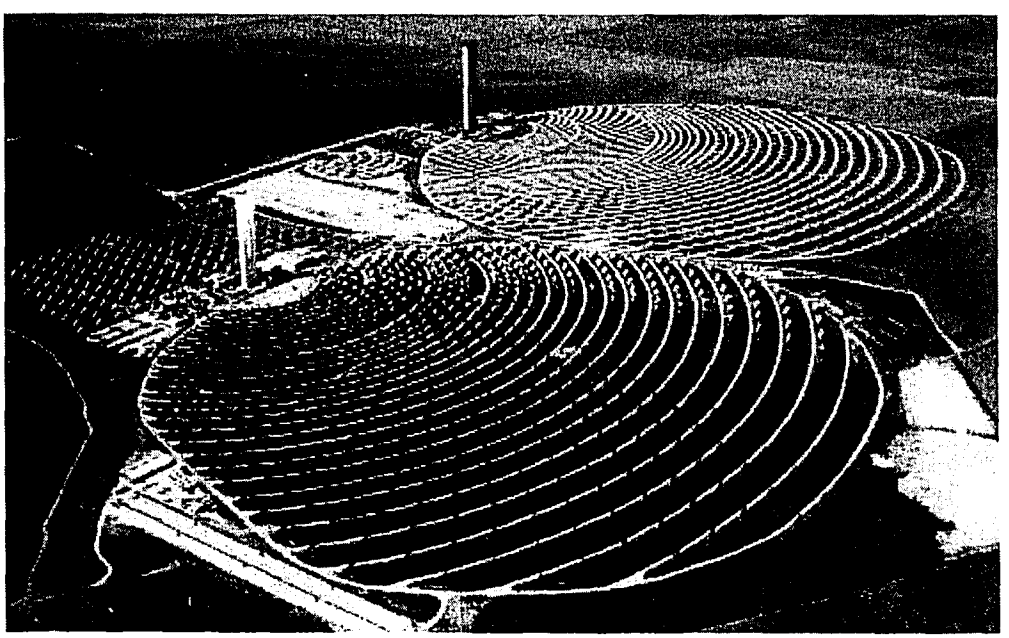

Figure 2.5: Solucar PS10 power tower plant

2.5 Parabolic Dish

Parabolic dish systems consist of bowl shaped surface which looks similar to a satellite dish that is covered with mirrors. Each mirror may have a distinct curved shape so the total array makes the shape of a parabolic dish or an effective parabolic shape as in a Fresnel dish. The mirrors focus light onto a receiver which is located at the focal point. A fluid is heated in the receiver that is located at or near the focal point, which could power an engine, e.g. a Stirling or Brayton cycle engine. Temperatures in the receiver can reach up to about 750°C. These systems have much promise, since they have a solar to electricity conversion efficiency of nearly 30%. This is the highest overall efficiency of any type of CST technologies [10]. This high efficiency is due largely in part to the fact that the dish is always pointed directly at the sun. Each dish is fit with a two axis tracking system similar to those on the power tower heliostats. This allows an extremely high optical efficiency of 85% (when the mirrors have a reflectivity of 93%). Typically either a polar or azimuthial tracking system is used.

Several parabolic dishes have been constructed and are in use today; they range in power output between 7 and 25kWe. Construction of one such dish began at Sandia National Laboratories in the early 1980's and much testing has taken place. Despite the high efficiencies of this type of dish, they still have yet to penetrate the market for large scale commercial use. High material and construction costs are most likely to blame. Figure 2.6 is a picture of a parabolic dish system located on Australian National University campus. This 400m^2 dish is considerably larger than most dish concentrators and is capable of 50kW$_e$ output[4].

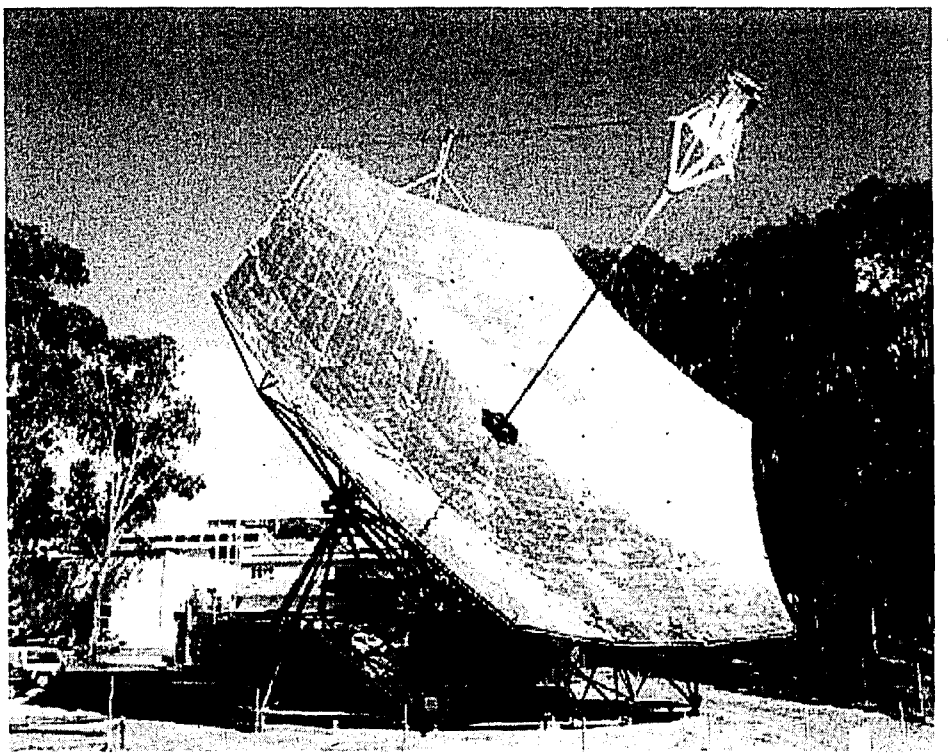

Figure 2.6: Parabolic "Big Dish" at ANU

Another prototype parabolic dish was designed by General Electric and built by Solar Kinetics Corp and tested in Shenandoah Georgia. This concentrator is about seven meters in diameter and consists of 21 Aluminum petals which are coated with FEK-244 reflective film and die-stamped to form the correct shape. The petals are supported by 21 sheet metal ribs, which are fastened to a central steel hub for stability. The dish sits on a steel tripod mount and is bolted to a concrete base. A counterweight and yoke system allows the dish to be moved via a two-axis tracking system by two 75W motor driven jackscrews. A microprocessor control unit located on the concentrator allows for total control over the tracking system under various conditions (including moving the dish to

the rest position during high winds, overheating, etc). Figure 2.7 shows a diagram of this dish.

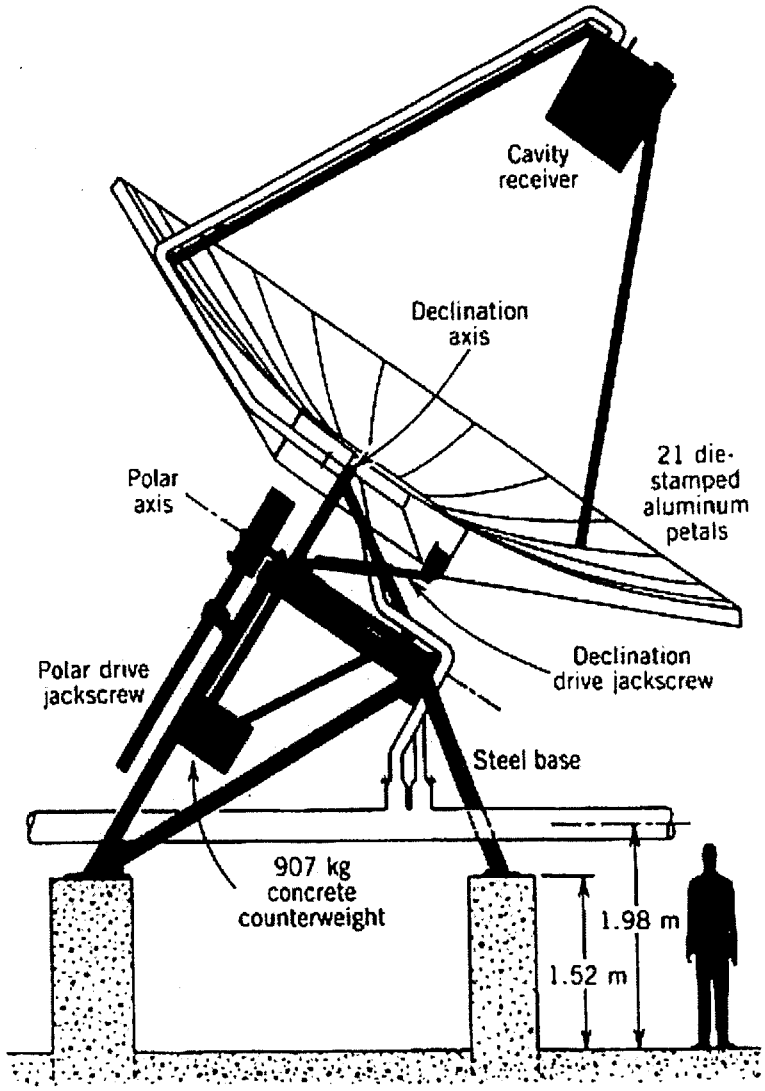

Figure 2.7: Shenandoah dish diagram

Two sets of flexible hoses carry the silicon based heat transfer oil (Dow Corning Siltherm-800) to and from the receiver. The fluid will be heated to a maximum of 400°C from an inlet temperature of 260°C. The insulated receiver will absorb over 98% of the radiation which enters the receiver cavity. Tests show that the concentrator has an

overall efficiency of about 61%. Figure 2.8 shows a picture of the actual dish constructed at Shenandoah. The Alpha-dish analyzed in this work is based on and is similar to the Shenandoah dish built by Solar Kinetics Corp. Though the concepts are similar, the Alpha-dish details are somewhat different [14].

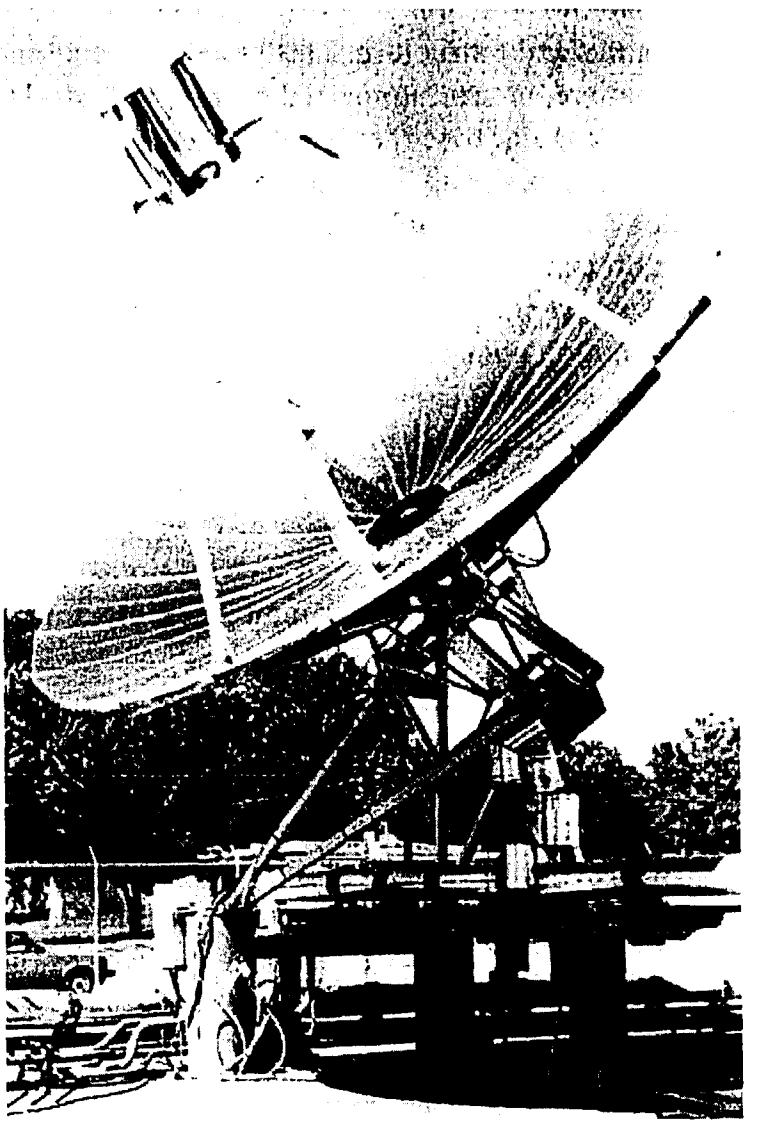

Figure 2.8: Shenandoah dish

2.6 Compact Linear Fresnel Reflector (CLFR)

CLFR systems are relatively new technology compared to the other CST systems discussed in this paper. CLFR are similar to parabolic trough systems in the way that they focus the light into a line, not a point. CLFR utilizes numerous long flat, or slightly curved mirrors which run parallel to a receiver tube. The mirrors are placed close to ground level and the receiver about ten meters above ground. The receiver is stationary, but each mirror has a single axis tracking device to keep the light focused on the receiver. Water or thermic fluid is used as the heat transfer fluid in the receiver to directly or indirectly generate steam to power a turbine. This system is typically run at a temperature of 265°C. These systems lend hope to lowering the cost due to the stationary nature of the receivers and relatively flat reflecting surface. The down side to this type of system, just as with the parabolic trough systems is the low collection efficiency. CLFR has efficiencies around 38%, which is an even lower rating than that for parabolic trough technologies. Part of this can be explained by extra heat losses in the receivers since they are not under vacuum or otherwise protected conditions.

CLFR technologies are just getting into the commercial market. A project in 2006 added a $14MW_{th}$ CLFR system to a coal fired power plant just outside of Sydney, Australia. The solar power generated is used to offset costs by preheating feed water to the coal plant [2]. Another project was launched in 2004 for implementation into the Liddell coal power station in Australia and is now in operation. Figure 2.7 is a picture of the $1MW_{th}$ CLFR test system which is up and running at Liddell. The field is to be expanded in two directions to supply the coal plant with up to $100MW_{th}$. Hopes are

high that projects like these will give the CLFR technology the testing and development it needs to then be implemented as fully operational solar plants [7].

The first CLFR plant in the U.S. is now up and running in Bakersfield, CA. The Kimberlina Solar Thermal Energy Plant owned by Ausra began production in October 2008. It generates up to $25MW_{th}$ energy to drive a steam turbine at a neighboring power plant to produce a peak output of $5MW_e$. Ausra is also currently is in the development stages of another $177MW_{th}$ plant in California.

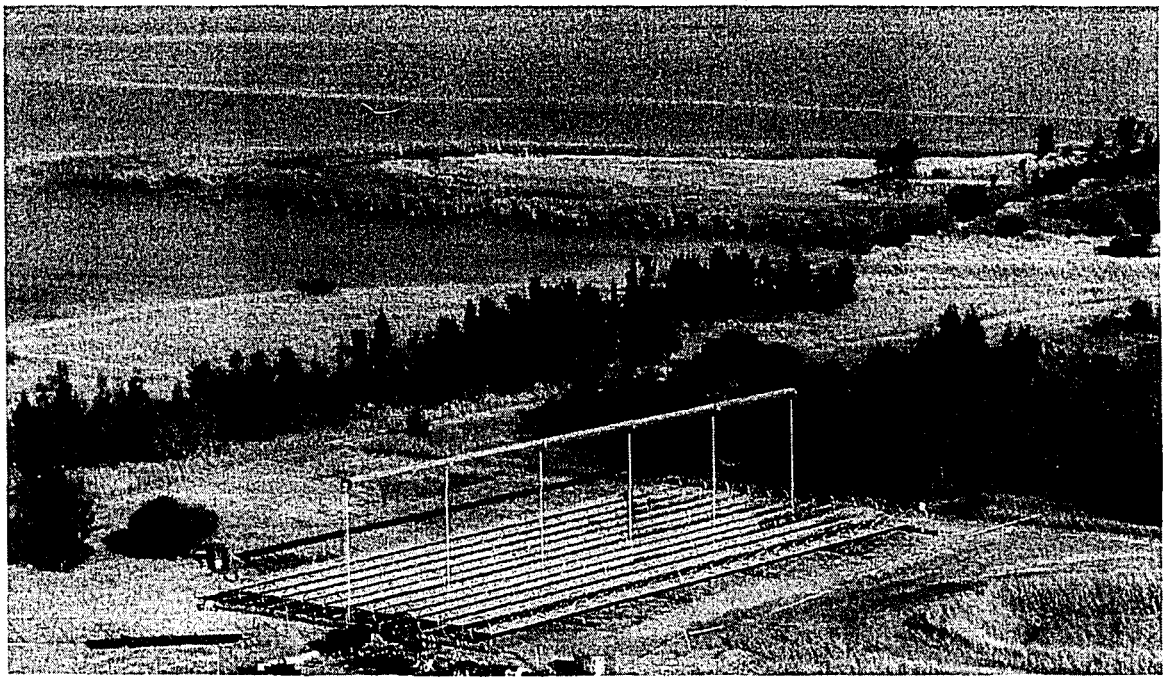

Figure 2.9: CLFR test system at Liddell coal power station

2.7 Point Fresnel

Point Fresnel systems are sort of a hybrid between dish concentrators and the CLFR systems. These use many small flat surface mirrors, located in a dish-like array, which

are all reflected onto a central point receiver, much like a parabolic dish. This could cost significantly less to manufacture since all the mirrors are flat, but this cost is offset by additional labor costs because each mirror has to be individually focused onto the receiver upon construction in the field. This technology is used in on rooftops in India to produce steam generators for cooking purposes. Figure 2.8 shows a $300m^2$ point Fresnel system used for testing at Sandia National labs [9].

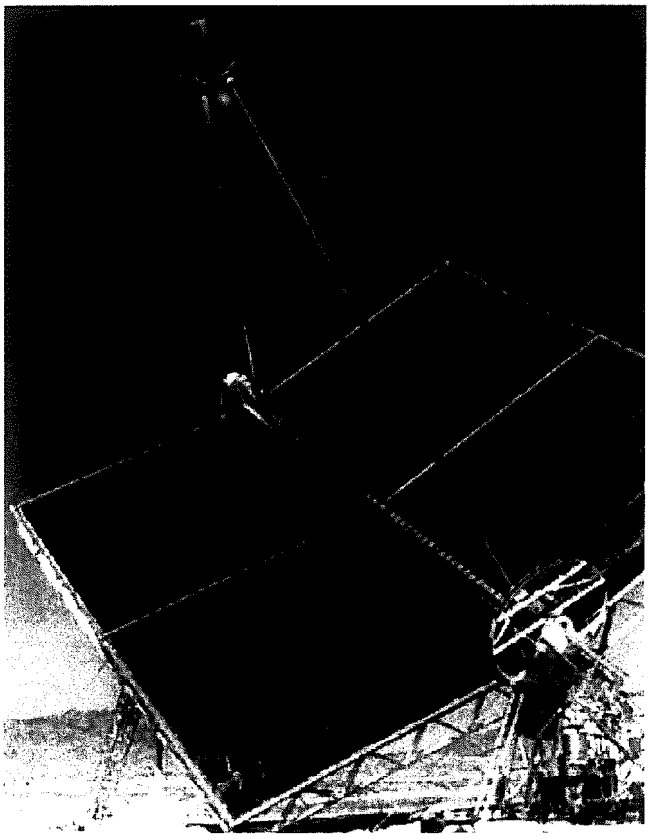

Figure 2.10: Point Fresnel system at Sandia National Labs

CHAPTER 3: DISH CHARACTERIZATION

3.1 Introduction

All of the previously discussed CST technologies have provided inspiration for the Alpha parabolic dish this work analyzes. Certain lessons were learned from all previously mentioned types of concentrators, and this design hopes to capitalize on some of the positive parts of each technology. The current Alpha dish most closely resembles the parabolic point dish concentrators, although it uses some principles from many of the other previously described types of CST technologies. The hope is to further reduce cost, while still maintaining high optical, thermal, and overall efficiencies.

The following sections will describe the physical characteristics of the dish. All dimensions are normalized with respect to the outer diameter of the reflecting surface (i.e. diameter = 1 arbitrary unit = 1au).

3.2 Support Structure

The CST design of the present Alpha dish is based on the one made by Solar Kinetics [14]. Figure 3.1 is a CAD model of the support structure without the reflecting surface and receiver attached. The dish is supported by a rigid collar which is 0.2au in diameter, and 0.003au thick. The 0.16au collar extends to the center of the reflecting surface, where it is attached for support. Eight trusses, which stretch from the collar to the outer edge of the reflecting surface, provide support to the dish. The collar will be the

attachment point to whatever base structure the dish is mounted on, two holes of 0.026au diameter are located on the collar for this purpose.

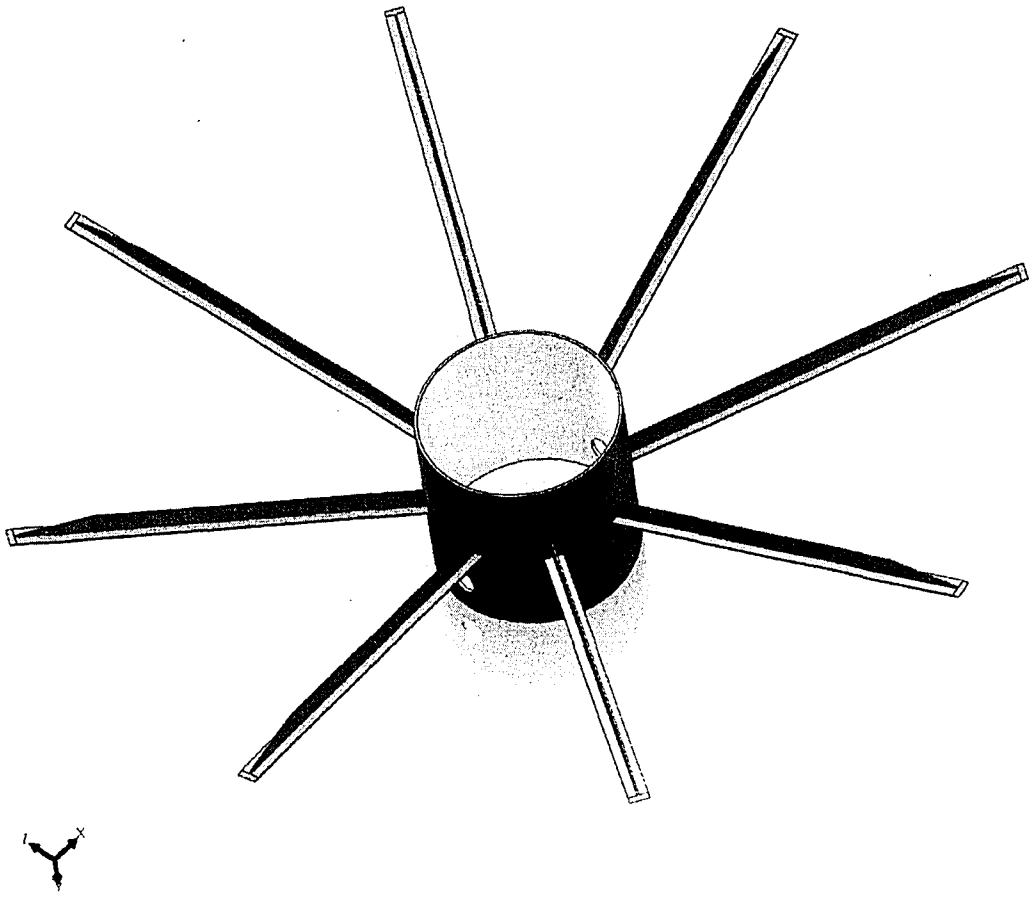

Figure 3.1: Dish Support Structure

3.3 Reflecting Surface

The design used by Solar Kinetics [14] is the basis dish design used here. The reflecting surface is made up of sixteen individual sheets. There is a 0.2au diameter flange located in the center of the dish to provide support and attach the petals to the

mounting collar. Welds are used to hold the petals together as well as to attach the reflecting surface to the frame. The reflecting surface is 2E-4au thick, and has an overall diameter of 1au. The surface is assumed to have a reflectivity of ninety seven percent. Figures 3.2 and 3.3 show the reflecting surface attached to the support structure from a front and rear view respectively.

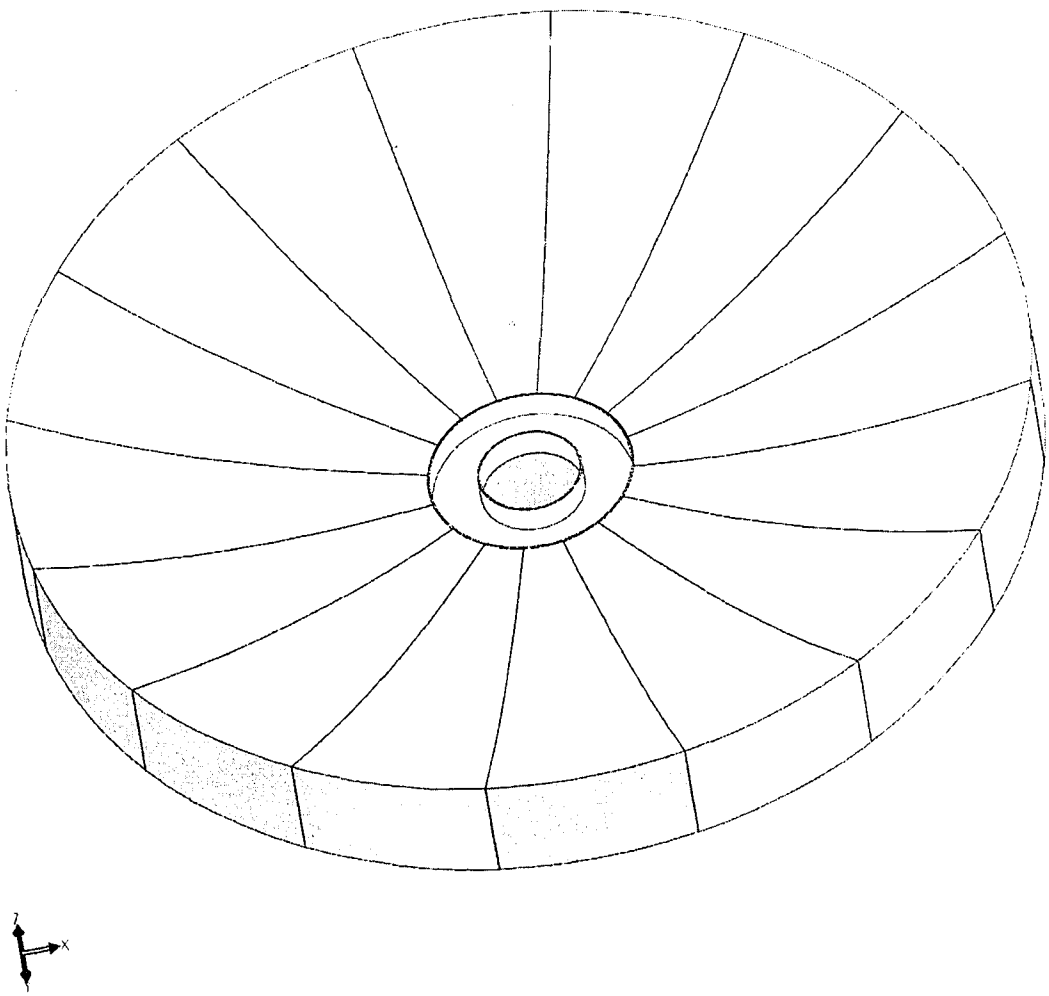

Figure 3.2: Reflecting surface (front view)

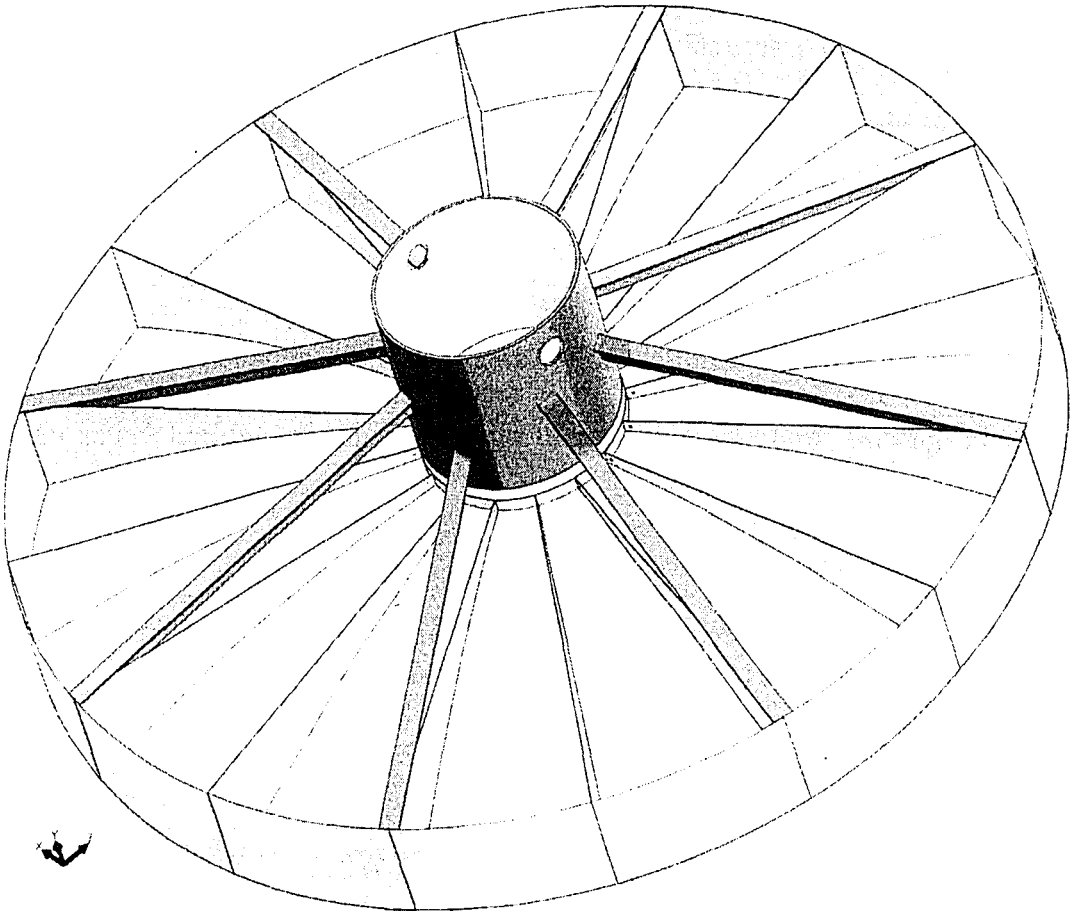

Figure 3.3: Concentrator Dish (rear view)

3.4 Receiver

Much research has been done on the efficiencies of cavity receivers for solar concentrators. These receivers all use some sort of heat transfer fluid with a heat exchanger or direct steam generation to power an engine. Refer to Wright [16], for complete analysis of a steam Rankine solar receiver. Receivers are usually coiled tubing

heat transfer surfaces with thermic fluid inside the tube and radiative heat flux input on the outside. To make the analysis easier, the coils are replaced with a cylinder with strong swirl flow through the heat exchanger. This system uses a 0.0067au thick cylinder with an inner radius of 0.024au. The receiver is 0.08au in height, with the heat transfer fluid flowing through it at a rate of 19.81g/s. This is housed in a 0.013au thick insulated cylinder with an outside diameter of 0.099au. The aperture diameter for the solar radiation to pass through is 0.072au. Figure 3.4 on the following page shows the receiver cylinder and its housing. As mentioned, the thermic fluid will have a strong tangential velocity to simulate flow through the coiled tubes.

The heat transfer fluid proposed for use in the receiver is Therminol VP-1. It has been used in solar thermal systems for over twenty years, including some of the previously mentioned solar trough systems. VP-1 is a synthetic fluid manufactured by Solutia Inc. which has some very favorable thermal properties for high temperature systems. It is stable in the liquid state from 13-400°C. Table 3.1 shows the thermal properties of Therminol VP-1 at 300°C; refer to attached Appendix 1 for complete details on VP-1 fluid properties.

Table 3.1: VP-1 thermal properties

Density	815 kg/m3
Viscosity	0.2 cp (mPa-s)
Heat Capacity	2319 J/kg-K

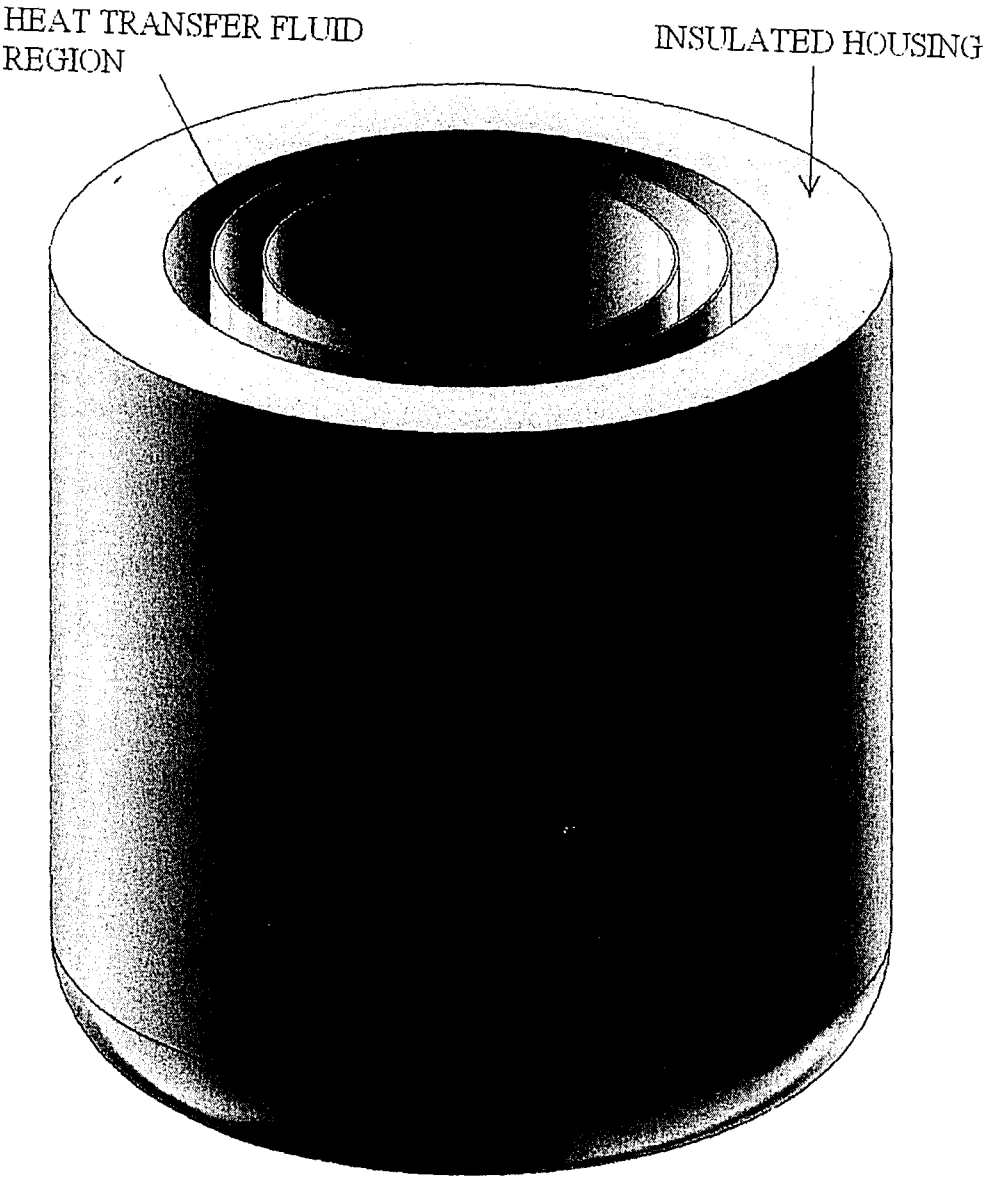

Figure 3.4: Receiver

Chapter 4: Theory

4.1 Finite Element Analysis of the Alpha-dish

Finite element analysis (FEA) was used to perform stress analysis for this study. Finite element methods have been studied for years and numerous papers and books have been published on the topic. This section will describe the computational methods used here.

The finite element method (FEM) is a numerical technique used to solve partial differential and other equations. The process works by discretizing the object into a finite set of smaller elements. Typically, the elements are rectangular, triangular or tetrahedral in shape, but can be of any polynomial depending on the complexity and shape of the object which is being modeled. The common points shared by the elements are referred to as nodes, the nodes and elements form a mesh throughout the object. Boundary conditions are applied at each node (forces, material properties, restraints, etc), and each node can have multiple degrees of freedom (dof). Each element is defined in matrix form, and systems of equations define the nodes. The equations are solved at each node by an iterative process solving for displacements for each node. Stresses and strains are then calculated using the displacements the defined material properties. Being a numeric solution, the FEM doesn't produce exact results, but with an accurately generated mesh the FEM can produce extremely accurate simulations and modeling of many types of engineering problems. In this study, the von Mises stress (maximum energy of distortion) will be evaluated. The governing equation for von Mises stress is:

$$\sigma_{vm} = \sqrt{\frac{1}{2}[(\sigma_1 - \sigma_2)^2 + (\sigma_2 - \sigma_3)^2 + (\sigma_3 - \sigma_1)^2]}$$

Where σ_1, σ_2, and σ_3 are the principle stresses.

4.2 Optics

Basic ray tracing principles along with the computation power of the ZEMAX program were used in this study to perform the optical analysis. At the earth's surface, the sun's rays are nearly parallel, this assumption was made for all analysis. When a ray strikes the reflecting surface, the angle of the reflected ray is equal to the angle of the incident ray with respect to the normal surface. Figure 4.1 from [3] shows this principle Snell's law. The curved nature of the dish will then focus the light into a circular profile on the receiver. A reflectivity of 97% is assumed for analysis in this study.

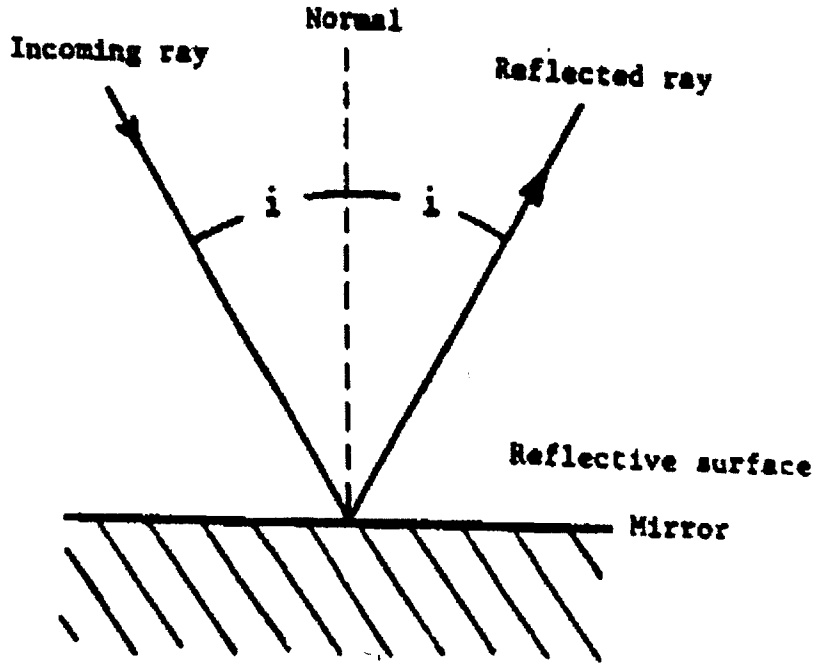

Figure 4.1: Ray tracing principle

4.3 Heat Transfer

The heat source for the receiver will be the incident radiant solar flux on the inner surface of the receiver cylinder. This flux profile is found using the ray tracing principles discussed in the previous section. The space in the cylinder will be heated by radiation from the heated surface. The outer wall of the cylinder will in turn be heated by reflected radiation from the insulated walls of the receiver housing. Conduction will take place in the walls of the cylinder, which will then heat the transfer fluid by convection. Convective and radiative losses will take place at the aperture of the receiver; these are assumed to be about 2.5% of the solar input [16]. An overview of the heat transfer principles which take place in the receiver will be discussed. For a complete thermal analysis of a solar receiver refer to Wright[16].

The radiation is governed by the Stefan-Boltzmann law, which is:

$$q = \varepsilon \sigma A (T_h^4 - T_c^4)$$

where:

q = heat transfer per unit time

ε = emissivity of the object

σ = Stefan-Boltzmann constant (5.67E^{-8} W/m^{2}K^4)

A= surface area of emitting object

T_h = temperature of emitting object (K)

T_c = temperature of cooler surroundings (K)

The conduction which takes place in the cylinder walls is goverened by Fourier's Law:

$$q = -kA\Delta T/t$$

where:

k = thermal conductivity (W/m-K)

A = surface area of the heat transfer

ΔT = Temperature gradient across the material (K)

t = material thickness

The convection which takes place between the cylinder wall and fluid as well as the air is governed by Newton's Law of Cooling, which is:

$$q = -hA\Delta T$$

where:

h = convective heat transfer coefficient (W/m^2-K)

A = surface area of the heat transfer

dT = Temperature difference between surface and fluid (K)

Chapter 5: Simulation Programs

5.1 CosmosWorks

Cosmos is part of the SolidWorks CAD/CAM software package. It uses finite element methods to perform stress analysis on CAD models. In this study, Cosmos was used for stress analysis of the dish structure; which was observed for simulation of different wind loading conditions. Cosmos allows the user to input all necessary parameters to ensure a realistic simulation process.

Once the CAD model is opened in Cosmos, the first step is to apply materials to the parts of the model. Materials can either be chosen from the Cosmos and SolidWorks libraries or can defined by material properties which the user inputs. Loads and restraints are then applied by the user; for this study, the attachment holes on the dish mounting collar were set as "fixed restraints" which allow no movement in any direction. Pressure loads were then applied to the face of the dish which are equivalent to certain wind loading conditions (these will be discussed in more detail in the following chapter).

Before the simulation process can be run, the mesh must be created for use in the finite element method. Results will only be as accurate as the mesh, for this reason, a fairly fine mesh used. Tetrahedral shaped elements were chosen, this is fairly common and accurate for many 3D models. A mixed mesh was chosen for this study; shell elements were used to model the thin petals, while a solid mesh was applied on the mounting collar and support trusses. All points where the solid and shell mesh pieces contact one another must be defined as "bonded" together, this allows smooth interaction

between the separate meshes. Once these parameters are defined, the mesh is then generated automatically by the program. The simulation can then be run, thus giving results. Figure 5.1 shows the dish with the mesh that Cosmos created. This mesh consists of 84,696 nodes and 41,779 elements.

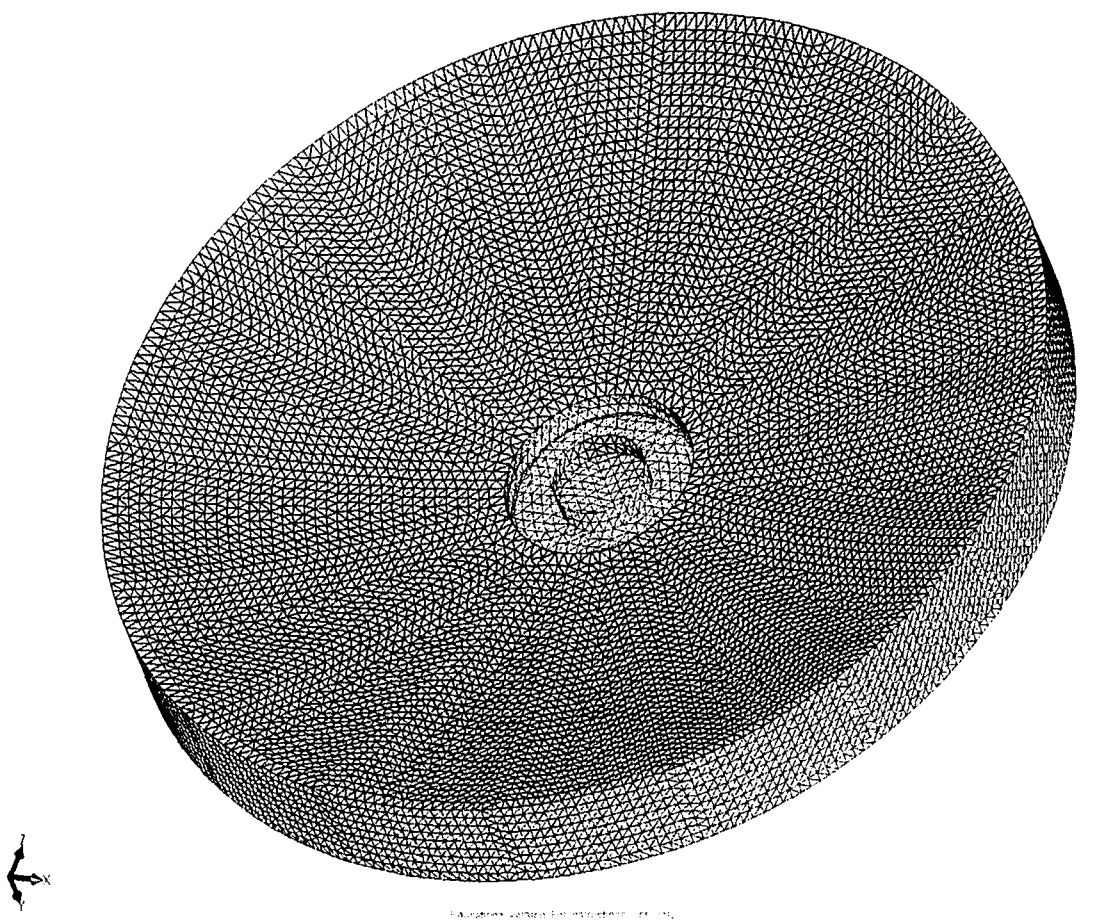

Figure 5.1: Cosmos mesh used for stress analysis

5.2 ZEMAX

ZEMAX is an optical design software package which was used for ray tracing simulation of the reflecting surface and optical system. ZEMAX-EE was used since we needed to model a physical system, it was run in non-sequential mode, which allows objects to be imported from other programs (i.e. CAD models of the dish). The ZEMAX program models optical systems by using ray tracing principles discussed in chapter 4. Each ray is emitted from a source which has a set power, the individual path of each ray is followed (as it reflects, transmits, or is absorbed by objects and lenses) until its path is intercepted by a collector or until the ray terminates. The user defines the number of rays which are traced; the power of each ray is a function of the power of the object and the number of rays emitted from that object. Data of interest for this study is total power, irradiance and where exactly each ray strikes the collector.

First, the SolidWorks model was saved in IGES format (a 3D vector graphics format supported by many different types of software). This model was then imported into ZEMAX as an object. To increase performance of the program, only the reflecting surface was imported, since this is the only part which will play a role in optical performance of the dish (the structure is hidden from any direct sunlight). Properties are then applied to the surface, for this study a reflectivity of 97% was defined. A source was then added which was designed to model the sun. A circular disk of the diameter of the dish (1au) was chosen, this will give parallel rays directed at the dish. The power of the source was chosen on the basis that most of the U.S. receives $1 kW/m^2$. The source was placed at an arbitrary point some distance away from the front of the dish. Since the

rays coming from the source we defined are parallel to one another, the distance is irrelevant and already models the sun being millions of miles from earth. Next, the detector must be added. A flat surface is chosen, it is placed at a distance of 0.53au from the center of the reflecting surface (between the source and dish). This represents the position of the receiver with respect to the dish assembly. When the simulation is run, data collected at the detector will be used for modeling of the receiver. Figure 5.2 shows the ZEMAX setup. This picture gives the general idea, but only shows a limited number of rays for viewing ease. During analysis, one million rays were used to ensure a high degree of accuracy

Figure 5.2: ZEMAX ray trace

rays coming from the source we defined are parallel to one another, the distance is irrelevant and already models the sun being millions of miles from earth. Next, the detector must be added. A flat surface is chosen, it is placed at a distance of 0.53au from the center of the reflecting surface (between the source and dish). This represents the position of the receiver with respect to the dish assembly. When the simulation is run, data collected at the detector will be used for modeling of the receiver. Figure 5.2 shows the ZEMAX setup. This picture gives the general idea, but only shows a limited number of rays for viewing ease. During analysis, one million rays were used to ensure a high degree of accuracy

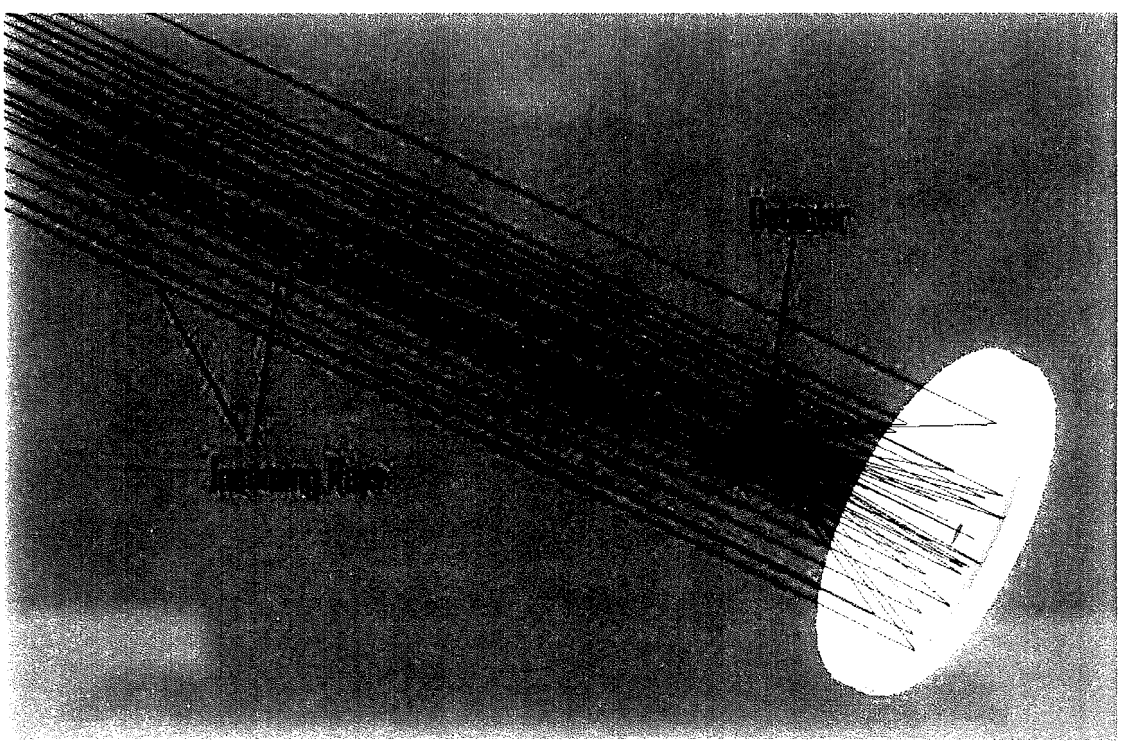

Figure 5.2: ZEMAX ray trace

5.3 Fluent 6.3

Fluent is a powerful CFD software package which was used to perform the heat transfer and fluid flow analysis of the receiver. An exact replica of the CAD model of the receiver shown in chapter 3 was constructed using Gambit (a CAD package which is part of fluent). A mesh must also be created for use in fluent similar to that created for the stress analysis using Cosmos. Gambit allows the user to create a mesh of any shape and size, instead of doing it automatically using finite element techniques as in Cosmos. Once the mesh was created, it is exported from Gambit for use in Fluent.

The mesh is imported to Fluent, and all relevant conditions are applied. Materials must be defined and each surface in the mesh is defined as a different type of boundary condition. The properties of VP-1 are input and a new material is created to be used on the interior of the mesh (the fluid flow region). The interior and exterior walls of the cylinder are set as stationary walls, material properties are also applied to these surfaces. A profile is created for the heat flux along the inner wall; this profile comes from the distribution of power received at the detector from ZEMAX. The outer wall is set to a constant radiation temperature of 400°C, to model the radiant heat inside the receiver. The bottom of the cylinder is defined as a mass flow inlet, which models where the VP-1 will enter the receiver. The mass flow rate is defined here as being 1.42kg/s. The top of the cylinder is defined as a mass flow outlet, no other parameters are applied. This is the region which where data will be collected on the fluid leaving the receiver. Figure 5.3 shows the meshed model of the receiver cylinder.

The VP-1 fluid mass flux is arranged to enter the cavity receiver at the inlet as axial motion with swirl in the form of tangential flow. This will be set such that the total flow out of the receiver is equal to the desired mass flow rate, discussed by Wright [16]. The enthalpy gain of the fluid is the desired output of this calculation.

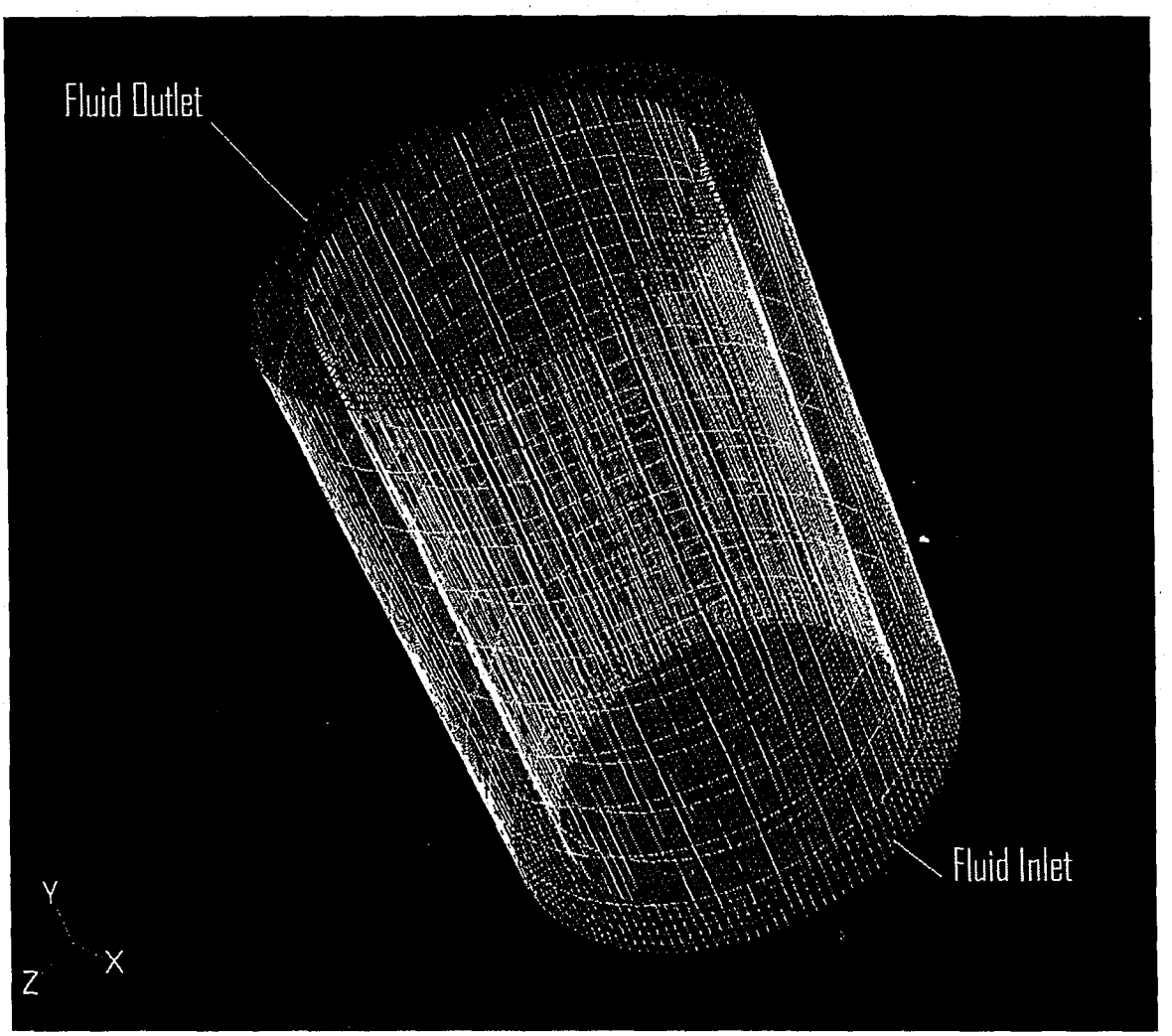

Figure 5.3: Fluent receiver model (tangential and axial motion through inlet)

Chapter 6: Results

6.1 Structural Analysis of the Alpha-dish

The stress analysis of the Alpha-dish was run under two different wind loading conditions. The first was for a head on wind at 30mph, and the second for a head on wind of 105mph. The 30mph case is for the operating conditions for the dish. The 105mph case is a typical design wind speed, this is a speed that is expected to occur only once every hundred years and is for non-operating conditions. In the field, in storms or high wind cases such as 105mph, the dish would be lowered to stowed position to avoid damage so it would be doubtful that the dish would ever face this high wind in the head on case. Despite this, the 105mph test is run as a worst case scenario and will help identify any areas of the dish which should be looked at more closely from a structural standpoint.

The applied load for both of these cases was calculated using the equation:

$$Load = P_{stag} \times A \times C_d$$

The stagnation pressure was found using the equation:

$$P_{stag} = \frac{1}{2} D \times V^2$$

Where:

P_{stag} = stagnation pressure

A = cross sectional area (1 m^2)

C_d = coefficient of drag (1.2 for dish was used here [18])

D = Density (1.2 kg/m^2 for air)

V = Velocity (m/s)

For the 30mph case, the applied load is 129.3N/m^2. The applied load for the 105mph case is 1590N/m^2.

30mph case

Table 6.1 outlines the key results from the 30mph test case. Figures 6.1 and 6.2 show displacement contour plots of the dish from front and rear views respectively. Likewise, Von Mises Stresses are shown in Figures 6.3 and 6.4. Figures 6.5 and 6.6 show the equivalent strain in the dish structure.

Table 6.1: 30mph wind load results

Maximum Deflection	8.64E-05 au
Maximum Von Mises Stress	1.49E06 Pa
Maximum Strain	1.60E-05

A = cross sectional area (1 m^2)

C_d = coefficient of drag (1.2 for dish was used here [18])

D = Density (1.2 kg/m^2 for air)

V = Velocity (m/s)

For the 30mph case, the applied load is 129.3N/m^2. The applied load for the 105mph case is 1590N/m^2.

30mph case

Table 6.1 outlines the key results from the 30mph test case. Figures 6.1 and 6.2 show displacement contour plots of the dish from front and rear views respectively. Likewise, Von Mises Stresses are shown in Figures 6.3 and 6.4. Figures 6.5 and 6.6 show the equivalent strain in the dish structure.

Table 6.1: 30mph wind load results

Maximum Deflection	8.64E-05 au
Maximum Von Mises Stress	1.49E06 Pa
Maximum Strain	1.60E-05

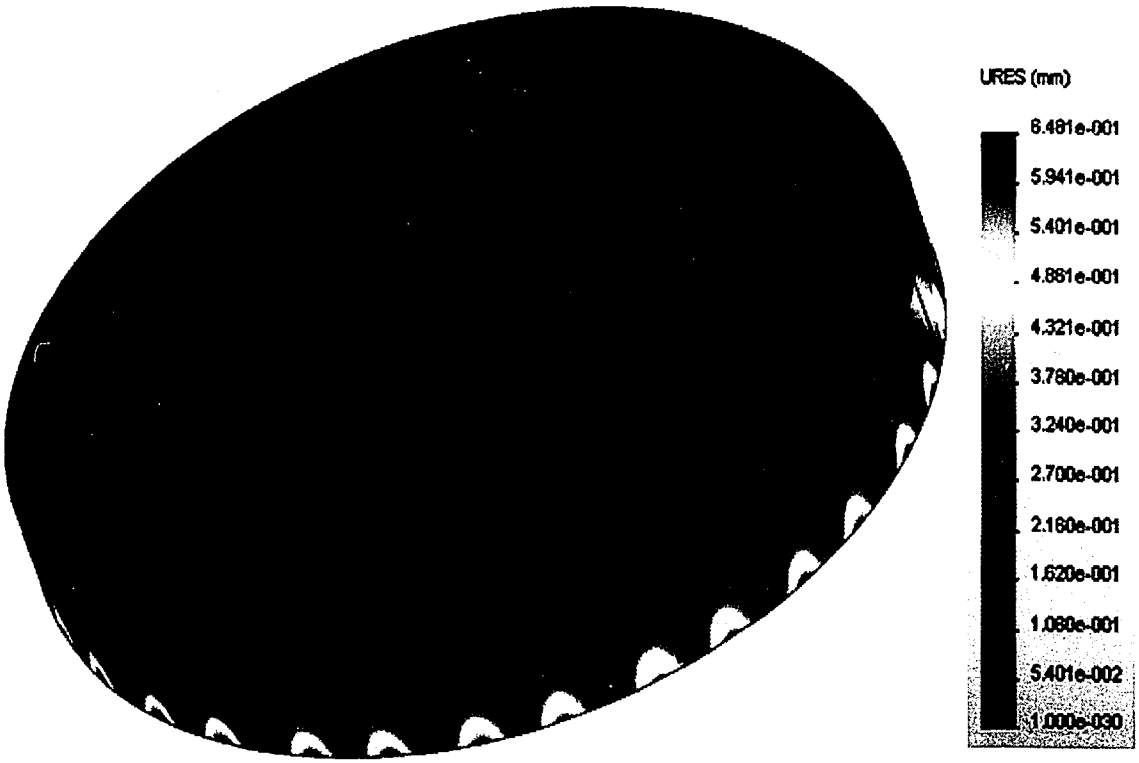

Figure 6.1: 30mph displacement (front view)

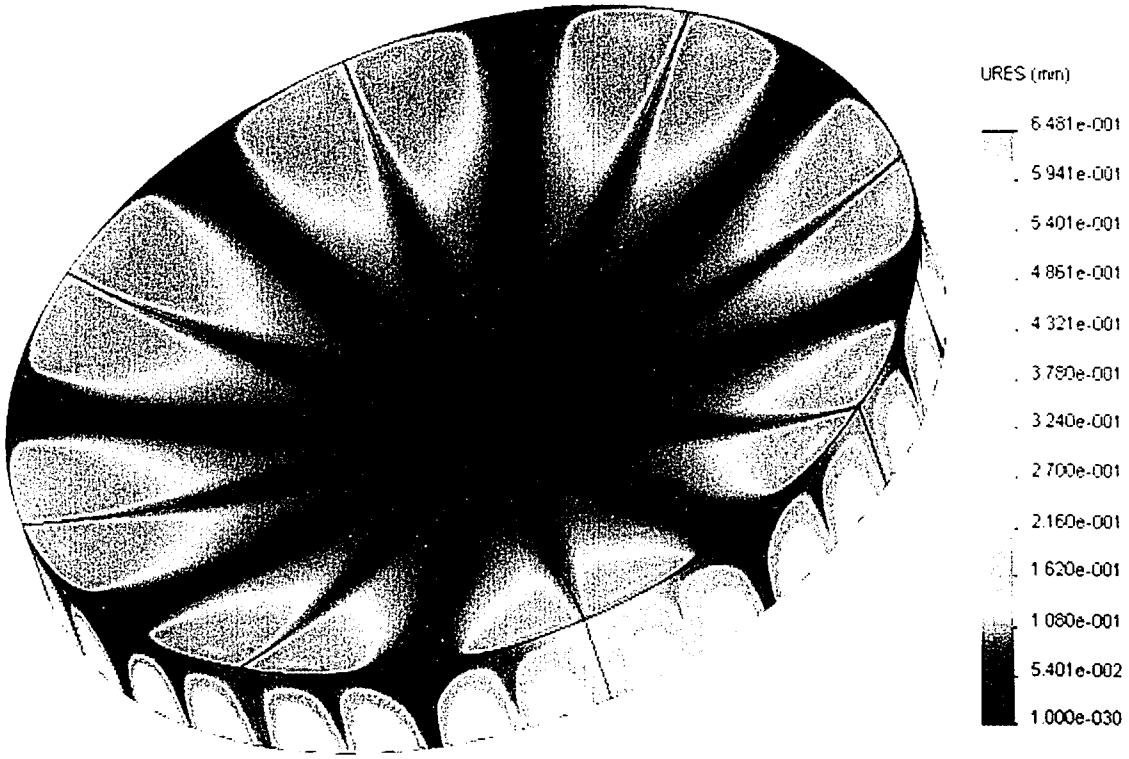

Figure 6.1: 30mph displacement (front view)

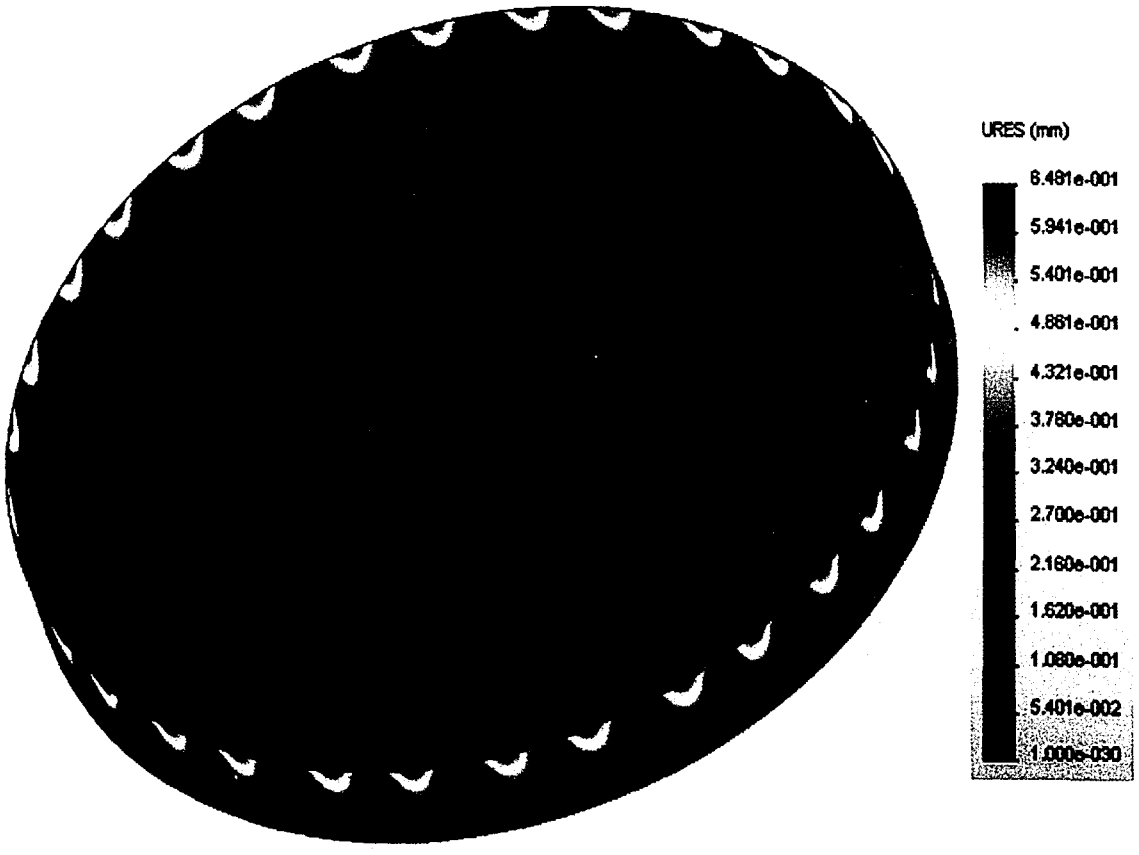

Figure 6.2: 30mph displacement (rear view)

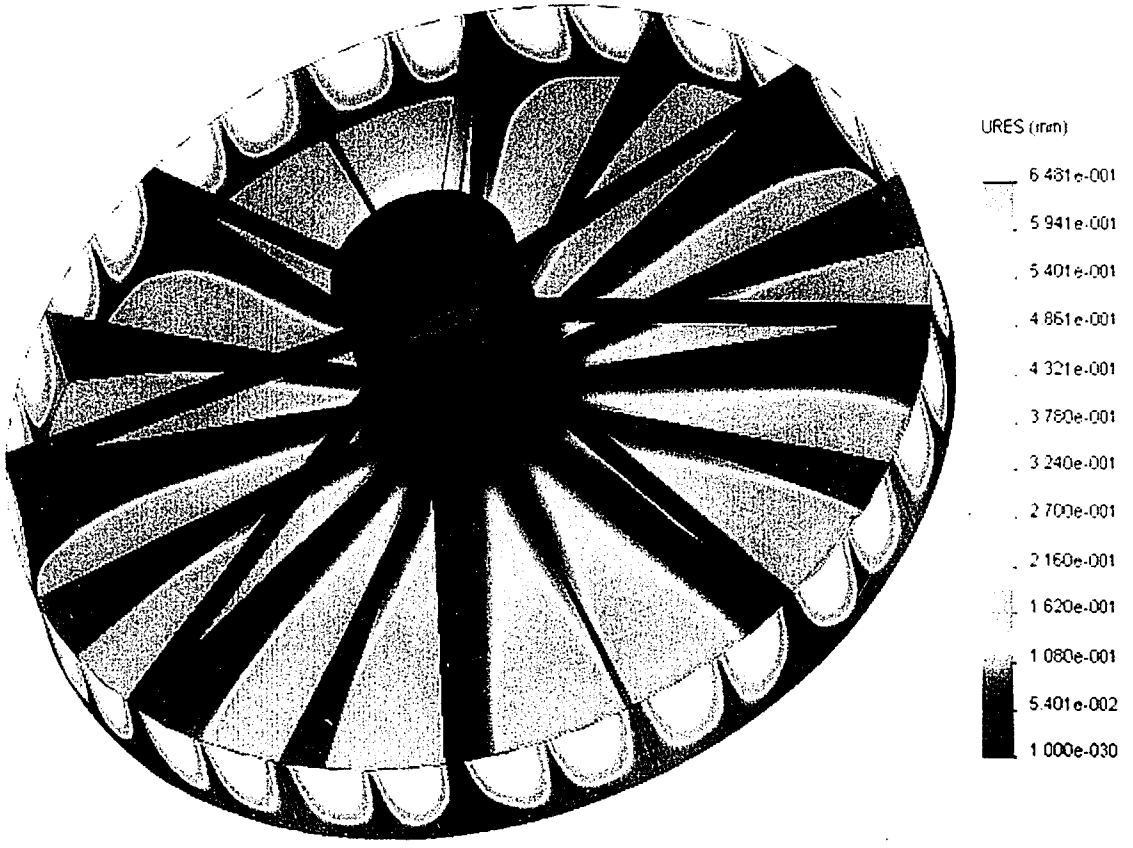

Figure 6.2: 30mph displacement (rear view)

Figure 6.3: 30mph Von Mises stress (front view)

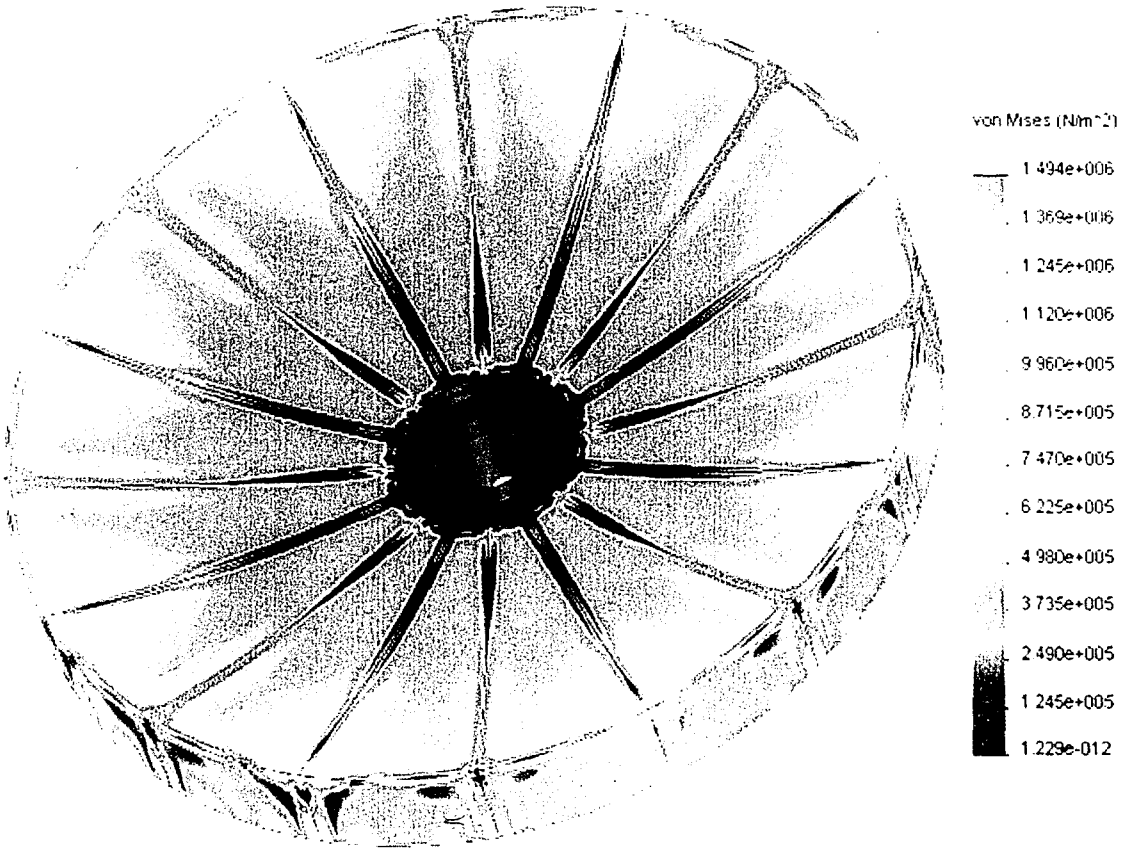

Figure 6.3: 30mph Von Mises stress (front view)

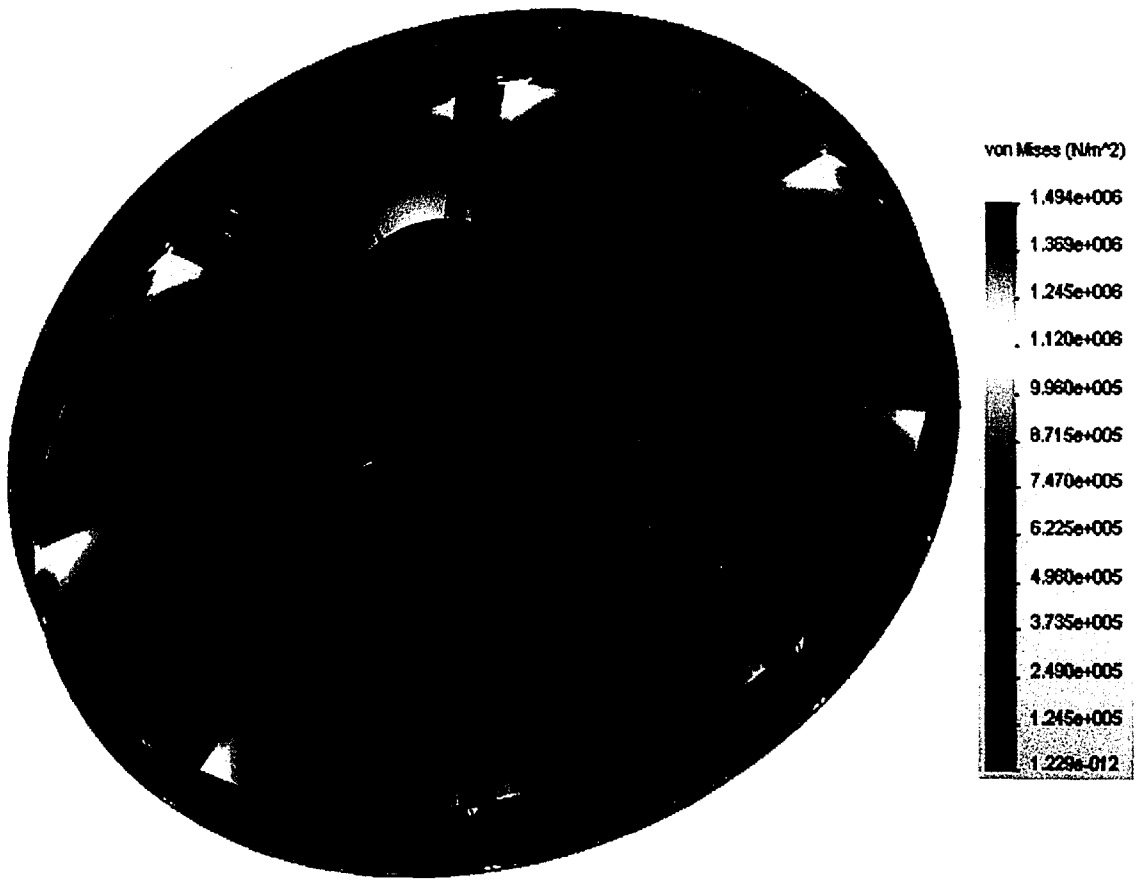

Figure 6.4: 30mph Von Mises stress (rear view)

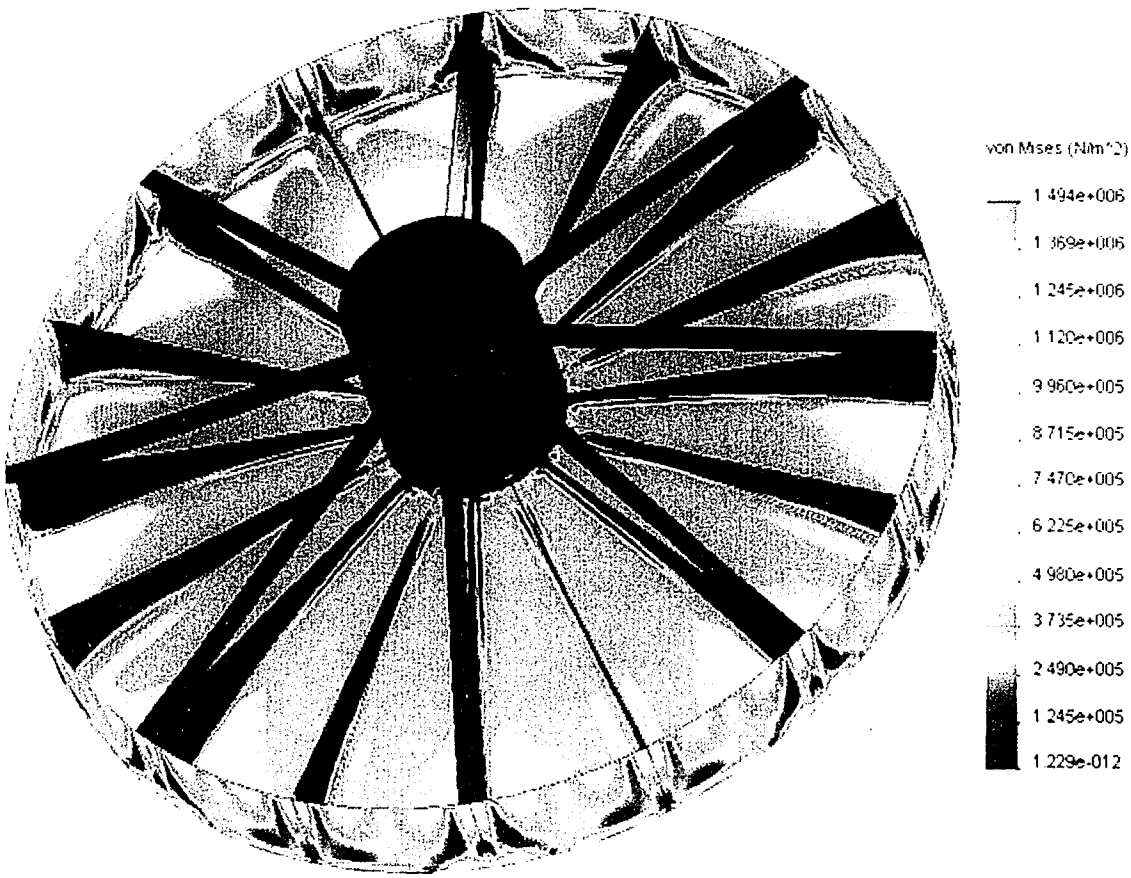

Figure 6.4: 30mph Von Mises stress (rear view)

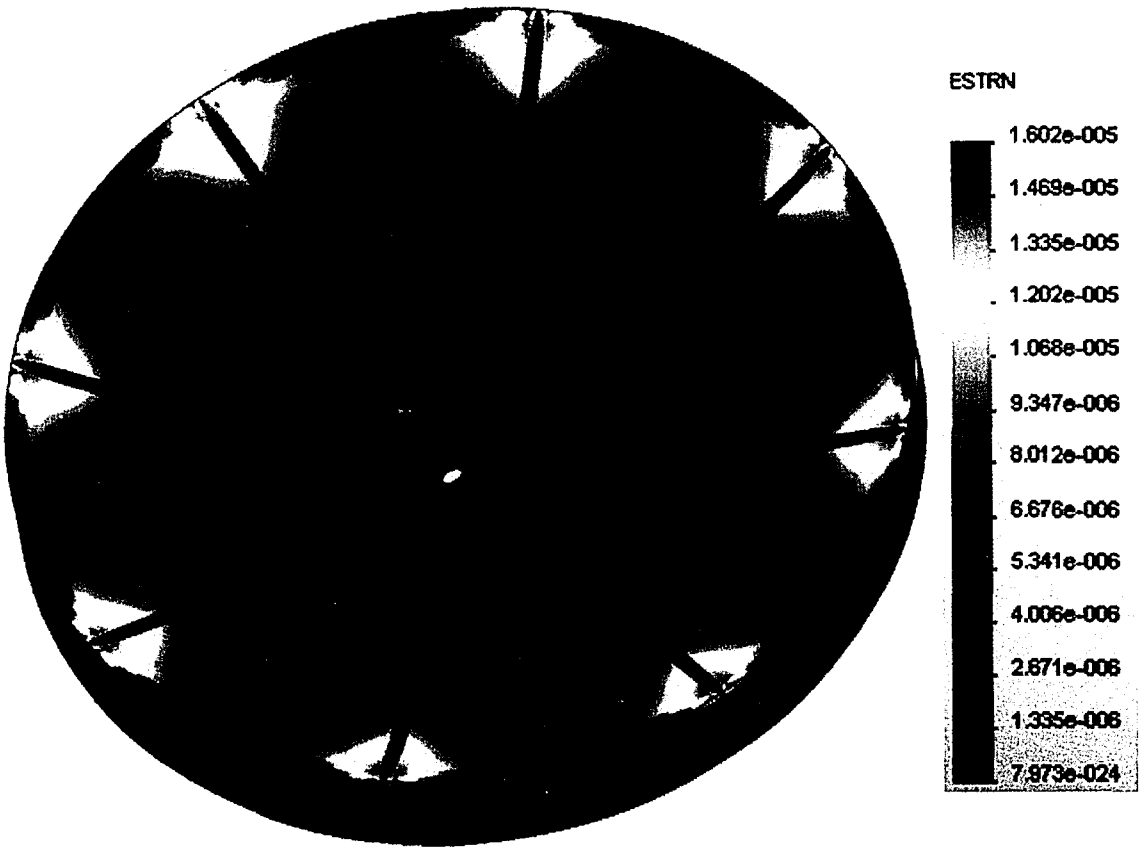

Figure 6.5: 30mph equivalent strain (front view)

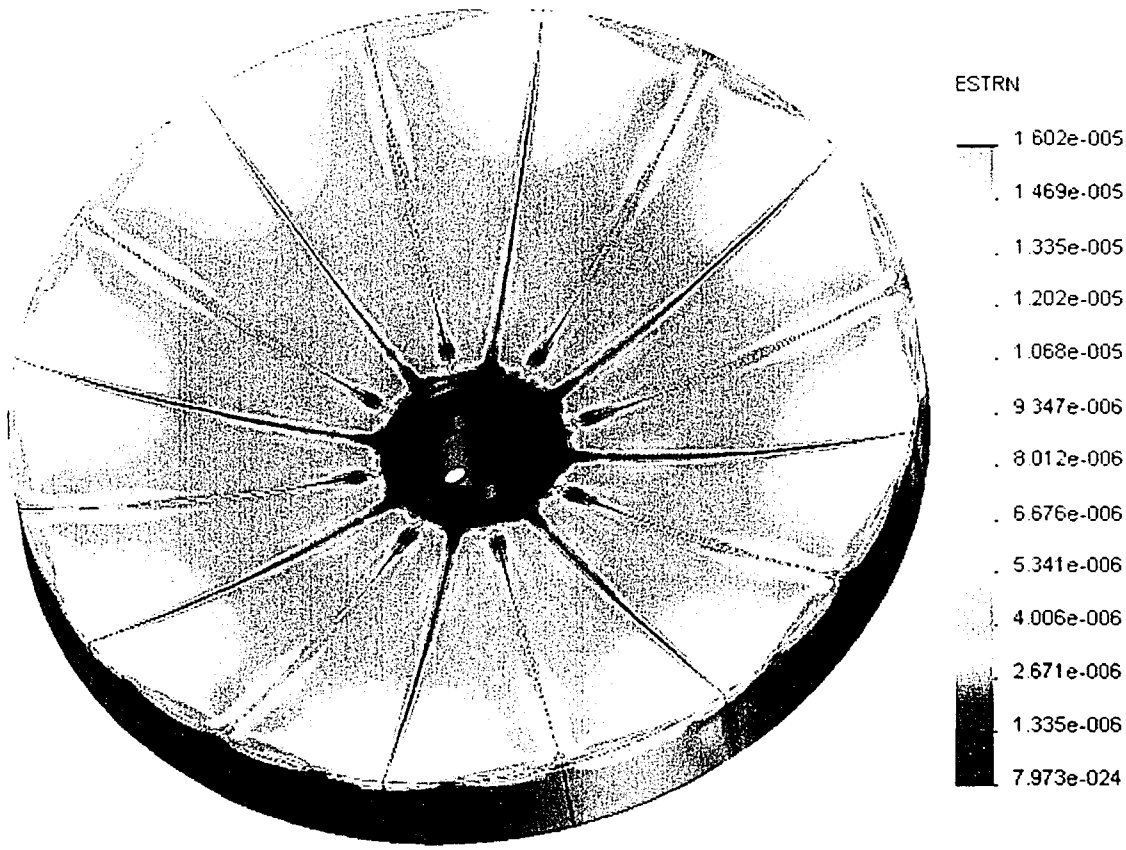

Figure 6.5: 30mph equivalent strain (front view)

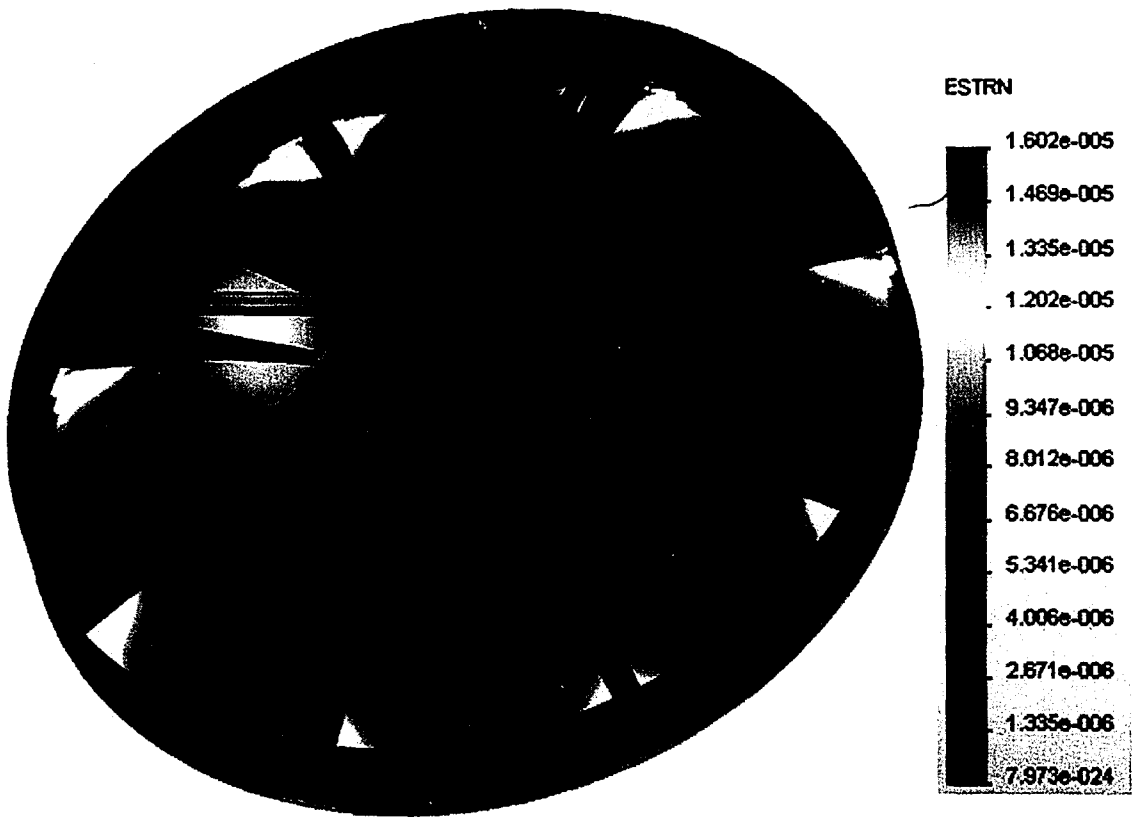

Figure 6.6: 30mph equivalent strain (rear view)

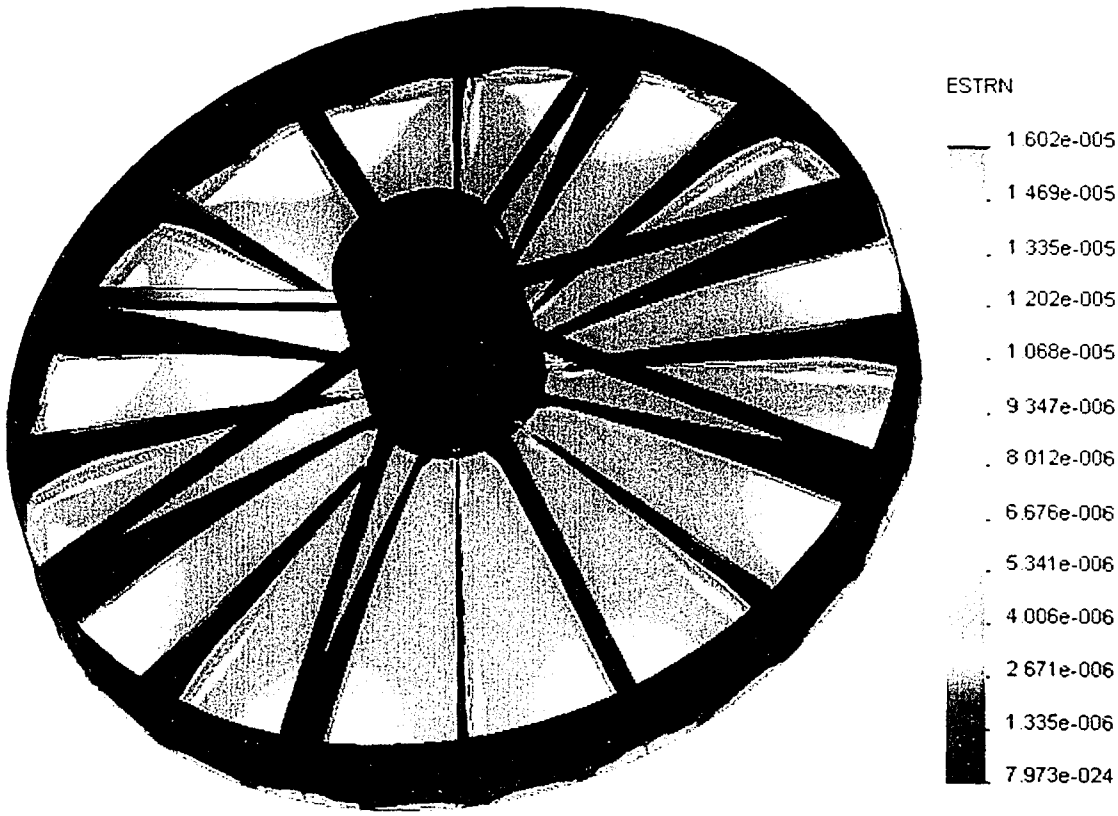

Figure 6.6: 30mph equivalent strain (rear view)

105mph case

Table 6.2 outlines the key results from the 105mph test case. Figure 6.7 and figure 6.8 show displacement contour plots of the dish from front and rear views respectively. Likewise, Von Mises Stresses are shown in Figures 6.9 and 6.10. Figures 6.11 and 6.12 show the equivalent strain in the dish structure.

Table 6.2: 105mph wind load results

Maximum Deflection	1.06E-03au
Maximum Von Mises Stress	1.84E07 Pa
Maximum Strain	1.97E-04

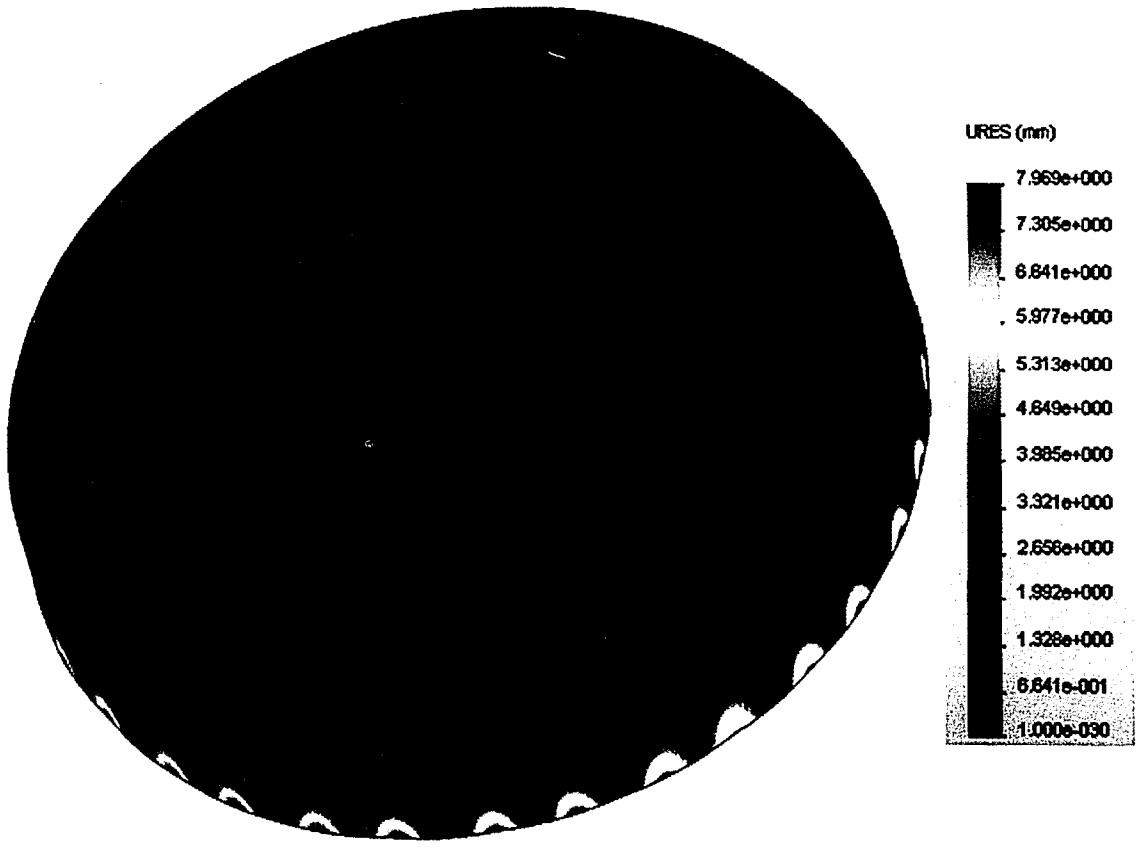

Figure 6.7: 105mph displacement (front view)

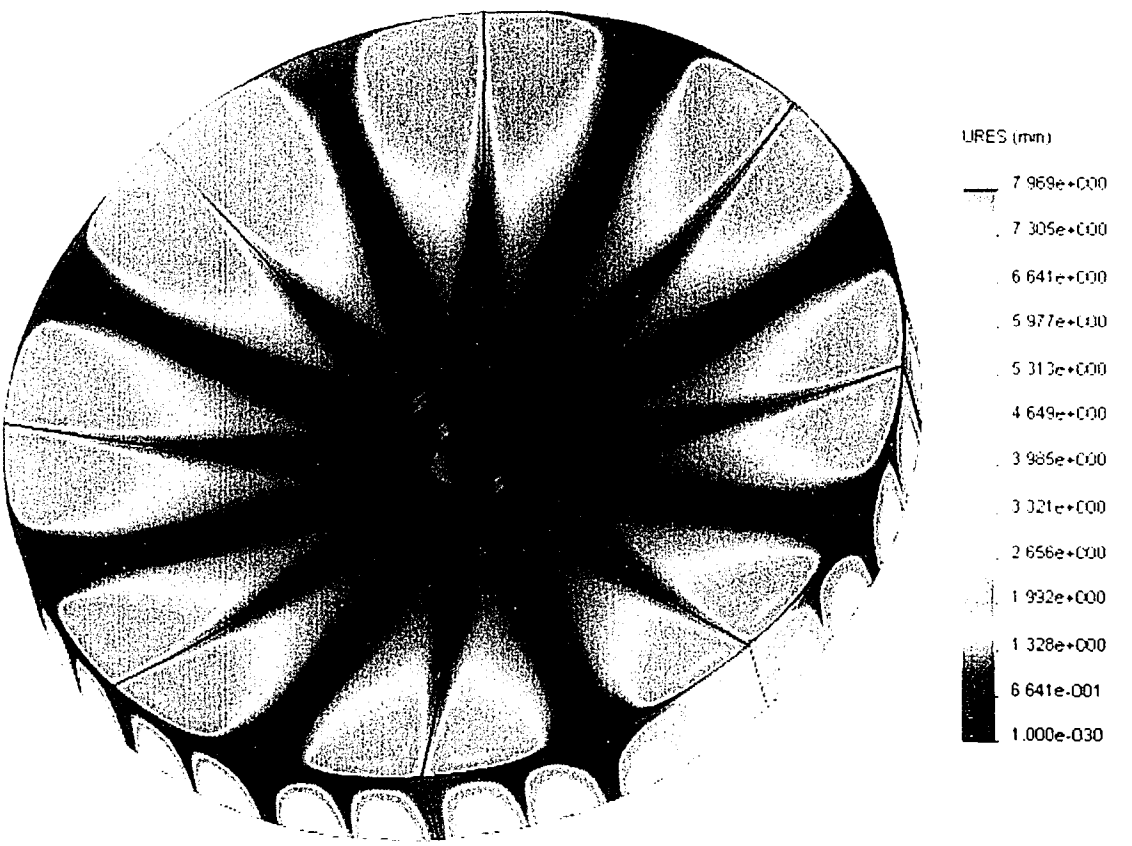

Figure 6.7: 105mph displacement (front view)

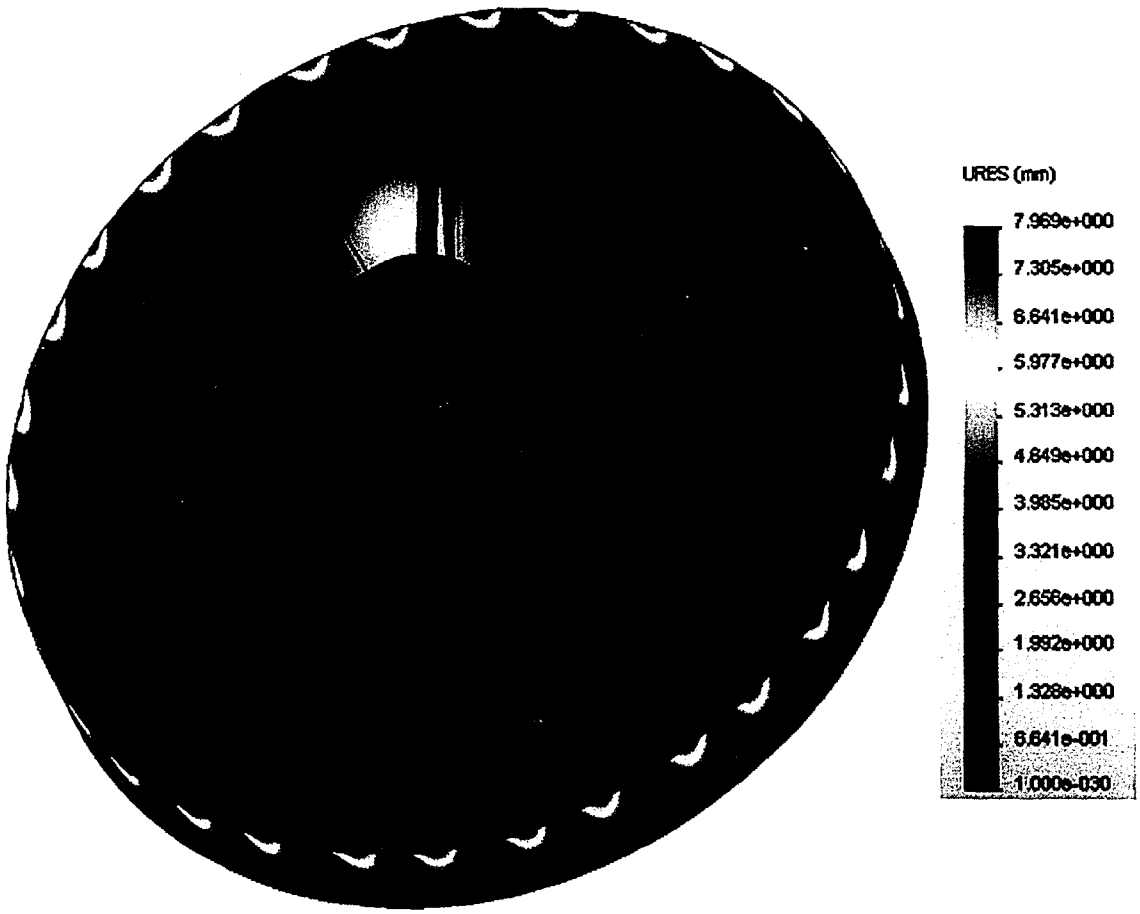

Figure 6.8: 105mph displacement (rear view)

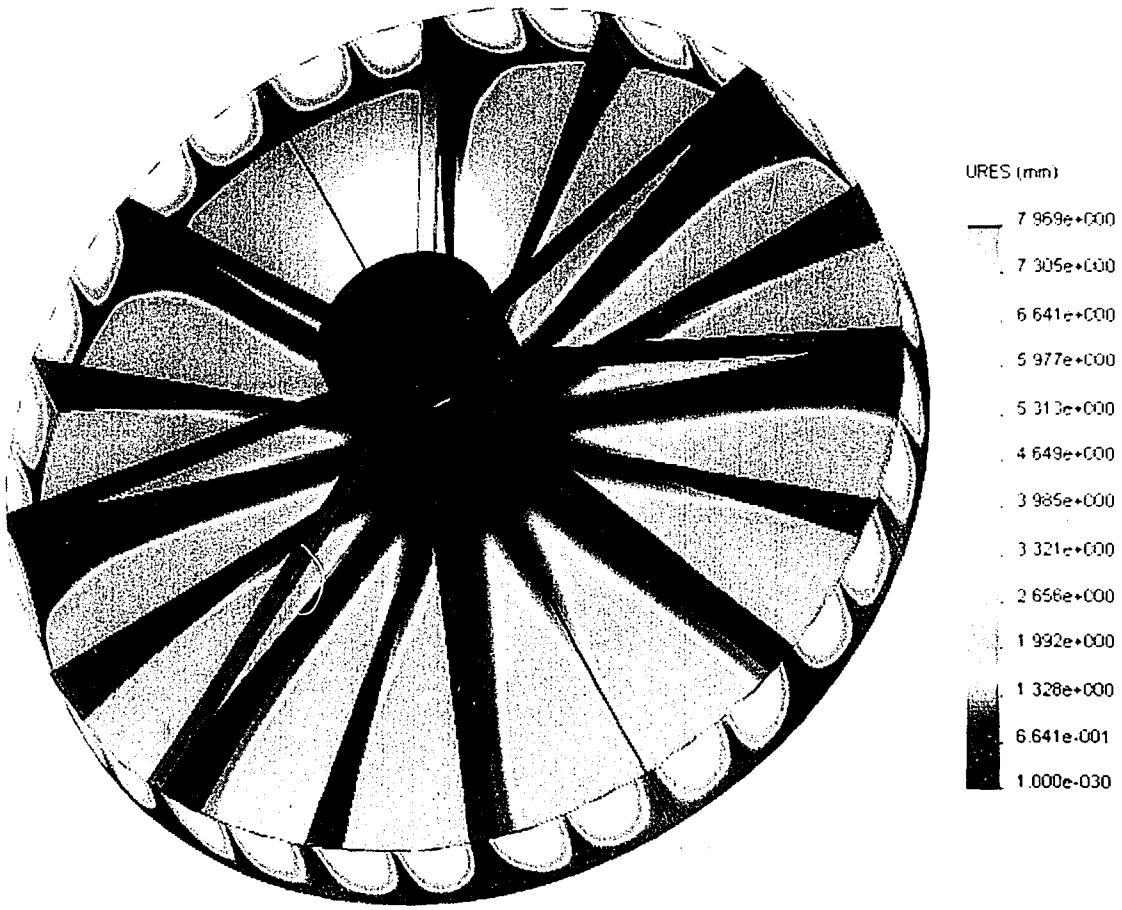

Figure 6.8: 105mph displacement (rear view)

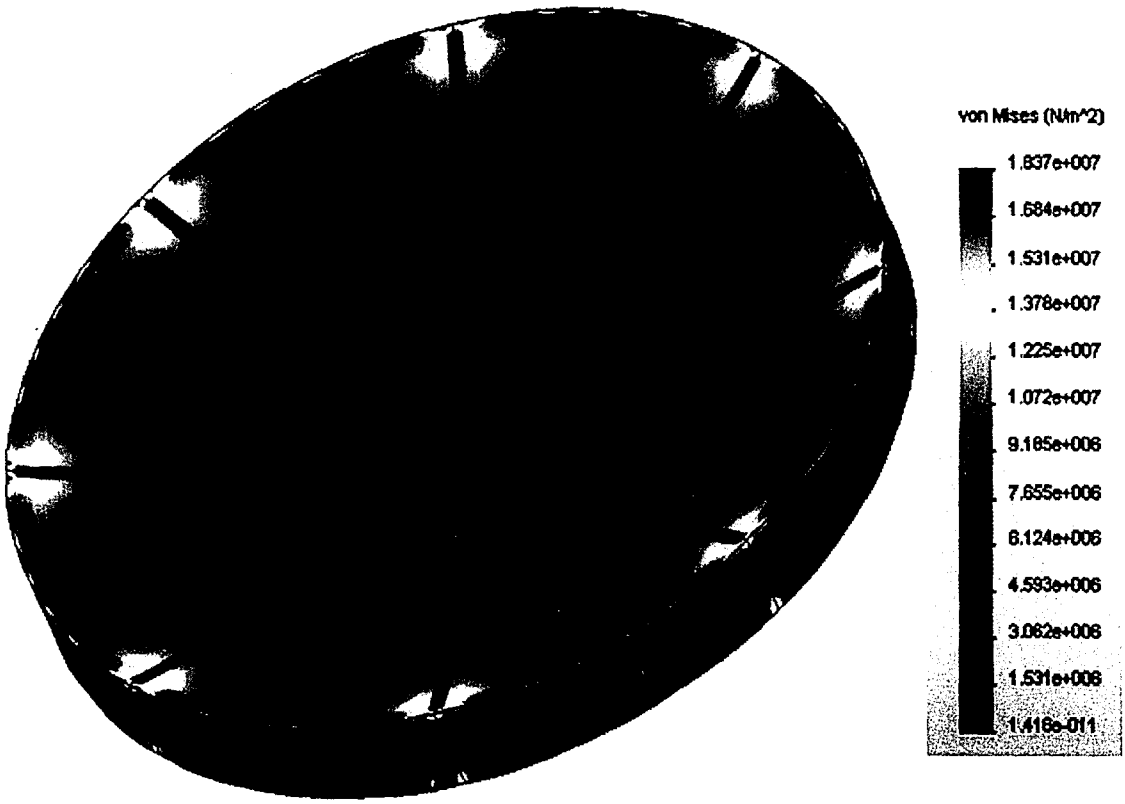

Figure 6.9: 105mph Von Mises stress (front view)

Figure 6.9: 105mph Von Mises stress (front view)

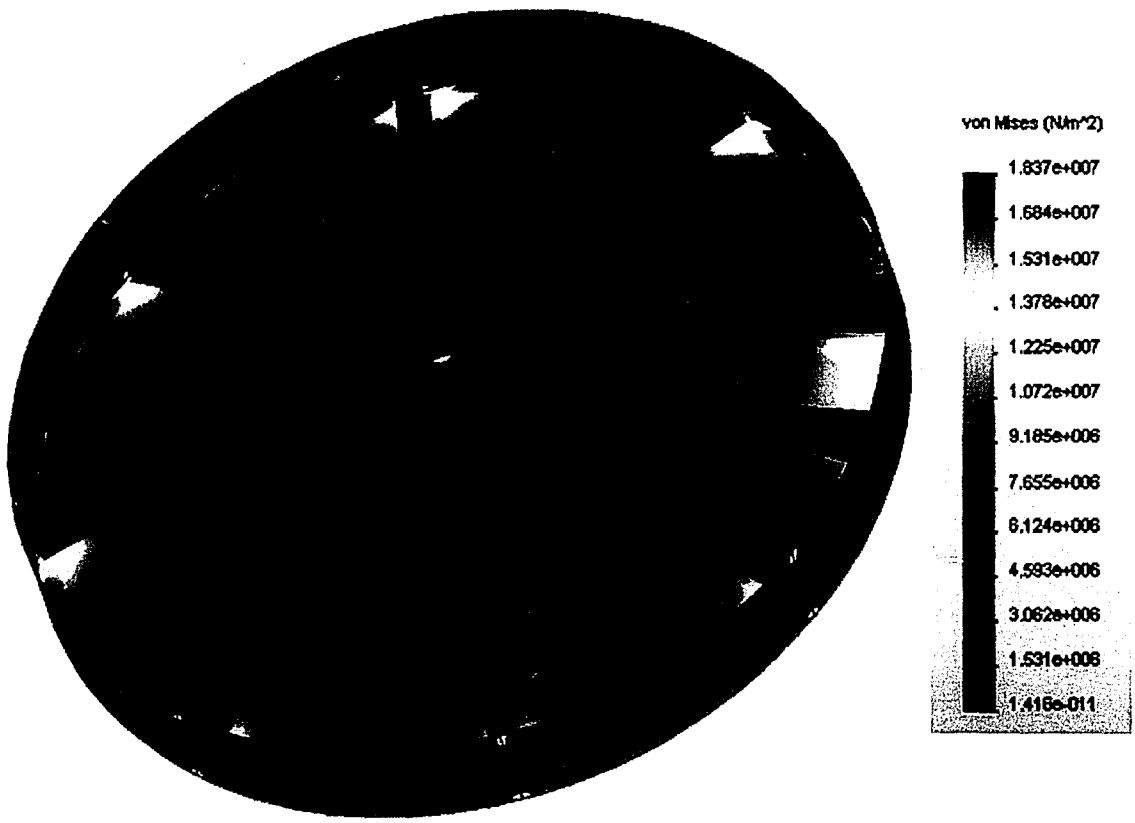

Figure 6.10: 105mph Von Mises stress (rear view)

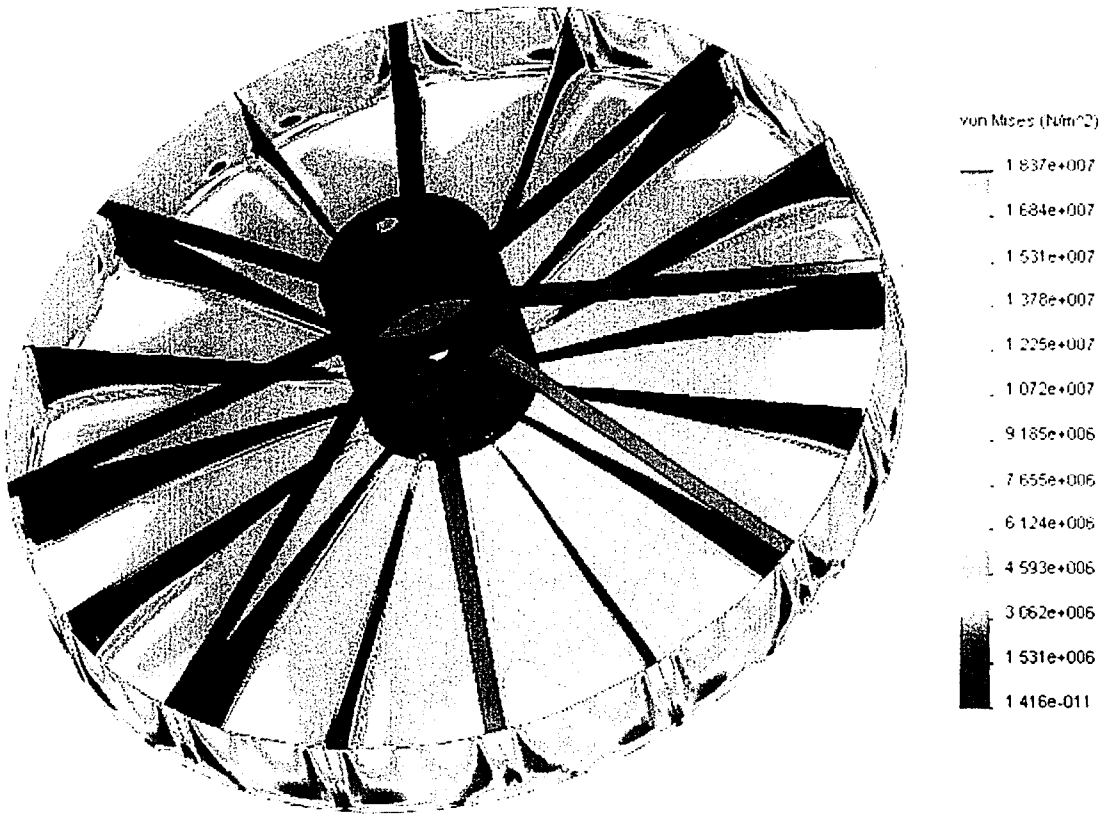

Figure 6.10: 105mph Von Mises stress (rear view)

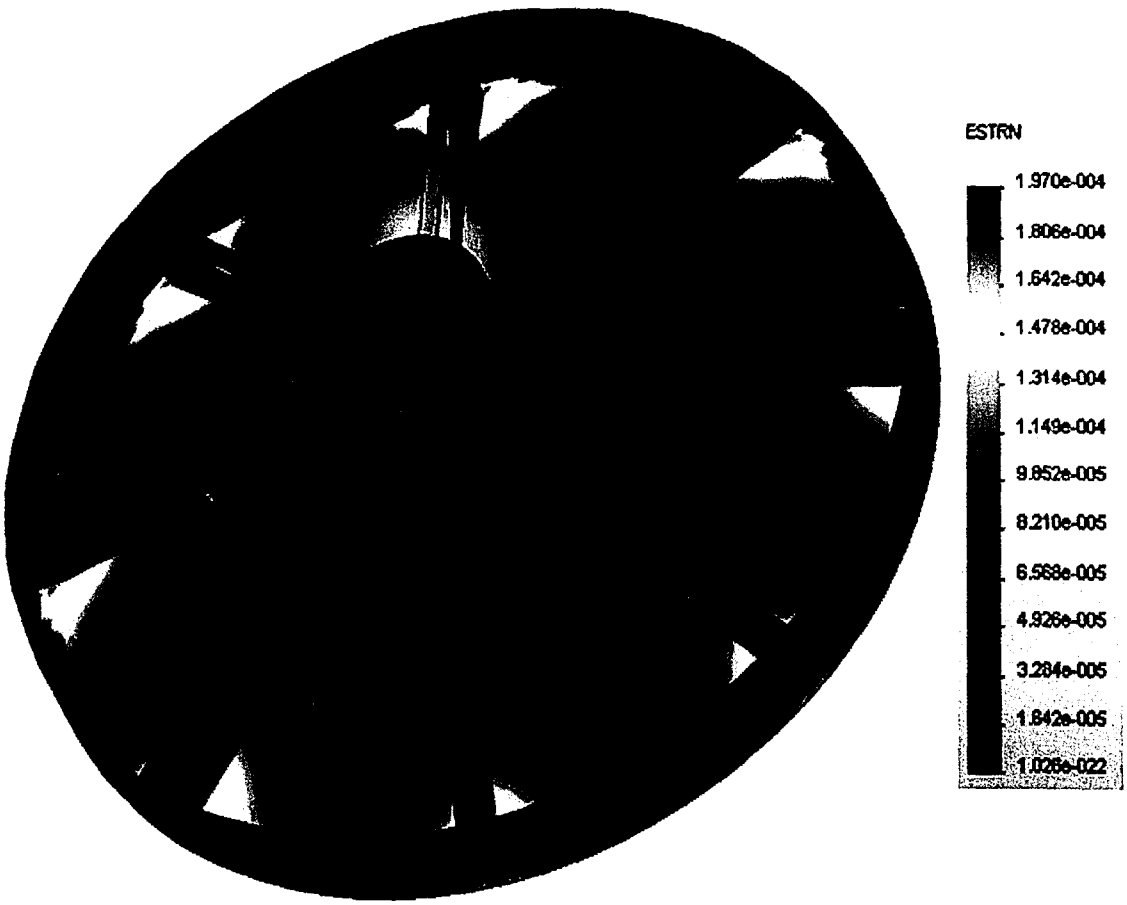

Figure 6.11: 105mph equivalent strain (front view)

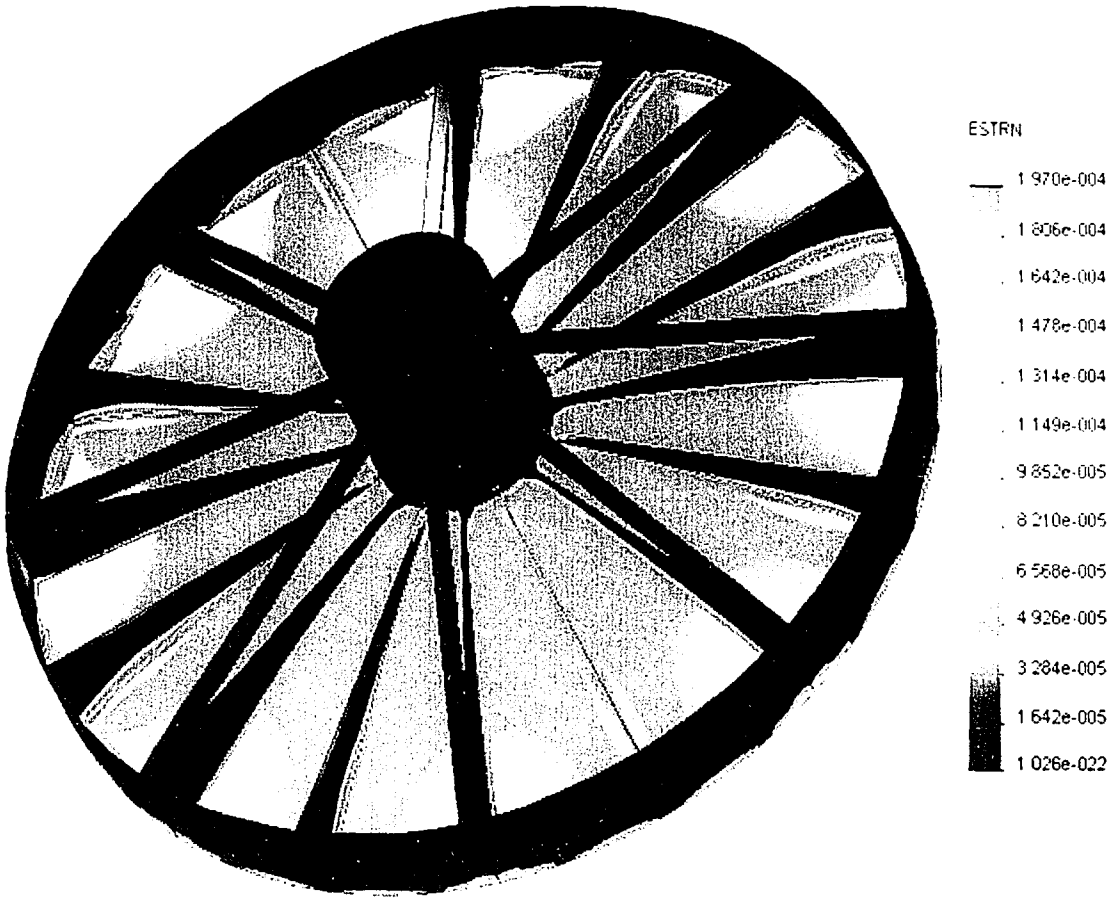

Figure 6.11: 105mph equivalent strain (front view)

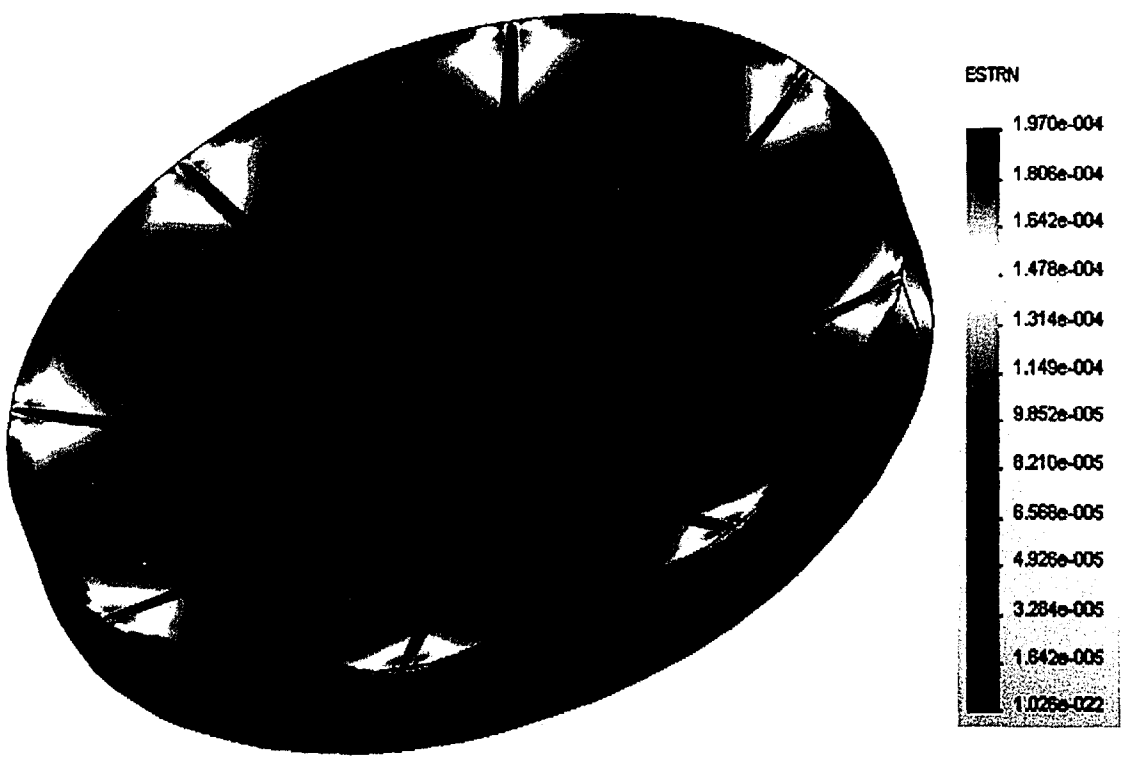

Figure 6.12: 105mph equivalent strain (rear view)

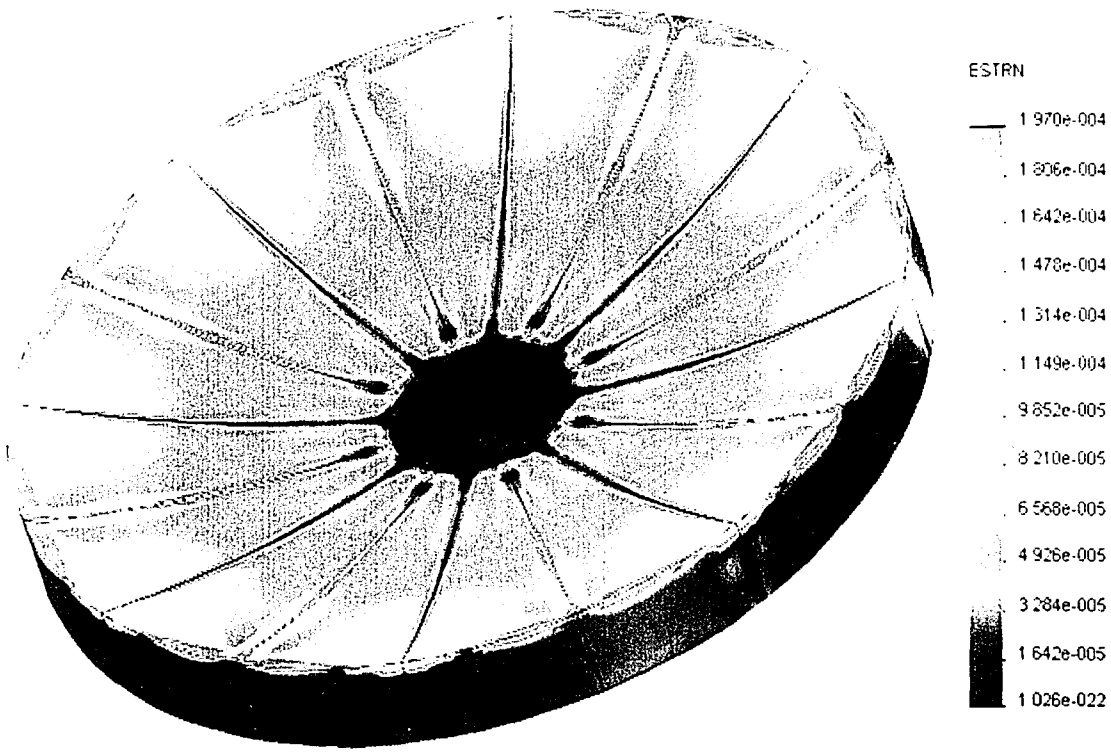

Figure 6.12: 105mph equivalent strain (rear view)

6.2 Optical Analysis

The ZEMAX program was used to model solar energy transmission and data was collected at the collector. Irradiance was specified, which provides the distribution of heat flux along the inner wall of the receiver. The maximum irradiance is focused into a ring on the concentrator at a value of 13.8 W/cm^2. The rest of the distribution is at a value of about 6.9 W/cm^2. The total power collected was 41.1kW. Figures 6.13 and 6.14 show the irradiance distribution at the detector at various zoom levels.

Figure 6.13: Irradiance

6.2 Optical Analysis

The ZEMAX program was used to model solar energy transmission and data was collected at the collector. Irradiance was specified, which provides the distribution of heat flux along the inner wall of the receiver. The maximum irradiance is focused into a ring on the concentrator at a value of 13.8 W/cm^2. The rest of the distribution is at a value of about 6.9 W/cm^2. The total power collected was 41.1kW. Figures 6.13 and 6.14 show the irradiance distribution at the detector at various zoom levels.

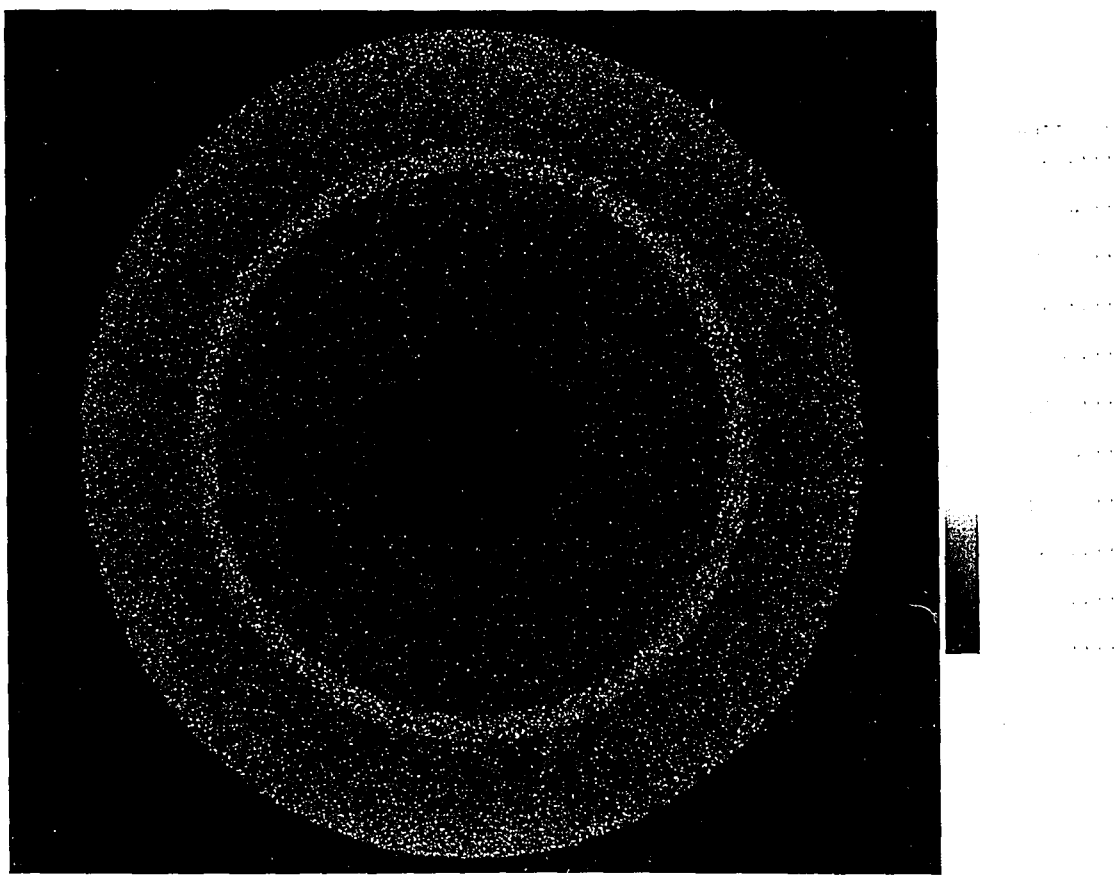

Figure 6.13: Irradiance

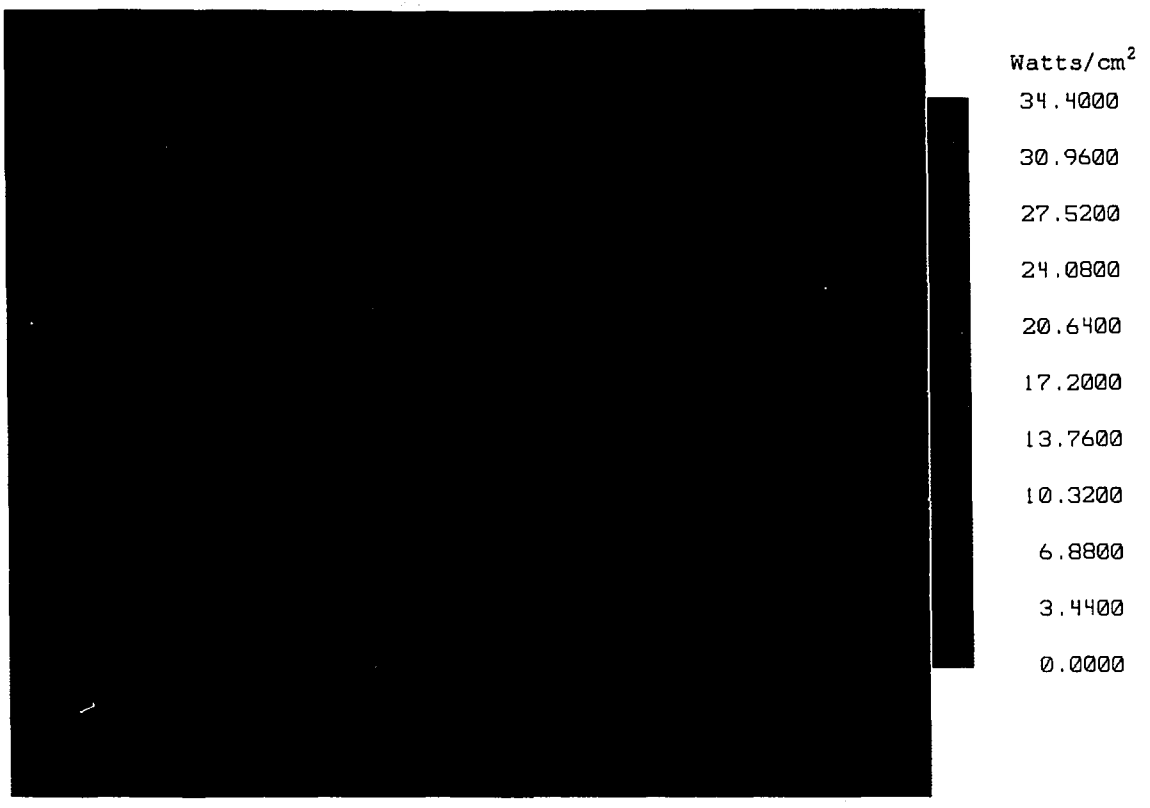

Figure 6.14: Irradiance (close-up)

6.3 Heat Transfer Analysis

The heat transfer analysis was modeled after the receiver studied at the Jet propulsion Laboratory which is described in detail by Wright [16]. The modeling is to find the maximum fluid outlet temperature which the receiver will produce. CFD heat transfer analysis was first run for a 0.6au long cylinder, which is the receiver cylinder previously described. The fluid entering the cylinder will have a strong tangential flow component (as well as an axial component) to more closely represent the motion through a coil. This design does not completely represent the coil cylinder used in the jet propusion paper due to the fact that the tangential velocity of the fluid will dissapate as it

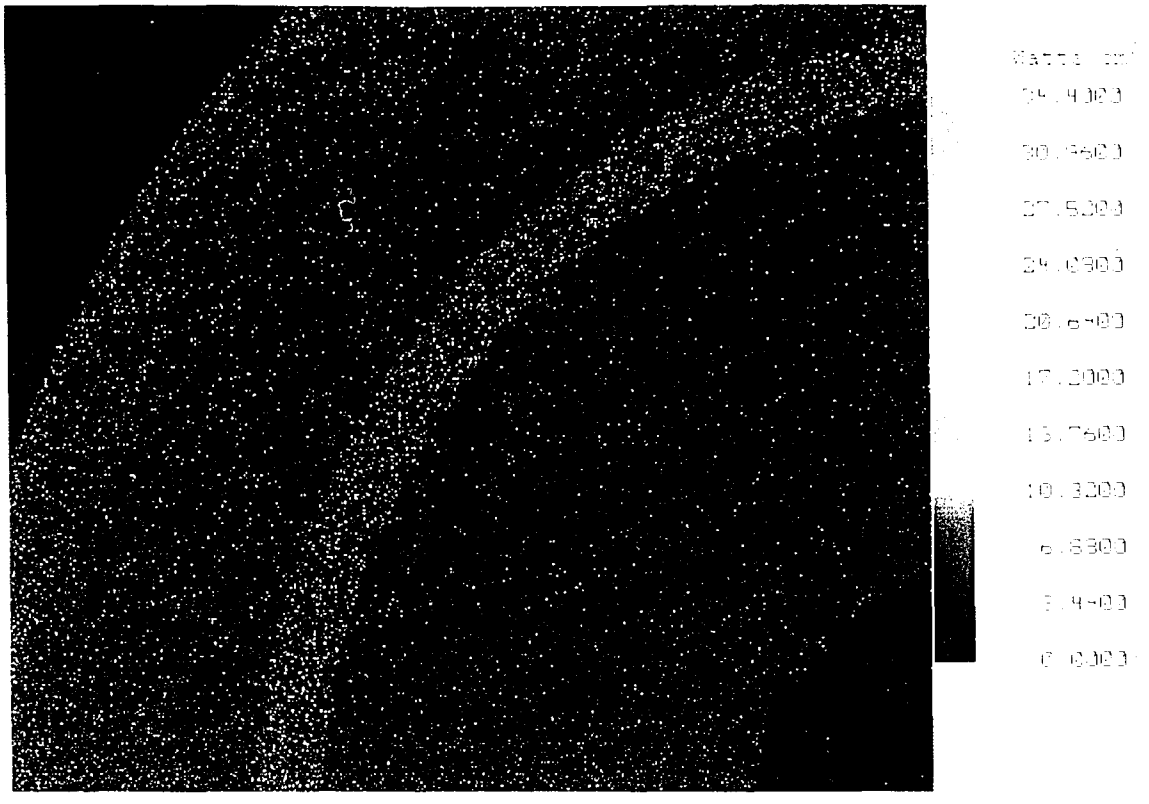

Figure 6.14: Irradiance (close-up)

6.3 Heat Transfer Analysis

The heat transfer analysis was modeled after the receiver studied at the Jet propulsion Laboratory which is described in detail by Wright [16]. The modeling is to find the maximum fluid outlet temperature which the receiver will produce. CFD heat transfer analysis was first run for a 0.6au long cylinder, which is the receiver cylinder previously described. The fluid entering the cylinder will have a strong tangential flow component (as well as an axial component) to more closely represent the motion through a coil. This design does not completely represent the coil cylinder used in the jet propusion paper due to the fact that the tangential velocity of the fluid will dissapate as it

travels further from the fluid inlet. To balance this effect, analysis was also run on cylinders which were extended in length by twenty, forty, and sixty percent (0.96au, 0.112au, and 0.128au respectively). This gives a more accurate representation of the final temperature, extending the cylinder length increases the amount of time the fluid contacts the cylinder, just as the swirling motion of the flow does. Table 6.3 shows the results for all four cases. A Reynolds number of 1830 was used for each of these cases; this was dictated by the mass flow rate of 1.42kg/s, which was chosen from research conducted by Wright [16] on a similar solar cavity receiver. Refer to figures 6.16-6.18 for contour plots of the temperature distribution for cylinders of length 0.8au, 0.96au, 0.112au, and 0.128au respectively Each case was for an inlet temperature of 100°C. It is clear to see that to get to the high temperature region of nearly 400°C which is desired, there needs to be a large amount of tangential flow throughout the cylinder, or a significant number of coils as in the Jet Propulsion receiver.

Table 6.3: Receiver outlet temperature results

cylinder length	Outlet temperature	Enthalpy gain
0.8 au cylinder	317°C	503.2kJ/kg
20% length increase	327°C	526.4kJ/kg
40% length increase	343°C	563.5kJ/kg
60% length increase	354°C	589kJ/kg

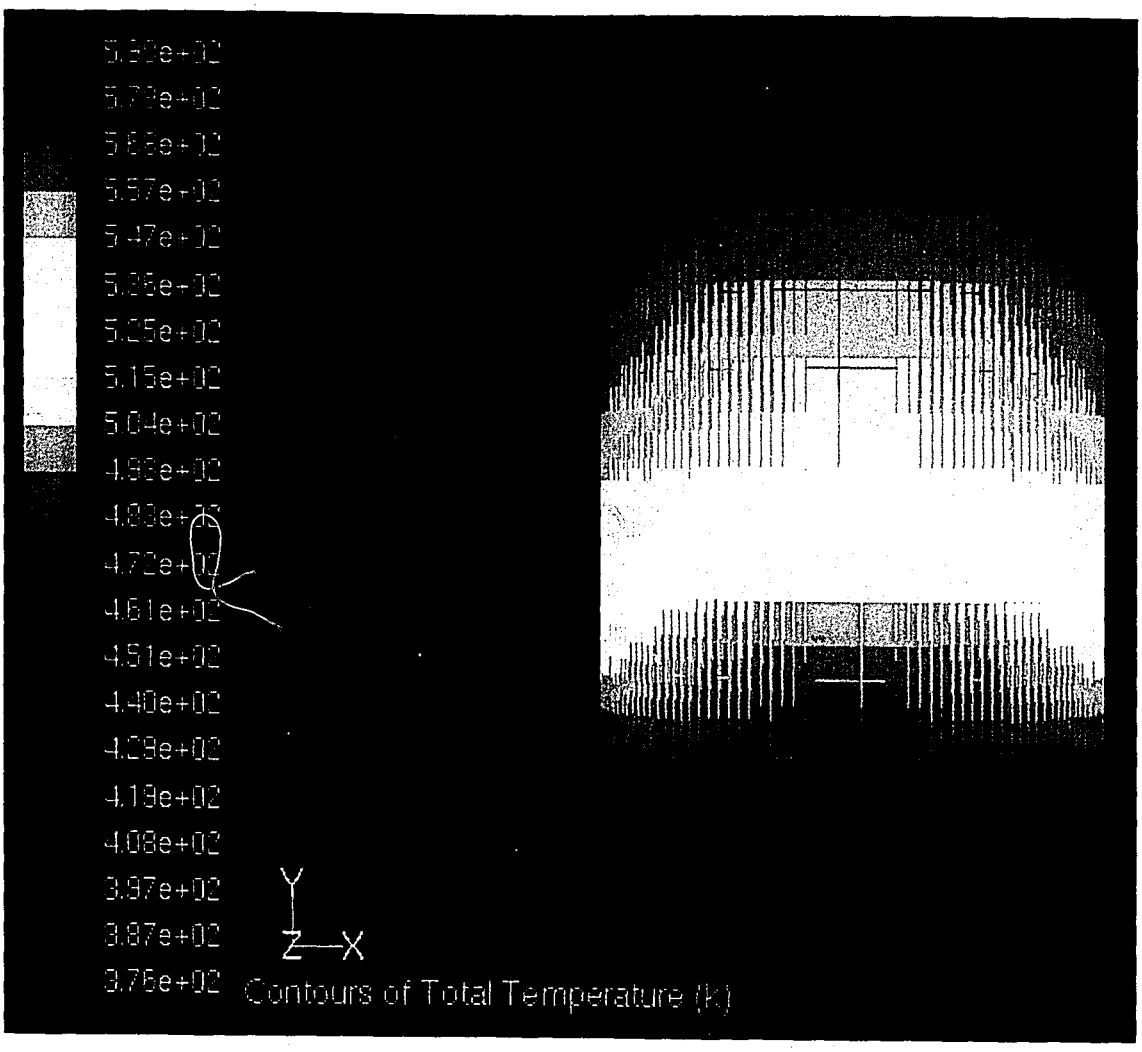

Figure 6.15: 0.8au cylinder outlet temperature

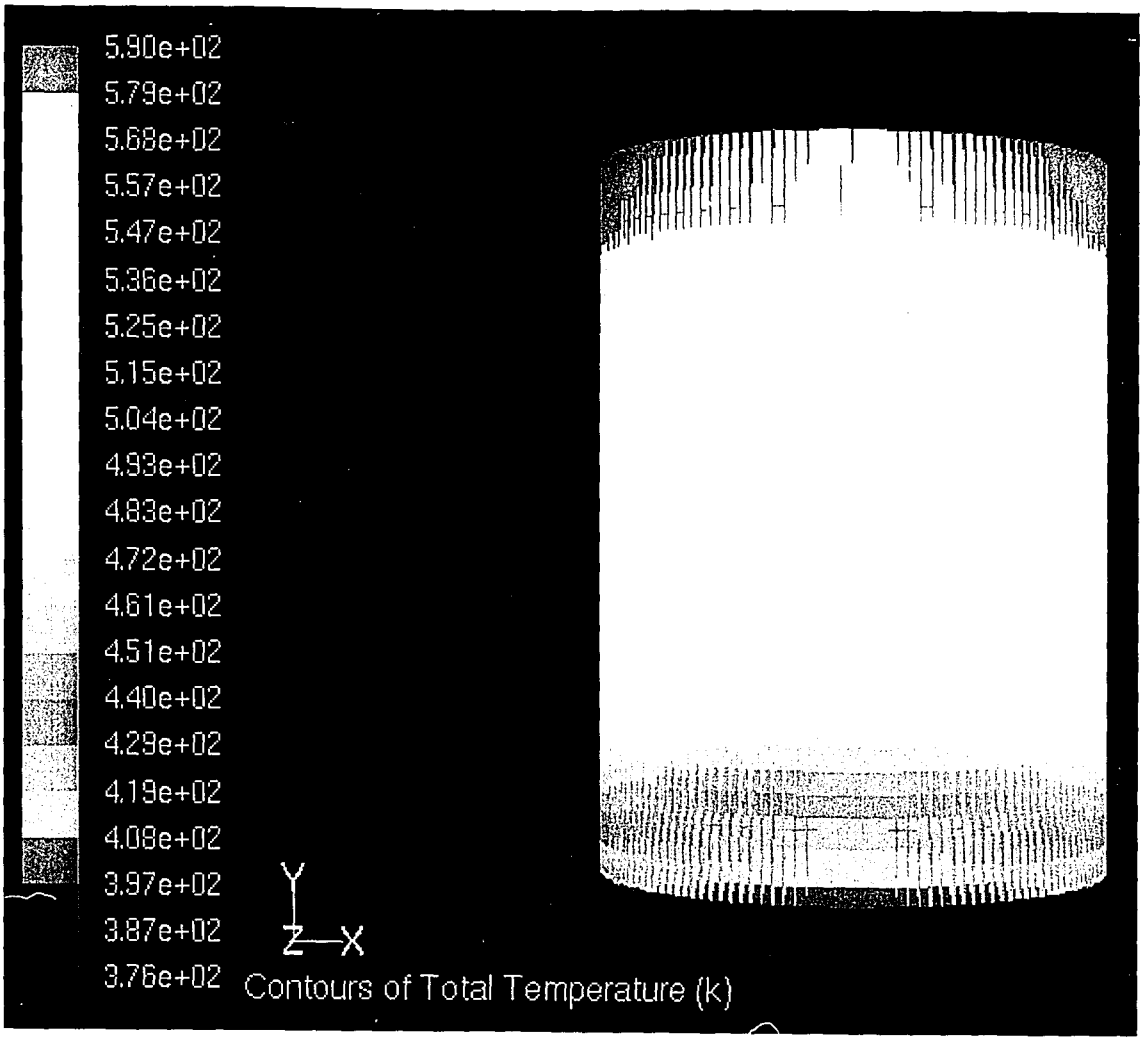

Figure 6.15: 0.8au cylinder outlet temperature

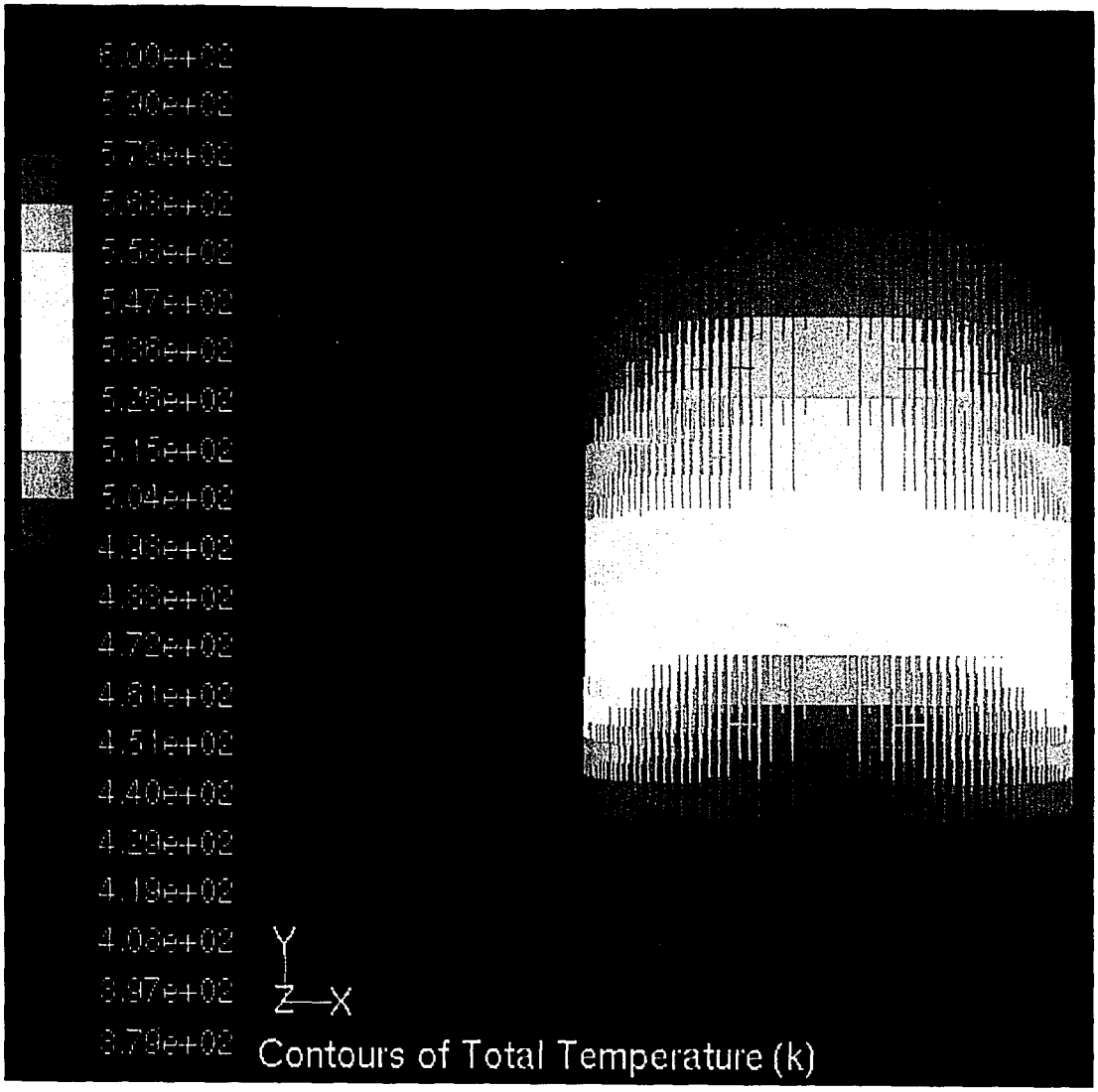

Figure 6.16: 20% extended length cylinder outlet temperature

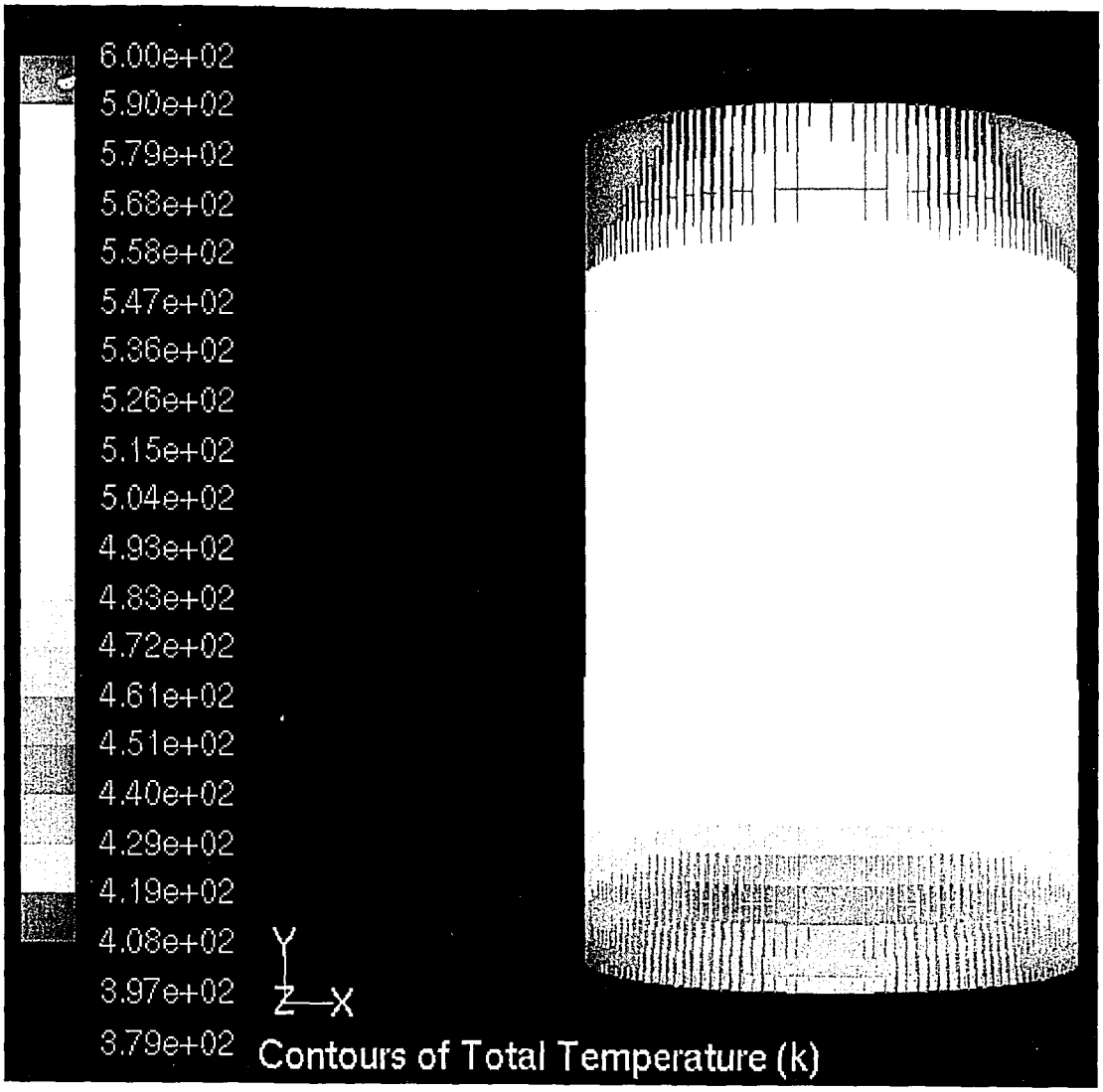

Figure 6.16: 20% extended length cylinder outlet temperature

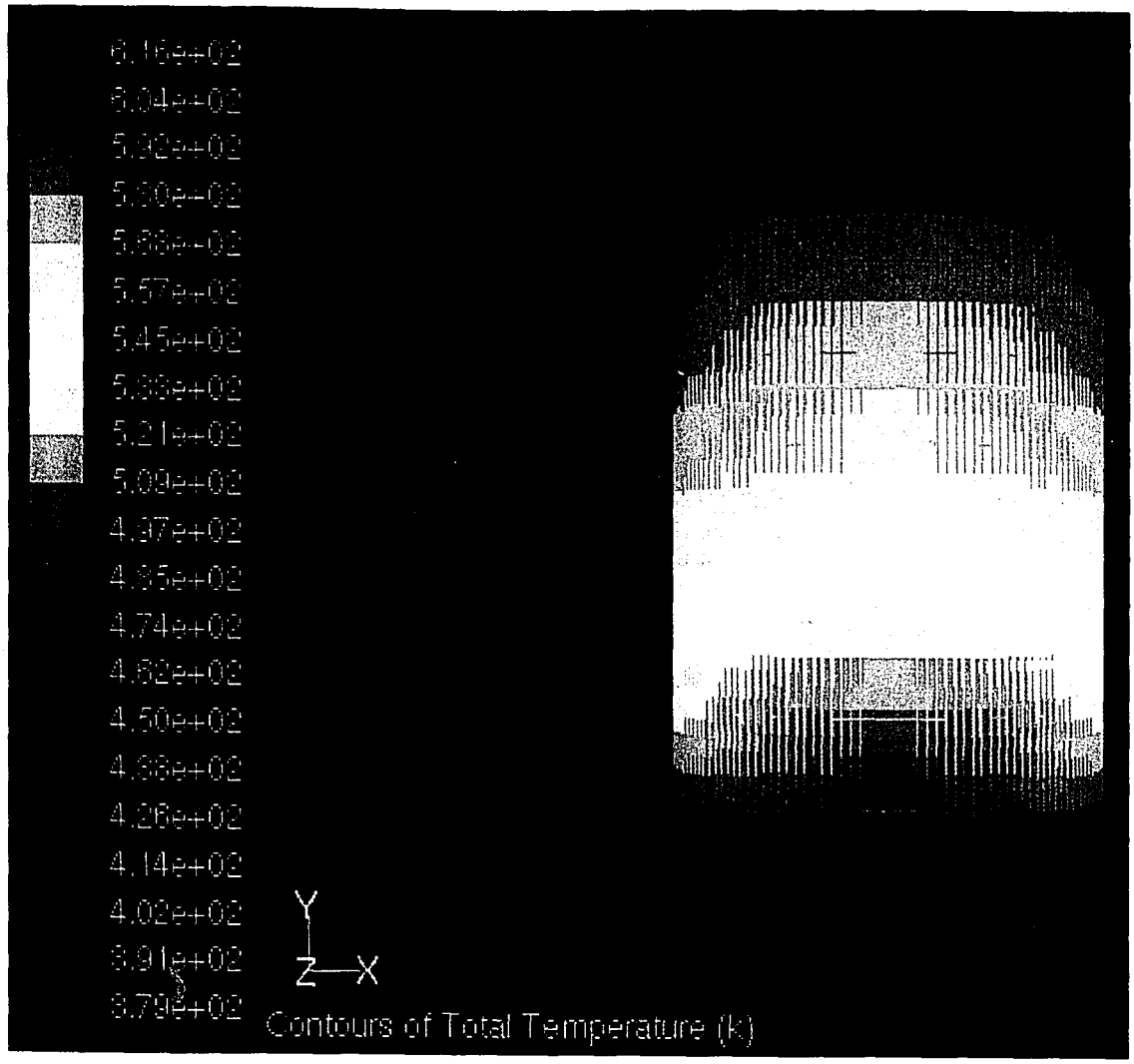

Figure 6.17: 40% extended length cylinder outlet temperature

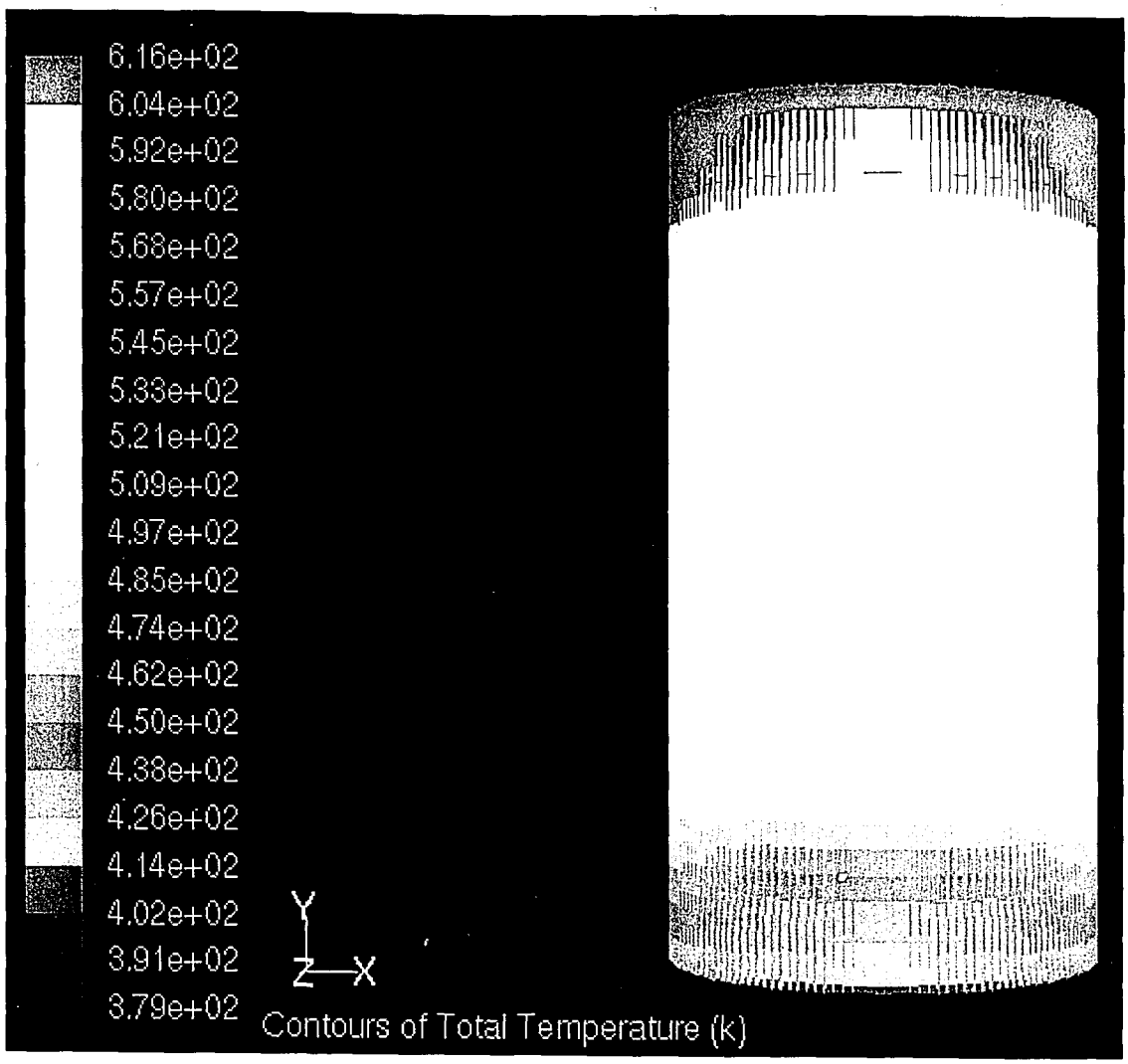

Figure 6.17: 40% extended length cylinder outlet temperature

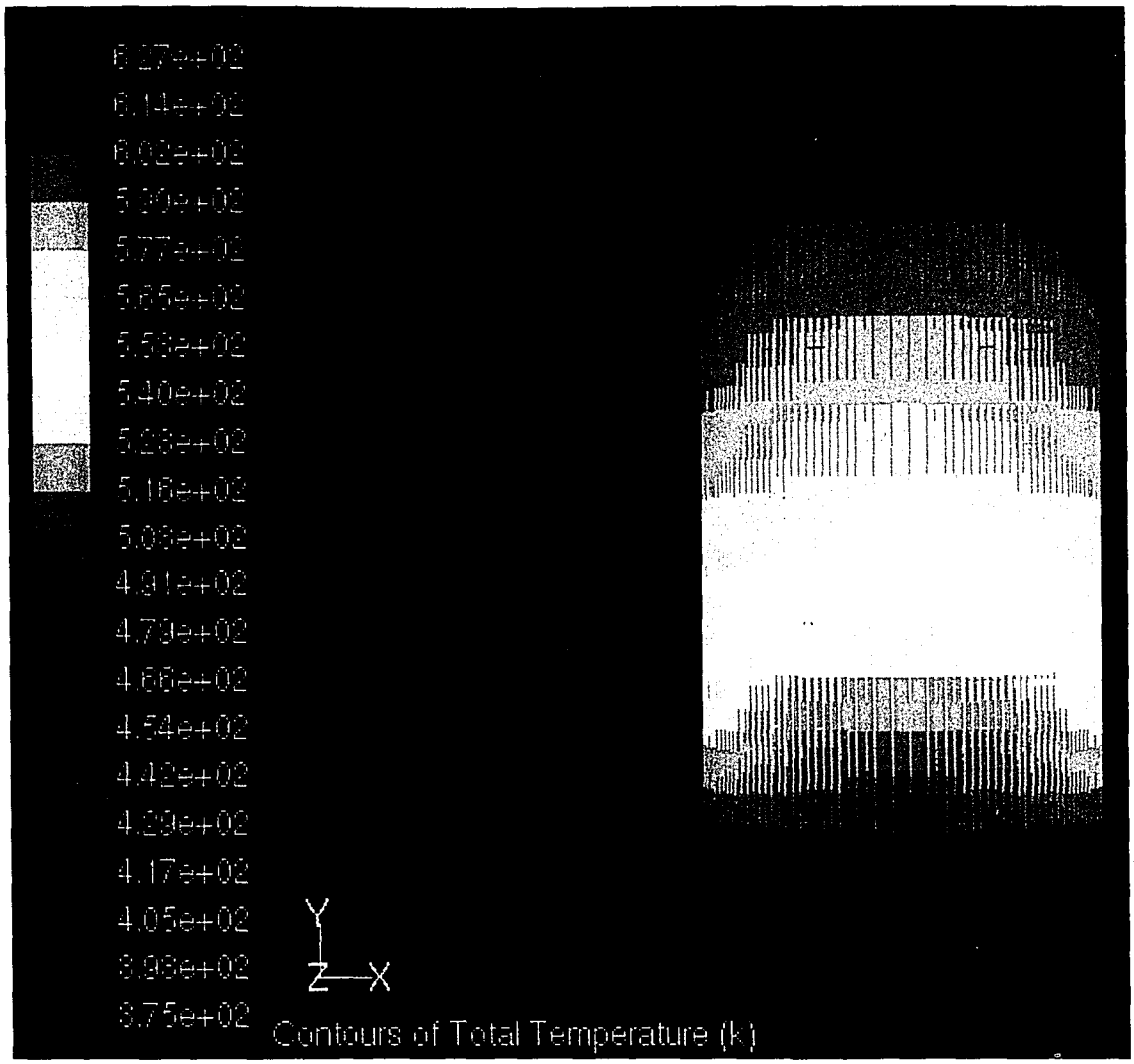

Figure 6.18: 60% extended length cylinder outlet temperature

The previous results show that the enthalpy gain increases with an increase in cylinder length (i.e. tangential flow or adding coils), the following examines the enthalpy gain as a function of Reynolds number (R_e). The 0.8au cylinder was used for all cases. The flow rate was varied from 0.1kg/s to 1.5kg/s (R_e from 129 to 1940 respectively). Table 6.4 shows results for the various trials. Refer to figure 6.19 for a graph of the enthalpy gain as a function of the Reynolds number.

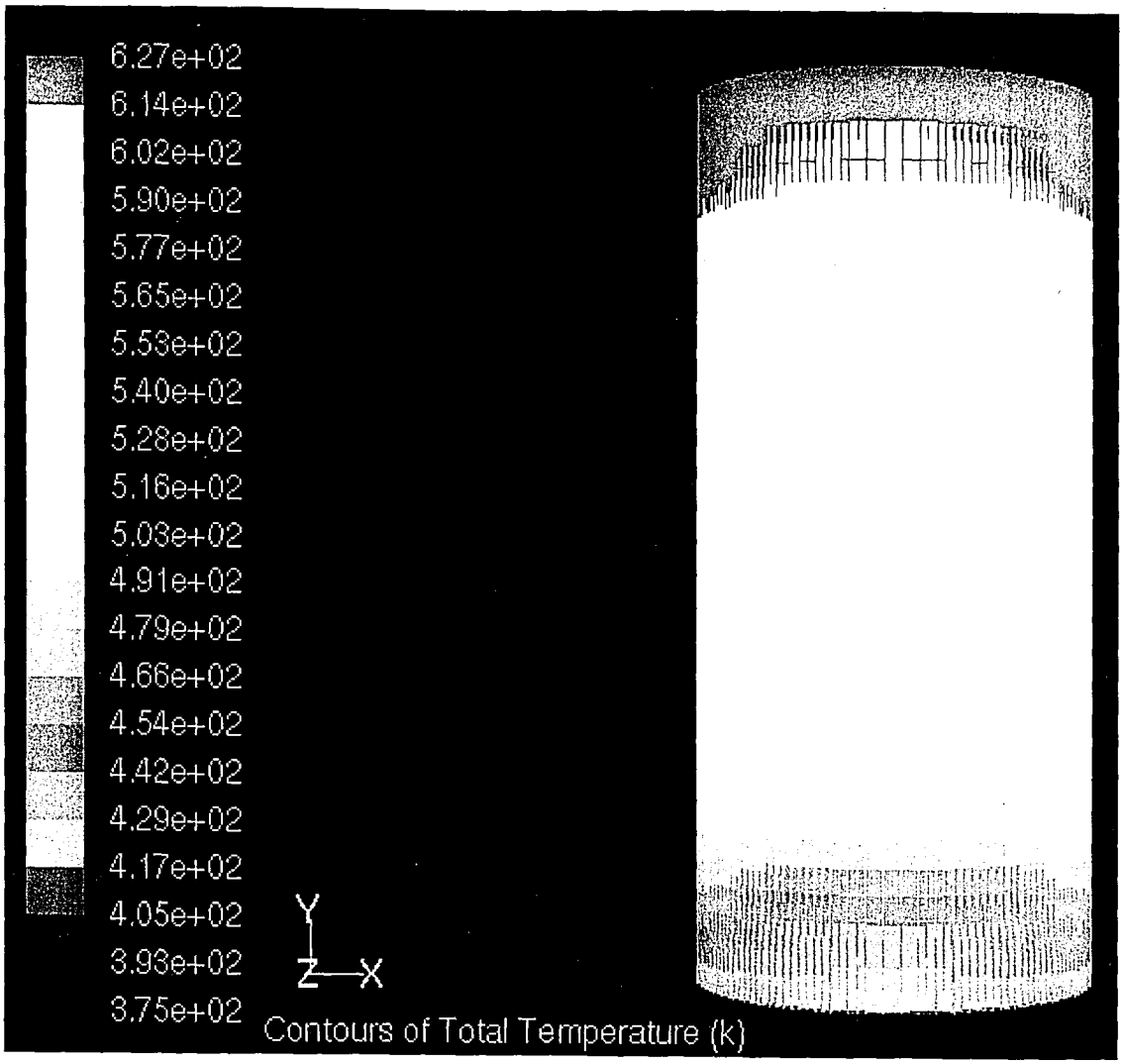

Figure 6.18: 60% extended length cylinder outlet temperature

The previous results show that the enthalpy gain increases with an increase in cylinder length (i.e. tangential flow or adding coils). the following examines the enthalpy gain as a function of Reynolds number (R_e). The 0.8au cylinder was used for all cases. The flow rate was varied from 0.1kg/s to 1.5kg/s (R_e from 129 to 1940 respectively). Table 6.4 shows results for the various trials. Refer to figure 6.19 for a graph of the enthalpy gain as a function of the Reynolds number.

Table 6.4: Varying Reynolds number results

R_e	Outlet Temperature (°C)	Enthalpy Gain (kJ/kg)
129	423	749.0
323	423	749.0
646	397	688.7
969	366	616.9
1290	344	565.8
1620	326	524.1
1940	312	491.6

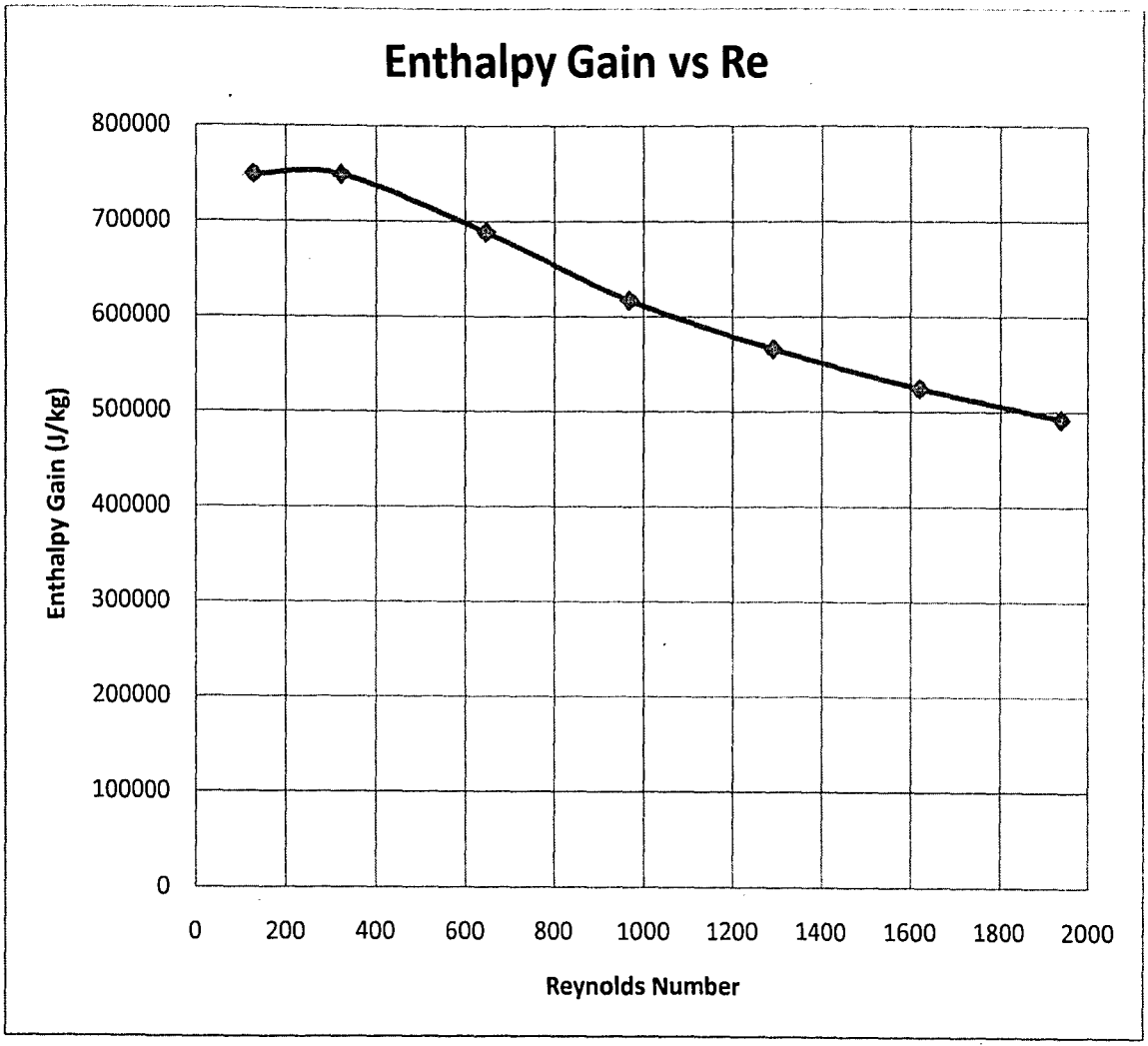

Figure 6.19: Enthalpy Gain vs. R_e

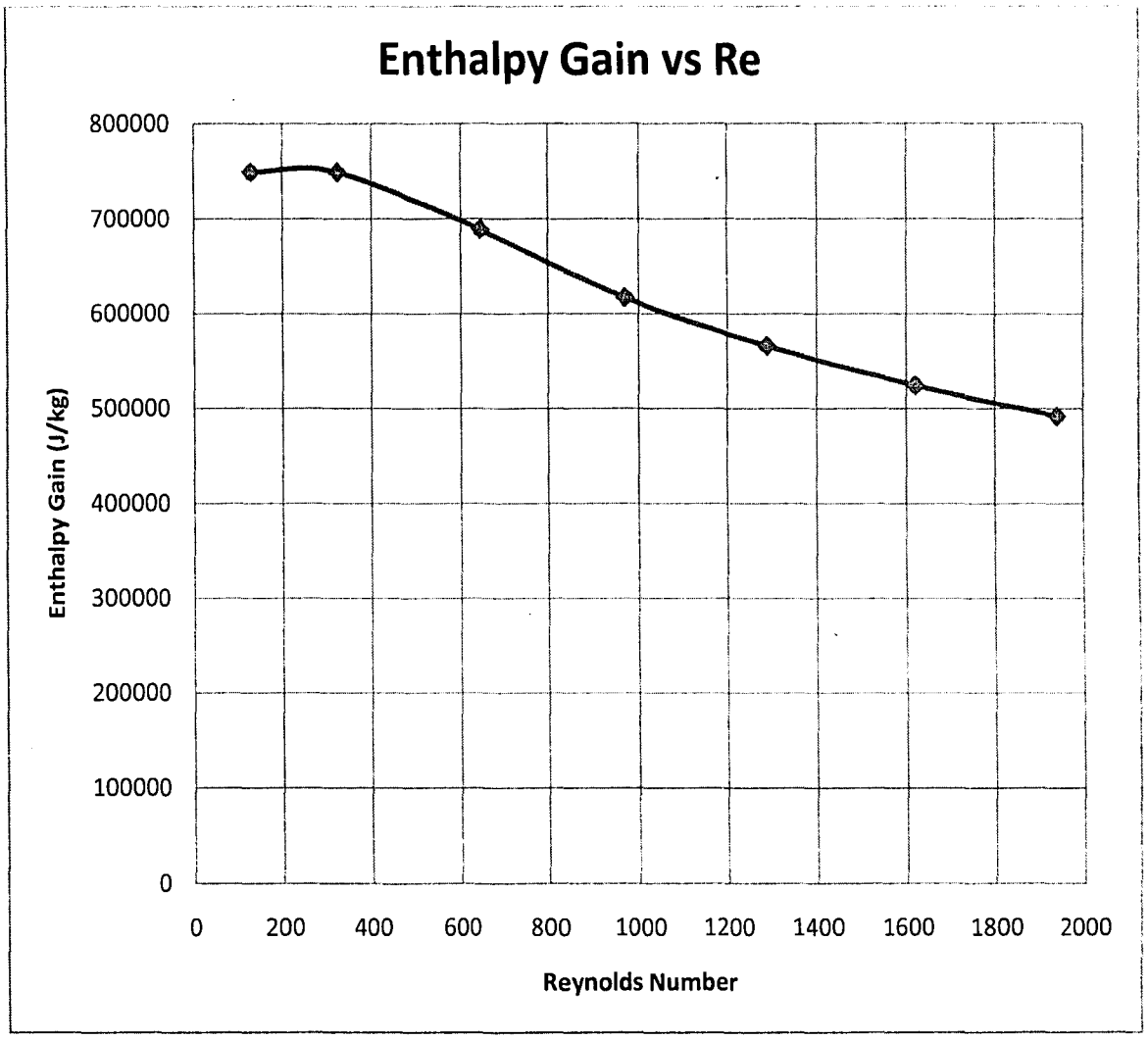

Figure 6.19: Enthalpy Gain vs. R_e

Chapter 7: Conclusions

An alpha-parabolic solar concentrator dish has been analyzed for stress analysis using FEM, optical analysis using ZEMAX, and thermal analysis using FLUENT software. The dish in this study follows the primary features of the Solar Kinetics dish designed by GE [14]. The design also called upon features from many of the various other types of CST technologies. The results show the proposed alpha dish performed well in all three of the simulated areas.

In the 30mph wind loading case, the maximum deflection the dish saw was 8.64E-5au, which is a near trivial amount. This shows the dish is expected to be able to still be operational in the event of 30mph winds. The maximum deflection for the 105mph wind loading case was only 1.06E-3au, which is still fairly small, and not catastrophic by any means. In the rare event that the dish were to face this extreme case (since it is only predicted to happen once every hundred years), our results show the dish would stay structurally sound. Obviously, the effeciency of the dish would suffer drastically, since these deflections would significantly change the optical properties of the concentrator. In theory, this would not be an issue because the dish would be in the stowed position to minimize these deflections and protect it from major damages.

For the optical analysis, the focused ring of irradiance was found in order to generate heat flux in the receiver. The focused ring was found to have an irradiance of 13.8W/cm^2. Overall, 41kW$_{th}$ were collected and concentrated into a ring in the receiver; this cooresponds to 95% of the direct solar radiation incident on the dish. It has been shown that a cavity receiver of this type, with proper insulation and interrior reflecting

surfaces, can capture 98% of this radiation [14]. Hence a thermal ouput of of over 40kW is predicted.

Thermal analysis shows the fluid with Reynolds number 1930 can be heated to a temperature of 354°C, which is an increase of 254°C from the inlet temperature (an enthalpy gain of 503.2kJ/kg). With better tangential flow in the receiver, it is predicted that this will further increase. Regardless, this is a greater increase than that of the Solar Kinetics dish, which only raised the temperature of the fluid 140°C (260-400°C) [14]. The results also show that enthalpy gain can by maximized by decreasing the Reynolds number. With a R_e less than 323, an maximum outlet temperature of 423°C was achieved using VP-1. This cooresponds to a maximum enthalpy gain of 749kJ/kg for the receiver.

In summary:

- 30mph max deflection = 8.64E-5au
- 105mph max deflection = 1.06E-3au
- 41kW_{th} total power transmitted to receiver (95% of incident solar radiation)
- Receiver maximum possible enthalpy gain of 749kJ/kg

All of the simulations done in this study show that that alpha-parablic dish has promise to compete with current solar technologies. Further research which can be done from this study could be to begin prototyping the dish for actual testing and collection of data in the field.

References

[1] Fujita, T. J. (n.d.). Comparison of Advanced Engines for Parabolic Dish Solar Thermal Power Plants. pp. 1747-1752.

[2] Graham L. M., and D. R. (2006). *Solar Thermal Power Systems- Stanwell Power Station Project.* Sydney.

[3] Kaplan, G.M., 2007, "Understanding Solar Concentrators," 30, Appropedia.

[4] Lovegrove, K. (2006). *Taking the ANU Big Dish to commercialization.*

[5] Lovegrove, K. (2006, October 6). *Solar Thermal Energy Research.* Retrieved May 25, 2007, from The Austrlian National University: http://engnet.anu.edu.au/DEresearch/solarthermal/high_temp/concentrato...

[6] Lovegrove, K., et. all. *Paraboloidal Dish Solar Concentrators for Multi-MegaWatt Power Generation.*

[7] Mills, D.R., and Graham, L.M., 2004 "First Results from Compact Linear Fresnel Reflector Installation," Solar Heat and Power Pty Ltd.

[8] Moran, S., and McKinnon, J.T., 2008 "Hot Times for Solar Energy," WorldWatch. March/April, pp. 26-31.

[9] Neti, S., Fangman, J., Shah, A.A., and Fangman, M., 2008, "Proposal for the Development of a Parabolic Dish for Concentrated Solar Thermal Power," Lehigh University, Bethlehem, PA.

[10] "Overview of Solar Thermal Technologies," CSP website 1999

[11] Price, H.W. and Kistner, R., 1999, "Parabolic Trough Solar Power for Competitive U.S. Markets," ASME, Maui.

[12] Schubnell, M., 1992, "Influence of Circumsolar Radiation on Aperture, Operating Temperature and Efficiency of a Solar Cavity Receiver," Solar Energy Materials and Solar Cells, 27, pp. 233-242.

[13] Steinmann, M. E. (2004). Modeling and Design of Direct Solar Steam Generating Collector Fields. *Solar Conference.* Portland: ASME.

[14] Stine, W.B., and Geyer, M., 2001, *Power From the Sun*, John Wiley, Chap. 9.

[15] Stoddard, L., and J. A. (2006). *Economic, Energy, and Environmental Benefits of Concentrating Solar Power in California.* National Renewable Energy Laboratory.

[16] Wright, C.C., and Bank, H., 1981. The Development of an 85-kW (Thermal) Steam Rankine Solar Receiver. *Parabolic Dish Solar Thermal Power Annual Program Review*, (pp. 67-74). Pasadena.

[17] Ulmer, S. W. (2002). Beam Characterization and Improvement with a Flux Mapping System for Dish Concentrators. *Solar Engineering ASME* , 286-292.

[18] Zang Chuncheng, L. B. (2004). Structural Design and Analysis of the Dish Solar Thermal Power System. *2nd International Energy Conversion Engineering Conference* (pp. 5645-5649). Providence: American Institute of Aeronautics and Astronautics.

Appendix A: VP-1 Properties

THERMINOL VP-1

Therminol VP-1 liquid/vapour phase heat transfer fluid, is a stable, high temperature medium that delivers process heat at temperatures up to 400°C with reliability and precise control.

Therminol VP-1 is a eutectic mixture of 73.5% diphenyl oxide / 26.5% diphenyl, and as such can be used in existing liquid, or vapour phase systems, for top-up or replacement of heat transfer fluids of the same composition. Vapour phase operation is possible at temperature above 257°C.

Heat Tracing System

Since Therminol VP-1 heat transfer fluid solidifies at 12°C, precautions must be taken to ensure lines do not freeze, particularly in outdoor installations. Heat tracing must be installed wherever lines run a danger of cooling below this point. All pipelines and equipment which may contain stagnant liquid should be traced, including all streams, vapour, drain and charge lines.

Thermal Stability at 400°C

Thermal stability of a heat transfer is one of the most important considerations in the selection of a fluid for operation under specific heat transfer conditions. Therminol VP-1 has a reputation for outstanding stability in operation.

Therminol VP-1 is based on raw materials of high purity produced by a first intent manufacturing process. This results in a reduced level of high boiler formation, superior thermal stability and benefits to the user in terms of extended fluid life and dependable trouble-free system operation.

Therminol VP-1 is thermally stable and suitable for operation over long periods at bulk temperatures up to 370-400°C.

Flammability

Although the DP/DPO eutectic can burn at elevated temperature, its chemical nature is such that its use as heat transfer medium in a properly designed and operated system does not normally constitute a serious fire or explosion hazard. Vapour freed into the air rapidly cools to below the fire point. High pressure mists, however, can form an explosive mixture with air.

Typical Physical, Chemical and Thermal Properties of Therminol VP-1

Composition		Diphenyl oxide/diphenyl
Appearance		Clear, sediment free liquid
Max. bulk temperature		400°C
Max. film temperature		430°C
Kinematic viscosity @ 40°C	DIN 51562 - 1	2.48 mm²/s (cSt)
Density @ 15°C	DIN 51757	1068 kg/m³
Flash point	DIN EN 22719	110°C
	DIN 51376	124°C
Fire point	ISO 2592	127°C
Autoignition temperature	DIN 51794	621°C
Pour point	ISO 3016	12°C
Boiling point @ 1013 mbar		257°C
Coefficient of thermal expansion		0.00097/°C
Moisture content	DIN 51777 - 1	< 300 ppm
Total acidity	DIN 51558 - 1	< 0.2 mg KOH/g
Chlorine content	DIN 51577 - 3	< 10 ppm
Copper corrosion	EN ISO 2160	<< 1a
Average molecular weight		166

Note: Values quoted are typical values obtained in the laboratory from production samples. Other samples might exhibit slightly different data. Specifications are subject to change. Write to Solutia for current sales specifications.

Properties of Therminol VP-1 vs Temperatures - Liquid Phase

Temperature	Density	Thermal Conductivity	Heat Capacity	Viscosity Dynamic	Viscosity Kinematic	Vapour pressure (absolute)	Enthalpy	Latent Heat vap.
°C	kg/m³	W/m.K	kJ/kg.K	mPa.s	mm²/s**	kPa*	kJ/kg	kJ/kg
12	1071	0,137	1,523	5,48	5,12	-	0	419,0
20	1064	0,136	1,546	4,29	4,03	-	12,3	414,7
30	1056	0,135	1,575	3,28	3,10	-	27,9	409,3
40	1048	0,134	1,604	2,60	2,48	-	43,8	403,9
50	1040	0,133	1,633	2,12	2,03	-	60,0	398,6
60	1032	0,132	1,662	1,761	1,707	-	76,4	393,3
70	1024	0,131	1,690	1,492	1,458	-	93,2	388,1
80	1015	0,130	1,719	1,284	1,265	-	110,3	382,9
90	1007	0,129	1,747	1,119	1,111	-	127,6	377,8
100	999	0,128	1,775	0,985	0,986	0,5	145,2	372,7
110	991	0,126	1,803	0,875	0,884	0,8	163,1	367,6
120	982	0,125	1,831	0,784	0,798	1	181,3	362,6
130	974	0,124	1,858	0,707	0,726	2	199,7	357,5
140	965	0,123	1,886	0,642	0,665	3	218,4	352,6
150	957	0,121	1,913	0,585	0,612	5	237,4	347,6
160	948	0,120	1,940	0,537	0,566	7	256,7	342,7
170	940	0,118	1,968	0,494	0,526	9	276,2	337,7
180	931	0,117	1,995	0,457	0,491	13	296,0	332,8
190	922	0,115	2,021	0,424	0,460	18	316,1	327,9
200	913	0,114	2,048	0,395	0,432	24	336,5	323,0
210	904	0,112	2,075	0,368	0,407	32	357,1	318,0
220	895	0,111	2,101	0,345	0,385	42	378,0	313,0
230	886	0,109	2,128	0,324	0,366	54	399,1	308,0
240	877	0,107	2,154	0,305	0,348	68	420,5	303,0
250	867	0,106	2,181	0,288	0,332	86	442,2	297,9
260	857	0,104	2,207	0,272	0,317	108	464,1	292,7
270	848	0,102	2,234	0,258	0,304	133	486,3	287,5
280	838	0,100	2,260	0,244	0,292	163	508,8	282,2
290	828	0,098	2,287	0,232	0,281	198	531,6	276,8
300	817	0,096	2,314	0,221	0,271	239	554,6	271,2
310	806	0,095	2,341	0,211	0,262	286	577,8	265,6
320	796	0,093	2,369	0,202	0,254	340	601,4	259,7
330	784	0,091	2,397	0,193	0,246	401	625,2	253,8
340	773	0,089	2,425	0,185	0,239	470	649,3	247,6
350	761	0,086	2,454	0,177	0,233	548	673,7	241,3
360	749	0,084	2,485	0,170	0,227	635	698,4	234,7
370	736	0,082	2,517	0,164	0,222	732	723,4	227,8
380	723	0,080	2,551	0,158	0,218	840	748,8	220,7
390	709	0,078	2,588	0,152	0,214	959	774,4	213,2
400	694	0,076	2,628	0,146	0,211	1090	800,5	205,3
410	679	0,073	2,674	0,141	0,208	1230	827,0	197,0
420	662	0,071	2,729	0,137	0,206	1390	854,0	188,0
425	654	0,070	2,760	0,134	0,205	1470	867,7	183,3

Note: Values quoted are typical values obtained in the laboratory from production samples. Other samples might exhibit slightly different data. Specifications are subject to change. Write to Solutia for current sales specifications.

Physical Property Formulae of Liquid

Density (kg/m³) = $-0,90797 \cdot T(^\circ C) + 0,00078116 \cdot T^2(^\circ C) - 2,367 \cdot 10^{-6} \cdot T^3(^\circ C) + 1083,25$

Heat capacity (kJ/kg.K) = $+0,002414 \cdot T(^\circ C) + 5,9591 \cdot 10^{-6} \cdot T^2(^\circ C) - 2,9879 \cdot 10^{-8} \cdot T^3(^\circ C) + 4,4172 \cdot 10^{-11} \cdot T^4(^\circ C) + 1,498$

Thermal Conductivity (W/m.K) = $-8,19477 \cdot 10^{-5} \cdot T(^\circ C) - 1,92257 \cdot 10^{-7} \cdot T^2(^\circ C) + 2,5034 \cdot 10^{-11} \cdot T^3(^\circ C) - 7,2974 \cdot 10^{-15} \cdot T^4(^\circ C) + 0,137743$

Kinematic viskosity (mm²/s) = $e^{\left(\frac{544,149}{T(^\circ C)+114,43} - 2,59578\right)}$

Vapour pressure (kPa) = $-0,190859 \cdot T(^\circ C) + 4,35824 \cdot 10^{-3} \cdot T^2(^\circ C) - 3,6106 \cdot 10^{-5} \cdot T^3(^\circ C) + 1,08408 \cdot 10^{-7} \cdot T^4(^\circ C) - 2,12329$

Latent Heat Vaporisation (kJ/kg) = $-0,526933 \cdot T(^\circ C) - 7,50103 \cdot 10^{-4} \cdot T^2(^\circ C) + 1,5622 \cdot 10^{-6} \cdot T^3(^\circ C) - 3,771 \cdot 10^{-9} \cdot T^4(^\circ C) + 425,18$

Properties of Therminol VP-1 vs Temperatures - Vapour Phase

Temperature	Density	Thermal Conductivity	Heat Capacity	Enthalpy*	Dynamic Viskosity
°C	kg/m³	W/m.K	kJ/kg.K	kJ/kg	mPa.s
12	-	0,0081	0,975	419,0	0,0057
20	-	0,0085	1,003	427,0	0,0059
30	-	0,0090	1,037	437,2	0,0061
40	-	0,0095	1,070	447,7	0,0063
50	-	0,0100	1,104	458,6	0,0065
60	-	0,0105	1,137	469,7	0,0067
70	-	0,0110	1,170	481,3	0,0069
80	-	0,0116	1,203	493,2	0,0071
90	-	0,0121	1,235	505,4	0,0073
100	-	0,0126	1,267	517,9	0,0075
110	0,042	0,0132	1,299	530,7	0,0077
120	0,065	0,0137	1,331	543,9	0,0079
130	0,099	0,0143	1,362	557,2	0,0081
140	0,148	0,0149	1,393	571,0	0,0083
150	0,214	0,0154	1,424	585,0	0,0085
160	0,303	0,0160	1,454	599,4	0,0087
170	0,422	0,0166	1,484	613,9	0,0089
180	0,575	0,0171	1,514	628,8	0,0091
190	0,772	0,0177	1,543	644,0	0,0094
200	1,02	0,0183	1,572	659,5	0,0096
210	1,33	0,0189	1,601	675,1	0,0098
220	1,71	0,0195	1,629	691,0	0,0100
230	2,17	0,0201	1,657	707,1	0,0102
240	2,72	0,0207	1,685	723,5	0,0104
250	3,38	0,0213	1,712	740,1	0,0106
260	4,17	0,0220	1,739	756,8	0,0108
270	5,09	0,0226	1,766	773,8	0,0110
280	6,17	0,0232	1,792	791,0	0,0112
290	7,42	0,0238	1,819	808,4	0,0114
300	8,86	0,0245	1,845	825,8	0,0116
310	10,5	0,0251	1,871	843,4	0,0118
320	12,4	0,0258	1,897	861,1	0,0120
330	14,6	0,0264	1,923	879,0	0,0122
340	17,0	0,0271	1,948	896,9	0,0124
350	19,8	0,0277	1,974	915,0	0,0126
360	22,9	0,0284	2,001	933,1	0,0128
370	26,5	0,0291	2,027	951,2	0,0130
380	30,5	0,0298	2,054	969,5	0,0132
390	35,0	0,0304	2,082	987,6	0,0134
400	40,1	0,0311	2,111	1005,8	0,0136
410	45,8	0,0316	2,142	1024,0	0,0138
420	52,4	0,0325	2,175	1042,0	0,0140

* the enthalpy basis is ideal gas at 12°C

Note: Values quoted are typical values obtained in the laboratory from production samples. Other samples might have slightly different data. Specifications are subject to change. Write to Solutia for current sales specifications.

Physical Property Formulae of Vapour

Density (kg/m³) = - 0.0303917 * T(°C) + 4.34615 * 10^{-4} * T²(°C) - 2.41006 * 10^{-6} * T³(°C) + 5.33458 * 10^{-9} * T⁴(°C) + 0.553905

Heat Capacity (kJ/kg.K) = - 0,003703 * T(°C) - 3.0274 * 10^{-5} * T²(°C) - 2.9324 * 10^{-8} * T³(°C) + 0.92709

Dynamic Viskosity (mPa.s) = + 2.0124 * 10^{-1} * T(°C) + 3.4557 * 10^{-3} * T²(°C) - 7.1288 * 10^{-6} * T³(°C) + 0.005449

Thermal Conductivity (W/m.K) = + 4.84257 * 10^{-5} * T(°C) + 2.9067 * 10^{-7} * T²(°C) - 6.5306 * 10^{-11} * T³(°C) - 0,0075110

Vita

Matthew Robert Devlin was born on April 22, 1985 in Coatesville, Pennsylvania. He is the son of Robert and Elise Devlin. Upon graduating from Coatesville Area Senior High School in 2003, he decided to attend Moravian College and pursue a degree in Physics. He received a Bachelor of Science degree from Moravian in 2007, where he graduated with honors. His honors thesis on the investigation of Ga substituted Cobalt Ferrite using Mössbauer Spectroscopy resulted in a publication in the Applied Journal of Physics in April, 2008. Upon completion of his studies at Moravian, Matt enrolled in the Mechanical Engineering Graduate program at Lehigh University. While at Lehigh, he was a TA, studied concentrated solar thermal technology with Dr. Neti, and worked for Lehigh's Industrial Assessment Center.

END OF TITLE